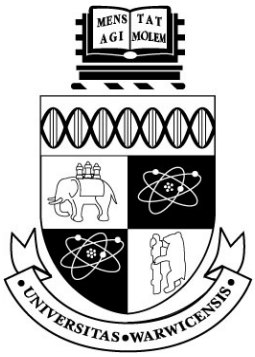

Mathematical Modelling of the Half-Sarcomere from a Human Skeletal Muscle.

by

Kay Patricia Guest.

Thesis

Submitted to the University of Warwick

for the degree of

Doctor of Philosophy.

Department of Physics

October 2013

THE UNIVERSITY OF WARWICK

Table of Contents

List of Tables

List of Figures

Chapter 4

Acknowledgments

It has been a bit of a trek, one I would not have completed without the unflagging encouragement and support of Professor Adrian Wilson, to whom I am greatly indebted.

My gratitude to J.P. for helping to put the wheels back on when they fell off and being ever ready with the puncture repair kit.

Declarations

Unless clearly stated and referenced otherwise, the work presented within this document is my own, carried out under the guidance of Professor Adrian Wilson within the Department of Physics at the University of Warwick. The content of this thesis has not previously been submitted for examination at any other institution.

Abstract

The character of the functional output of a motor unit within skeletal muscle has been linked experimentally to the proteins found in the sarcomere, the smallest contractile unit of muscle fibre. Current mathematical models focus on either individual chemical reactions or the bulk properties of muscle with limited reference to the internal processes and structures within the muscle. Without an understanding of those internal properties, the normal function of muscle cannot be simulated and consequently muscular diseases and their treatments cannot be accurately modelled.

In this project, a mathematical model has been developed which relates the chemo-mechanical cycle of individual events (crossbridges) to the transfer of mechanical energy through an actin filament, myosin cofilament and, by incorporating the protein titin, the mechanical properties of the interconnecting proteins in a section of sarcomere. Evaluation and parameterisation of the model were made by comparison with in vitro test data from the published literature at the level of a single crossbridge and single filaments. At the single filament level, the model was evaluated against two conditions: a low load high displacement (concentric contraction) and a high load low displacement (isometric contraction).

In isometric loading the peak force level per unit length of actin filament was higher than that observed in vitro, the difference being attributable to the greater compliance in the substrate used in vitro to hold the myosin fragments (~37pN compared to ~12pN). The mean number of concurrent crossbridges was consistent between the model and in vitro data. Under low load the model demonstrated filament movement at speeds comparable to those measured in in vitro motility studies, although longer filaments in the model were required than those in vitro to reach the higher speeds (7μm vs. 2μm for ~8μm/s).

By making the pre-lever reaction duration of the crossbridge cycle strain dependent it was possible to obtain long reaction cycles in low load scenarios comparable to those observed for fragments in solution while generating the actin filament speeds observed in vitro. It was necessary to have a distribution of attachment times across the filament in order to generate and maintain filament movement in the model; the variation being governed by the tension distribution in the filament. By applying a passive loading as

generated by the titin protein the filaments moved more rapidly, with an increased contribution from each crossbridge to filament movement.

Initial results indicate examination of the strain dependency of the post-lever reaction duration may modify filament speeds and will increase the proportion of each crossbridge movement that contributes to the actin filament propulsion (increase crossbridge efficiency). Examination of a selection of the model's parameters gave an initial evaluation of how the model could be 'tuned' to change the number, reaction state and distribution in time of crossbridges to achieve changes in filament contraction speed, isometric force generation and the efficiency with which crossbridges are used; noting that one desired output may conflict with another.

The interaction of the passive components in the structure of the sarcomere with the strain dependent reaction cycle at each crossbridge demonstrated the potential limitations of scaling and averaging localised events without consideration of the passive structures present in the fibre and muscle bulk. The model provides a means to examine the mechanisms and parameters of the sarcomere's function and how those parameters may be adjusted to achieve different output characteristics. The model provides a foundation for the emulation of muscle fibres and a motor unit in health and disease.

Chapter 1

1 Introduction

Skeletal muscle performance is large ranging from delicate finger movements to the moving of heavy loads, responding with speed and endurance depending on the task. Many factors contribute to this versatile performance range; based on a literature review a summary can be found in Figure 1.1. The function of a muscle is a composite of the dimensions, orientation and internal properties of the individual muscle fibres, the muscle's shape and its anatomical environment e.g. tendons, limb geometry, mass and interactions with other muscles.

The basic contractile unit of skeletal muscle is the sarcomere; that is where chemical energy is translated into mechanical energy. Previous studies (described in more detail in Section 2.1.3) have experimentally linked the function of motor units to the type of proteins found in the sarcomere. These proteins and motor units fall into three distinct types, summarised in Table 2.1. The observed link to the motor unit means that if the sarcomere components can be modelled and their interaction understood the behaviour at that level can be translated through the geometry and connective tissue of the larger scale fibres in order to characterise a motor unit. From the combination of different numbers of, size and type of motor units the diverse range of muscle function can be simulated.

There are mechanistic models that allow the properties of whole muscle to be simulated (Section 2.3) and models that focus on the thermodynamics of individual chemical reactions before extrapolating to the bulk muscle. However, these types of model do not make reference to the internal processes and structures within the muscle without which it is not possible to adequately simulate muscular diseases and their treatments. Models exist of some of the components of the sarcomere but these tend to focus on the detail of the chemical interactions rather than the mechanical structure. Currently no model of the sarcomere has been found which incorporates the chemical processes and mechanical structures including the passive connective proteins. Therefore, in this thesis a section of sarcomere has been examined and modelled in order to begin the process of building a bulk muscle model. The interdependency of

the mechanical, passive components of the sarcomere and force-displacement generating chemical interactions that drive the muscle's function is examined. Physical principles are used to define the models structure with a view to creating a predictive output the components of which can be analysed.

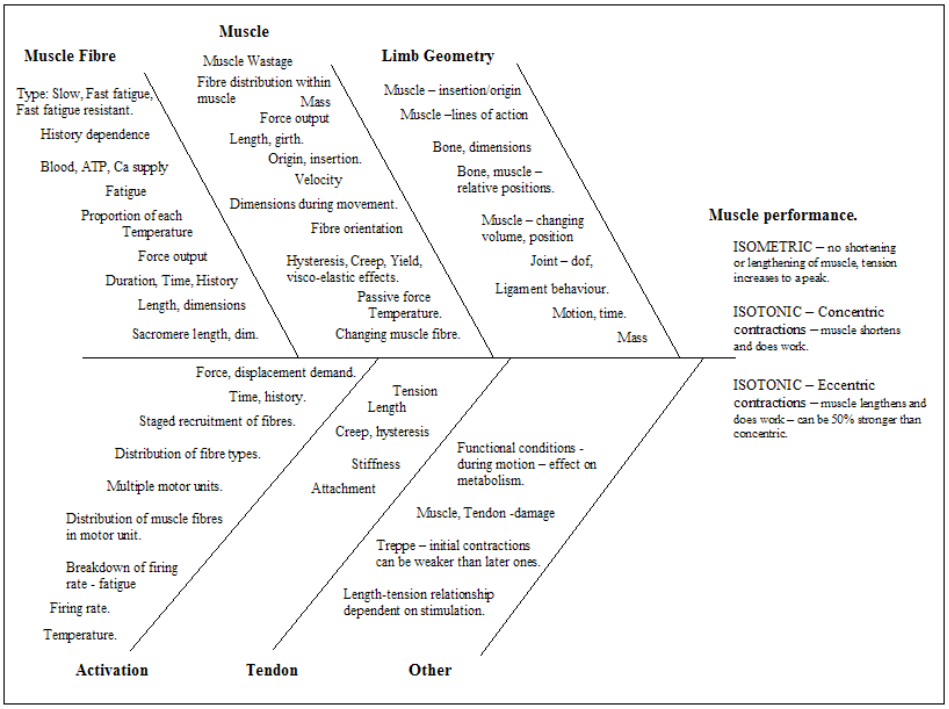

Figure 1.1, Outline of functional characteristics of individual muscles and the surrounding structures, which combine to generate limb movement and influence the actual and apparent performance of the muscle.

1.1.1 Overview of Biological Components.

A muscle is composed of bundles, fascicles, of fibres. The bundles are arranged in different patterns depending on the function of the muscle e.g. longitudinal or pennate (at an angle) and multipennate. In Figure 1.1.1, the hierarchy of the substructures of skeletal muscle are shown with an indication of the number or volume at each level. A muscle can be broken down into functional groups of fibres called motor units. These groups of fibres are stimulated by the same nerve but are spatially distributed across the muscle. Each muscle fibre, a single muscle cell, is composed of myofibrils, which are fibre like structures aligned with the length of the fibre. Each myofibril is itself divided cross-sectionally into blocks termed sarcomeres, which are stacked end to end. Within the sarcomere, thick (myosin cofilaments) and thin (actin) filaments align parallel to the fibre in an ordered structure causing the dark and light banding which

gives skeletal muscle its alternative name: striated muscle (Figure 1.1.2). Chemical interactions form crossbridges between the thick and thin filaments and these provide the mechanical energy for a muscle contraction. An individual crossbridge produces piconewton forces and nanometre displacements but the number of crossbridges within a muscle is many: ~10^{16} per fibre (see Figure 1.1.1). In the fibre connective tissue, perimysium, maintains the ordered structure of the fibres and transfers loads. In the sarcomere, proteins provide the support structure.

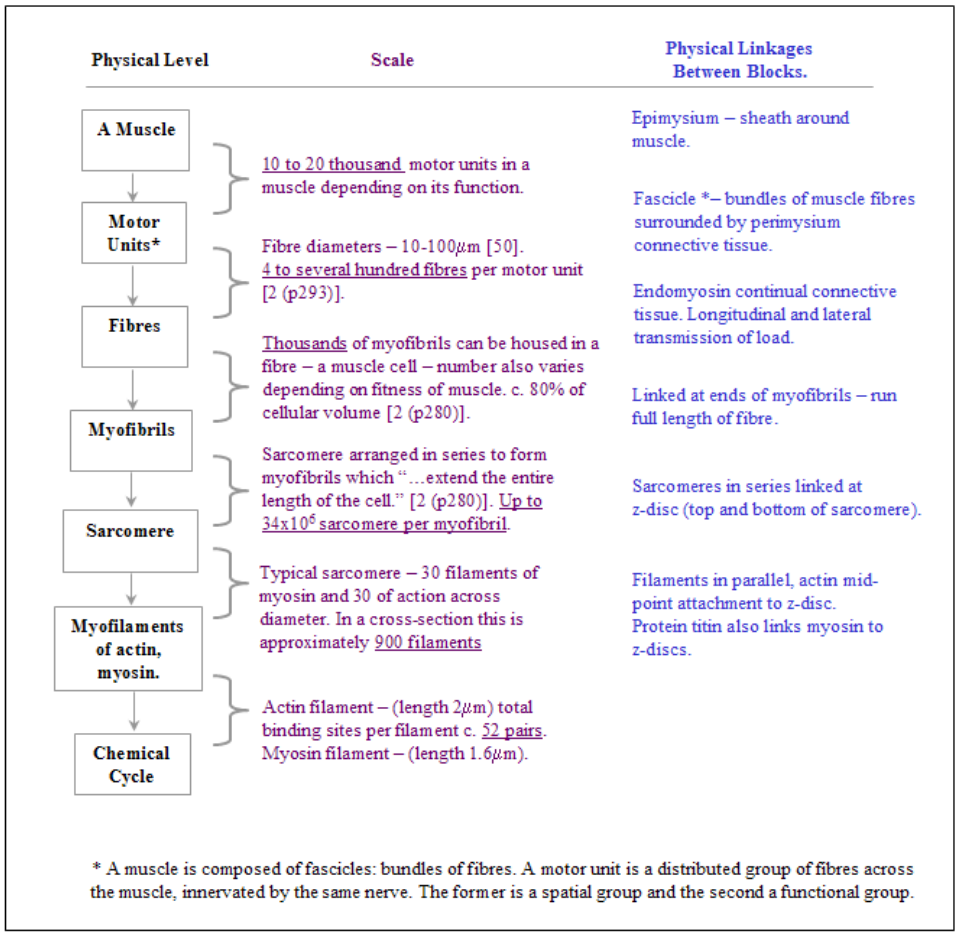

Figure 1.1.1, The structural hierarchy of muscle and linking fibres, sources [1,2].

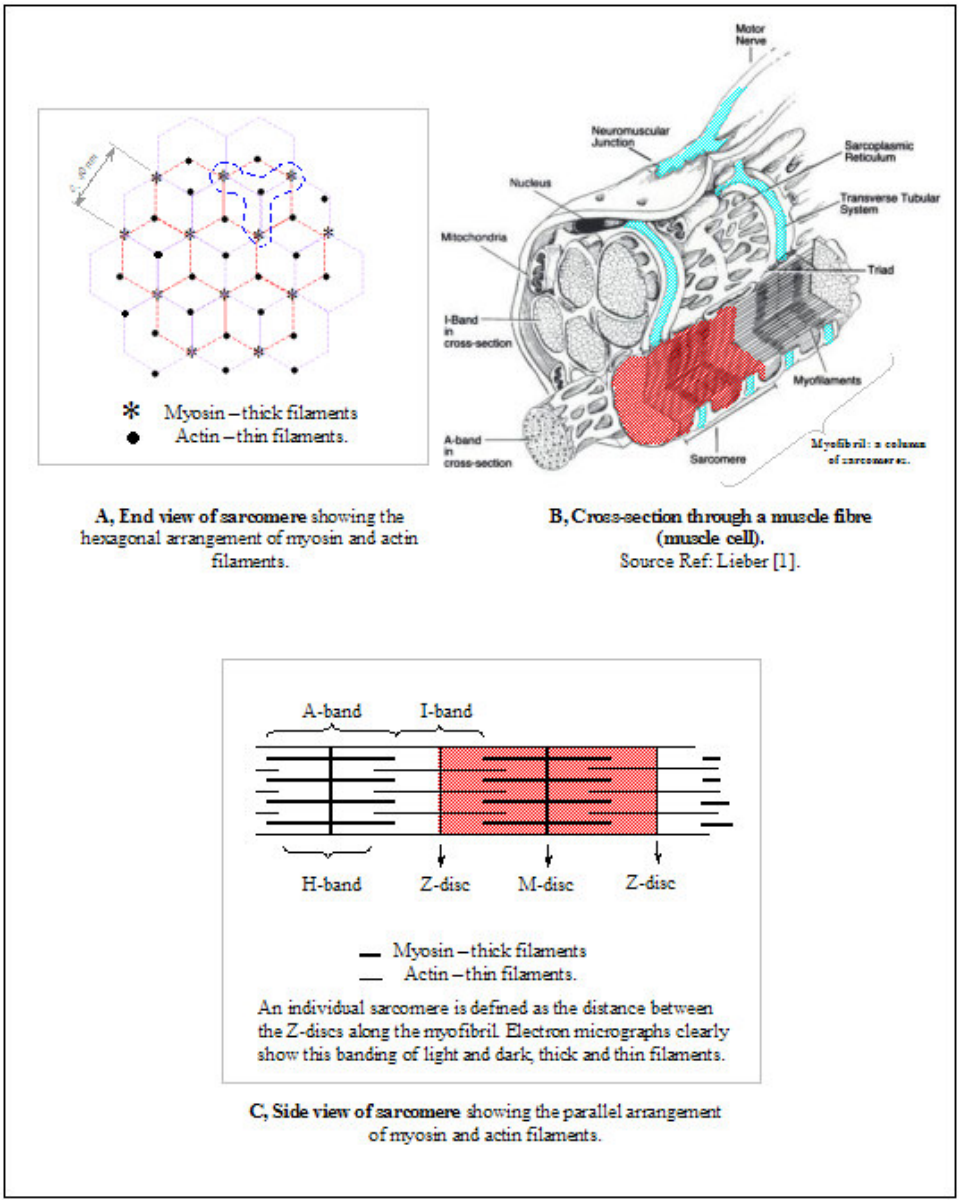

A, End view of sarcomere showing the hexagonal arrangement of myosin and actin filaments.

B, Cross-section through a muscle fibre (muscle cell). Source Ref: Lieber [1].

C, Side view of sarcomere showing the parallel arrangement of myosin and actin filaments.

Figure 1.1.2, Cross-section through a muscle fibre (B) with a single sarcomere highlighted in red. The ordered structure of a sarcomere is shown in A and B: end and side views. Diagram B locates, in blue, the neuromuscular junction; where the nerve terminates at a chemical synapse. Also highlighted in blue is the transverse tubular system, which carries the Na^+ ion stimulated excitatory postsynaptic current to the sarcomere.

1.1.2 Model Overview.

The model described in this thesis, which will be referred to as the Baseline Model, is of a section of sarcomere. A cross-section through a sarcomere is shown in Figure 1.1.2.A. The dashed 'T' shape encompasses a unit repeated throughout the ordered structure of the cross-section. This repeated unit contains three myosin (thick) cofilaments each presenting 120^o of its cross-section to a single actin filament. The

Baseline Model is of this 'T' shaped repeat unit, as it is the simplest repeatable unit within the fibre, the function of which can be scaled up to the level of the fibre. To simplify the modelling the three-dimensional structure was transformed into one-dimension by combining the three partial myosin cofilaments into one composite filament.

The sarcomere blocks are shown longitudinally in Figure 1.1.2.B and C where the actin and myosin filaments can be seen to follow an ordered pattern with a plane of symmetry at the M-disc which bisects the myosin cofilament. During a contraction, the Z-discs are drawn together towards the M-disc, maintaining the striation pattern. Due to this symmetry the Baseline Model was set at a half-sarcomere length; M to Z-disc in length. The M-disc was considered to have a fixed position and force and displacement was measured at the Z-disc. The ordered structure of the sarcomere is maintained by a number of proteins. The dominant linkage between the Z-discs is the giant polypeptide titin. Titin provides a passive force restoring the sarcomere to its rest length. Six titin proteins are present per myosin cofilament. In the Baseline Model, this equates to six titin proteins per actin filament and so the composite model titin is equivalent to six titin proteins.

The biological components have been extrapolated to a one-dimensional problem with three distinct functional elements represented: the chemical reaction which drives the crossbridge formation, the expression of that chemical energy as mechanical energy and the mechanical properties of the actin, myosin and titin filaments. The chemical reaction may be considered as a sequence of events limited by geometry, temperature, concentration and strain while the mechanical dynamics problems can be represented with springs and dampers. A model was required to bring these components together in a single, cohesive framework.

An initial survey of muscle anatomy and physiology identified a very high number of parameters, 50+ (Appendix B, Table 1-4), are required to describe multiple concurrent events in this complex system. The wide range of lengths ($<<10^{-9}$ to 10^{-6} m) and time scales ($<10^{-6}$ to 10^{-3}secs) make the system computationally stiff. Software such as Facsimile can manage this type of stiffness but is not adaptable enough to model the other structural components of the model, where as, the opposite may be said of software such as SimuLink. Therefore, a compartmental modelling structure was favoured with a customised solver. Any scientific programming language could have been used but Matlab was deemed appropriate due to its inbuilt functions for

manipulation of arrays, plotting capabilities and the accessibility to tabulate and visualise variables during model development. A generally accessible and flexible program is advantageous to integrating the model into future work.

The different aspects of the model are isolated into separate functions with a controlling script and post-processing scripts. All model parameters are defined in the control script, as are loads and the selection of data to be recorded for future analysis. The individual functions include: initial geometry layout, crossbridge formation, reaction rates, a record of individual bond sites and an equation formulation and solution of the system. This object-orientated structure isolated the input, output and internal functions of key aspects of the model allowing localised modifications to part of the model to be made independently of the remainder of the model.

Time steps of fixed duration were used but in instances of rapid length and therefore, stiffness changes in the myosin cofilament (see Section 3.2.2), the time step was subdivided a pre-defined amount (10 in the Baseline Model) and the system re-evaluated. In Appendix A, a summary of the half-sarcomere sub-unit model is given showing the components modelled, the flow and processing of data and type of output generated. Figure 3.8.1 shows how data moves through the Matlab script and Appendix E contains flow diagrams of the key functions that are used in the model.

1.1.3 Thesis plan

To provide a context for the model Chapter 2 describes muscle anatomy and physiology in more detail. Methods of muscle classification are considered in order to relate the complex range of muscle function to the properties of the Baseline Model. For model validation and parameterisation the availability and limitations of published experimental data are evaluated. Alternative modelling approaches are considered and how they relate to the model described in this thesis.

In Chapter 3 the development of the model is described. Firstly, the structural components, actin, myosin and titin filaments are considered. Focus is then placed on the individual crossbridges. These are considered in terms of their functional characteristics: the chemical reactions, what governs the meeting of bond sites and how the chemical energy is converted into mechanical energy. Finally, the influence of titin on the overall structure is considered. For each aspect of the model, a detailed

biological description is given and alternative modelling approaches and theories are reviewed. Each sub-section includes a detailed description of the representation in the Baseline Model. Where possible the model component is tested and parameter values identified and evaluated in the context of the published literature.

In Chapter 4 the Baseline Model is used to simulate two extremes of muscle function at the filament level: the rapid, low load shortening of the sarcomere (a concentric contraction) and the development of force in the absence of shortening (isometric contraction). These experiments allowed the interaction of crossbridges to be examined and in particular the exploration of the strain dependent reaction parameters. In Chapter 5 the results of Chapter 4 are compared to the results and model structure developed in Chapter 3 with consideration given to observations and measurements found in the published literature.

Finally, the observations and many parameter values (Appendix B, Table 1-4) identified in previous sections are reviewed in terms of muscle function (Figure 1.1), the fibre types identified in Chapter 2 and the protein isoform.

Chapter 2

2 Model Background

2.1 Form, Function and Scaling of Properties.

In the introduction, the general structure and interactions of muscle were presented. The sarcomere was identified as the basic contractile unit of the muscle. In Figure 1.1.2, this unit can be seen in the context of the muscle fibre. In this section the stimulation, energy supply and the source of the contraction in the sarcomere and fibre are considered. Finally, the relationship between the sarcomere, the Baseline Model and the motor unit's function is explored.

2.1.1 Fibres in the Motor Unit.

The spatial distribution of activated fibres in a motor unit spreads the contractile load through the muscle avoiding asymmetric deformations. Additionally fibres do not necessarily run the full length of the muscle or fascicles; some begin and end within the muscle bundle [3,4]. Therefore, loads must be transmitted laterally through the interconnecting tissue and non-innervated fibres, as demonstrated experimentally by Street [5]. The tension developed by individual motor units varies greatly. Those motor units producing higher tension having many more fibres of larger diameter [6]. All the fibres in a motor unit are stimulated simultaneously; the motor unit is an all or nothing system. Depending on its function, a muscle may have ten motor units or twenty thousand.

2.1.2 Contraction Stimulation.

The process of contraction is initiated by the stimulation of a nerve. A major mylinated motor nerve branches into finer non-mylinated tendrils that are attached to individual fibres within the motor unit. On activation of the motor nerve, these tendrils carry an action potential in the form of a wave of depolarisation to each fibre. A model of the generation and propagation of this action potential was presented by Hodgkin

and Huxley [7]. Although the experimental evidence to support the model was based on a giant squid axon, it has repeatedly been found to be a good representation in other experimental studies.

The action potential arrives as an ion imbalance at a chemical synapse known as the neuromuscular junction which is on the surface of the fibre, (Figure 1.1.2.B). The ion influx stimulates the release of calcium ions which enable the release of the neurotransmitter acetylcholine. Acetylcholine molecules migrate across the gap between the nerve and fibre, known as the synaptic cleft, binding to the surface of the fibre at the motor end plate. It is worth noting that a significant number of drug interactions disrupt this process and therefore muscle activity. Nerve gases and organophosphate insecticides over-stimulate the action of acetylcholine and botulinus toxin, barbiturates and curare (a muscle paralysis agent) inhibits it [1].

Once present at the motor end plate the acetylcholine opens ion gates in the membrane of the muscle fibre initiating an ion influx (Na+) into the cell generating another wave of depolarisation. This wave of depolarisation (excitatory postsynaptic potential) is carried deep into the fibre to the sarcomere via a network of transverse-tubules (shown in blue in Figure 1.1.2.B) where it stimulates the release of calcium ions into the sarcomere. By binding to the actin filaments the calcium ions open myosin receptive bond sites, providing opportunities for crossbridges to form with the myosin cofilament.

2.1.3 Sarcomere Crossbridges: the source of the contraction.

The myosin's bond sites are located on heads attached to arms that protrude from the thick cofilament. Figure 2.1.1, shows a sketch of this formation. In the chemical reaction (2.1.1) (full cycle shown in Figure 3.3.1) between the two bond sites, the initial state is a crossbridge between an actin bond site (A) and a myosin bond site (M). A single molecule of adenosine triphosphate (ATP: the chemical energy transporter within the human body) binds to the myosin site expediting the release of the crossbridge.

$$A{\cdot}M + ATP \rightarrow A + M{\cdot}ADP{\cdot}Pi \leftrightarrow A{\cdot}M{\cdot}ADP{\cdot}Pi \leftrightarrow A{\cdot}M \qquad (2.1.1)$$

While unattached the myosin catalyses the conversion of ATP to adenosine diphosphate (ADP) and a γ-phosphate (Pi) and in so doing energy is stored in the myosin head in the form of a structural distortion. The energised myosin site is then ready to bind to a new, receptive actin site. Having bound, ADP and Pi molecules are expelled initiating the release of energy into the new crossbridge, 'ratcheting' the actin filament a small parallel distance relative to the myosin bond site/cofilament (see Figure 2.1.1). This "crossbridge cycle" of formation and release is explained in more detail in Chapter 3 and diagrammatically in Figure 3.3.1.

Sequences of multiple crossbridge events combine to form the overall contraction of the sarcomere with the cumulative effect that each fibre is capable of producing a transient contractile force of a few tens of grams. This description of the distorted myosin head movement is based on the rotating crossbridge model proposed by Huxley [8] in 1957, which he based on his own experiments together with those of many others. He proposed that the expression of energy (ATP) stored in the myosin head could be approximated as the release of tension in a spring termed the "power stroke model" (considered in greater detail in Section 3.5). His interpretation identified key features in the system providing a foundation for future work.

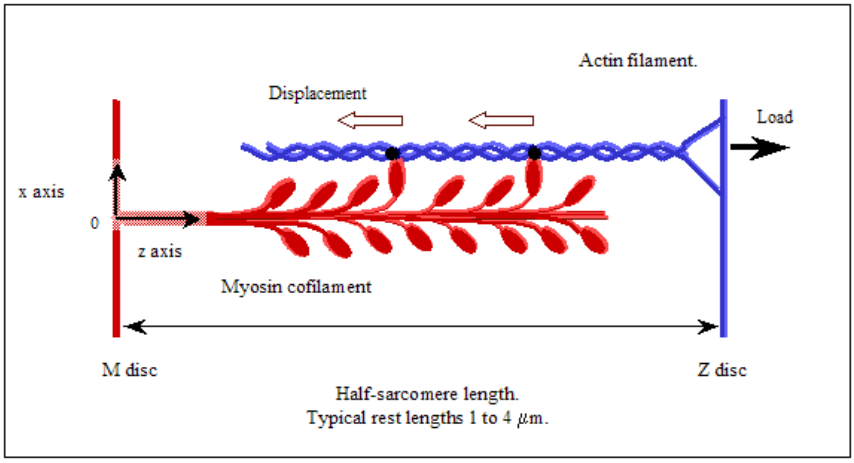

Figure 2.1.1, Schematic representation of the interaction of actin and myosin myofilament over a half-sarcomere length. Movement is towards the M Disc: the mid point of the sarcomere. Typical sarcomere length 1.01 to 4.41μm for human gastrocnemius [9], see Section 3.7. Load indicates resistance to the contraction/ actin movement.

2.1.4 Fuelling the Contraction.

Whilst the chemical synapse and ion gates in the fibre require energy in the form of ATP, the dominant consumption of ATP is in the crossbridge formation (Section

2.1.3). Approximately sixty percent of this energy is released as heat [10,11,12]. A visible manifestation of this is shivering, which is a means whereby body temperature is increased by working the muscles.

In response to the stimulus to contract, the muscle can draw on four methods of ADP production. These processes are outlined in Figure 2.1.2. Oxidative (aerobic) glycolysis produces 95% of the muscle's energy and can do so for hours but this process takes time to begin production. Initial energy demands are met by the simpler and faster creatine phosphate enzyme cycle, which can produce maximum muscle tension for ~15s before the required chemicals are exhausted. This provides enough time for non-oxidative (anaerobic) glycolysis to begin producing energy. It can maintain output for 30-40s. at maximum muscle tension. The non-oxidative glycolysis production rate is 2.5 times faster than oxidative glycolysis. If energy demand persists, the oxidative glycolysis process takes over the energy production. The other processes of energy production re-activate if energy demand is high.

Oxidative and non-oxidative glycolysis converts glucose to ATP. Sources of glucose include glycogen polymers stored in the muscle (drawn on in anaerobic conditions), blood glucose and intracellular glucose. Glucose is a more accessible source of energy but when the supply is exhausted, in more sustained activities, fats are broken down in the mitochondria in oxygen hungry β-oxidation. Blood flow is vital to the dissipation of excess heat from the muscle in addition to transporting oxygen and other basic substrates required to maintain the muscle's function and removing waste products such as lactate, carbon dioxide and water.

When there is a deficiency of ATP, a physiological inability to contract the muscle occurs, which is part of the pathway to muscle fatigue. In fatigue, contractures occur producing a high resistance to movement caused by crossbridges forming in the sarcomere that are unable to disengage. The muscle is effectively locked, as in rigor mortis. More importantly, ion pumps in the chemical synapses may become imbalanced resulting in a failure to transmit or only intermittently transmit the action potential required to simulate the muscle fibre contraction.

2.1.5 Classification: linking the sarcomere to the motor unit.

There are numerous ways of classifying skeletal muscle: physiological, biochemical, histological and morphological. Skeletal muscle's mechanical output range is such that attempts to group behaviour is rather artificial but doing so identifies some of the key features of muscle function in humans and animals [1]. In Table 2.1. key studies of a) motor unit functions, b) fibre function and energy production capabilities and c) the isoforms of myosin proteins are shown. The results of these three studies identified three types of fibre linking isoforms to ATP/energy production and overall motor unit performance. This indicates extrapolation of some of the motor unit's function based on a study of the sarcomere is valid.

The widely used metabolic classification developed by Peter *et al* [13] evaluates the rate and means by which a fibre produces ATP using three histochemical experiments. These experiments are: (1) the overall rate of ATP production/hydrolysis, also known as ATPase activity, (2) non-oxidative glycolysis (glycolytic potential) and (3) oxidative glycolysis (via mitochondrial activity: oxidative fibres have high concentrations of mitochondria). Via this means 95% of fibres fall into three categories, see Table 2.1, columns 1 to 4. Barany [14] observed that the maximum contraction speed of fibres is directly proportional to ATPase activity which provided the key to connecting these properties to the motor unit physiological output. In Table 2.1, this alignment can be seen to be fast fatigable (FF) fibres, fast fatigue resistant (FR) and slow fibres (S).

Within each muscle fibre, subtle variations in the expression of proteins in the sarcomere termed protein isoforms have been identified [15]. Three types of myosin II isoform (see Section 3.2) have been shown experimentally to influence ATP binding, contractile force and speed in normal humans [16] (Table 2.1 footnotes). Each of these isoforms can be associated with a particular fibre type (Table 2.1). Other isoforms do occur in humans: embryonic and perinatal forms and MyHC-IIb, common to small mammals, has been observed in humans in special circumstances.

Isoform expression is dynamic in response to motoneuron stimulation, hormonal changes and mechanical loading meaning adult muscle is adaptive [15,17]. This adaptability to changing stimulation has also been demonstrated at the whole muscle level [5 (p175) summary of multiple papers] where, depending on the type and duration of stimulation, modification takes days or months. Adaptation implies the

occurrence of transient states and this may explain Martin *et al*'s [18] observation that the fibres within a motor unit are not necessarily uniform. Isoforms shape the force-velocity-displacement relationship of the contracting sarcomere and the multiple sarcomere, fibre length and structure, and ATP supply scale that profile up to the motor unit's contractile characteristics [1].

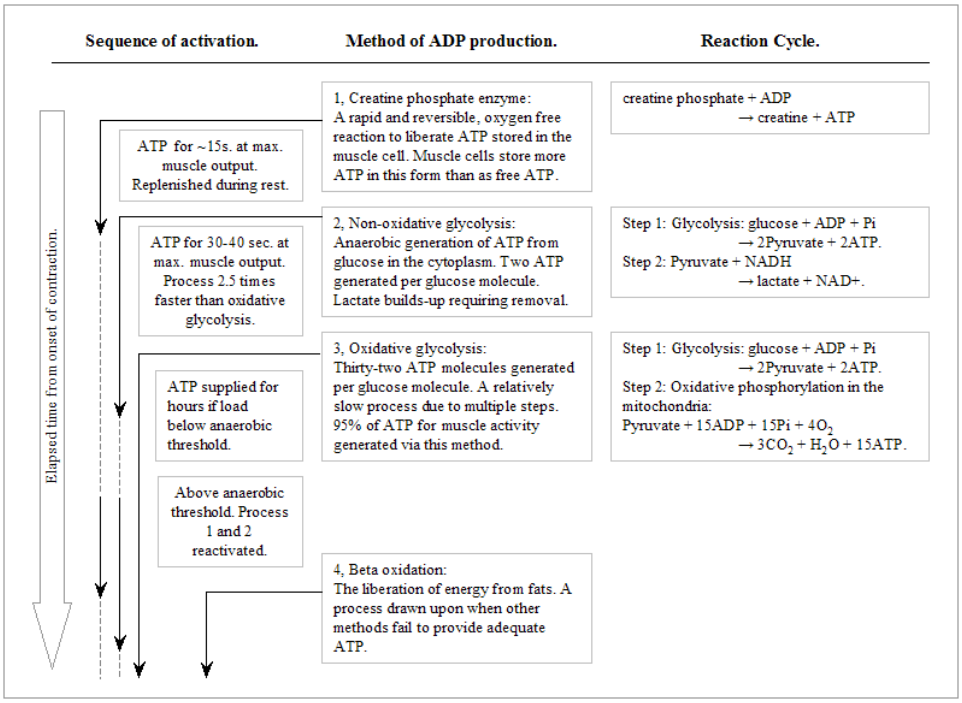

Figure 2.1.2, Methods of energy production to meet the demands of the muscle. ATP, adenosine triphosphate, ADP, adenosine diphosphate, NADH a coenzyme called nicotinamide adenine, NAD+ in an oxidised state. Pi, O, CO_2, H_2O, phosphate, oxygen, carbon dioxide and water respectively.

Table 2.1, Summary of fibre types based on metabolic classification previous described and, experimentally determined motor unit designation and isoforms.

Fibre designation *(a)*	ATPase activity (F or S). *(b)*	SDH activity (O) ~ mitochondrial activity. *(c)*	α-GP activity (G) ~ glycolytic potential. *(d)*	Motor unit designation. *(e)*	Associated myosin II isoforms. *(f)*	Type I (slow)/Type II (fast)
Fast glycolytic (FG)	High	Low	High	Fast fatigable (FF): rapid response, high force output, sustainable for short periods, exhausted within a minute.	MyHC-IId *(g)*	Type II
Fast oxidative glycolytic (FOG)	High	High	High	Fast fatigue resistant (FR): slower response than FF, maximum force half of FF but sustainable beyond sixty minutes.	MyHC-IIa	Type II
Slow oxidative (SO)	Low	High	Low	Slow (S): slow to reach a much lower maximum force than FF or FR but sustainable for hours.	β-MHC (MHCIB)	Type I

(a) The three assays gauging ATP production, (b,c,d), were performed on 6-8μm frozen sections of tissue (2-4 sarcomere thick). In the assay, a key product of the reaction is tagged, producing visible colour changes dependent on its rate of production, which can then be visualised microscopically. If a fibre is crudely scored high or low on each of these tests 2^3 fibre groups are possible. 95% of fibres fall into three categories. (b) Pi (γ-phosphate), a by-product of ATPase production, when artificially reacted with calcium produces an observable precipitant. High Pi levels appear dark indicating a higher ATPase rate; this observation was made in fast contracting fibre samples. Paleness indicating low ATPase activity has been identified in slow fibre samples.(c) Succinate dehydrogenase (SDH), a mitochondrial enzyme is 'tagged' to indicate the level of mitochondrial activity. High numbers of mitochondria are associated with oxidative fibres, low with non-oxidative fibres.(d) α-glycerophosphate dehydrogenase (α-GP) is used to identify glycolytic potential (ATP production in the absence of oxygen). α-GP acts as a shuttle transporting NADH into mitochondria for ATP production. Similar to an SDH assay it has the advantage of not being organelle based.(e) Due to their distributed nature, identifying motor groups is difficult; depleted and radioactive glucose techniques have been used but tend to identify only certain fibre types. Burke et al [19,20] approached the problem by stimulating axioms in live cats. This allowed them to examine and categories individual units. They considered motor unit twitch tension, tetanic tension at an intermediate stimulation frequency and fatigability against a standardised protocol noting that some units have a 'sag' or decline in output after a given period. As with fibre types the motor units tended to fall into three categories.(f) Classification of fibre isoforms in normal humans [16,2009]. MyHC-IIb (MHCIIb) – is commonly expressed in small mammals but only occurs in humans in special circumstances. There are other pecialised isoforms MyHC – Extraocular, MyHC – Embryonic and MyHC – Perinatal. In addition to these pure fibre types hybrids have been identified by electrophoretic analysis [21]: Pure type I, type IIA, type IID, Hybrid I/IIA of composition: MHCIβ > MHCII, HybridIIA/I of composition: MHCIIa > MHCIβ,Hybrid IIAD of composition: MHCIIa > MHCIId,,Hybrid IIDA of composition: MHCIId > MHCIIa.In-vitro motility studies of unloaded filaments [16, 22] show the relative ATPase rate of MHC isoforms, follow the pattern of fibre types e.g type II (fast fibres): MHC-IIb > MHC-IId > MHC-IIa as does the speed of motility MHC-IIb < MHC-Iid < MHC-IIa. (g) MHCIId was previously classified as MHCIIb in humans [23].

2.2 Available Test Data.

Measurements taken from the biological systems are required to understand the function and structures to be modelled and to provide numerical values for model implementation. Muscle poses a number of issues in terms of the measurement of its properties. For the detail required in this model the muscle must be considered in the abstract form of in vitro experiments: individual proteins, filaments and myofilaments within the fibre. Outside of the body, artificially maintained and stimulated, the function of these components may be unintentionally modified. Due to availability, samples used in the experimental work come from an assortment of animals and anatomical sites. At times, it is necessary to extrapolate from one animal to another or one muscle to another, knowing that the two may perform differently. In addition, experiments tend to be performed below body temperature and with modified chemical concentrations in order to slow processes down and make observations easier ($<<37^{o}C$).

The author has not made any biological measurements, the data used to compare against the model have been extracted from the published literature. Explicit references have been given when these data have been used. Model tests have been performed for direct comparison with optical tweezer and microneedle experiments noting that measurement techniques on this piconewton-nanometer scale are continually being refined and with this, the precision of the values obtained.

In Chapter 3, particular reference is made to in vitro experiments where an actin filament clamped by optical traps is manoeuvred to form a single crossbridge with a myosin fragment bound to a substrate. The technique, pioneered by Finer *et al* [24], provides a means to measure force and displacement generated by an individual crossbridge. In Chapter 4, the movement and force generation of multiple crossbridges along lengths of actin filaments and myosin are compared to in vitro data. Sheetz *et al* [25] demonstrated heavy meromyosin (HMM: myosin cofilament fragments see Figure 3.2.1) coated fluorescent beads, in the presence of ATP, move across actin filament bundles sourced from giant algal cells (Nitella), [26,27] thus showing the actin-myosin interaction generates movement. In refinements of this experimental technique actin filaments are monitored traversing a myosin coated nitrocellulose substrate [28]. Various myosin fragments (HMM, S1, myosin) and cofilaments have

been used in these displacement (motility) studies. Further enhancements have come with the use of optical traps: attached to the actin filament they can be used to monitor movement and filament force development [29,30,31 are examples]. A discussion of the practicalities of studying crossbridges in action is given by Spudich *et al* [32,33].

2.3 Previous Modelling Approaches.

There are numerous approaches to modelling muscle. At the bulk muscle level there are mechanistic models based on the work of Hill (spring and dashpot) as shown in Figure 2.3.1.

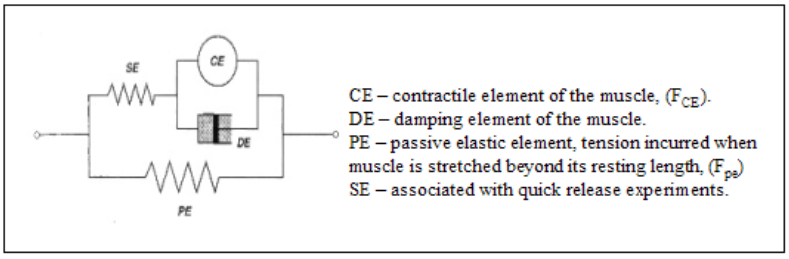

Figure 2.3.1, A classic Hill model, taken from Yamaguchi [34].

If such models are to represent an 'ideal' muscle, non-linear functions are required to fully replicate the force length and force velocity characteristics of real muscle. The generated force, the contractile element, F_{CE} (CE in the diagram) from the muscle model, is summed with a passive force, F_{PE} that is a returning tension incurred when muscle is stretched beyond its resting length. The contractile component may be considered to include activation force, F_{act}, a force length relationship, F_{len} and a velocity dependent relationship, F_v, fatigue, F_{fat} such as in:

$$F_{total} = F_{CE} + F_{PE} = F_{act} \cdot F_{len} \cdot F_v \cdot F_{fat} + F_{PE} \qquad (2.3.1)$$

Further modifications include properties such as creep and hysteresis. This type of model is dependent on the measurement of muscle samples to parameterise the individual elements. In vivo measurements are confounded by the connective components: the ligaments, tendons, bones etc. Therefore, data are usually gathered from artificially stimulated in vitro samples. A prominent example is Hill's 'characteristic equation' derived from experimental results, derived from frog muscle at 0^{o}C, [Ref. 35, review by Hill including his 1938 paper]. The underlying assumption in this approximation is that the rate of heat liberation with speed of shortening and

the total rate of energy liberation (heat + work) both increase linearly as the load drops below isometric tension. The force velocity relationship can then be shown to be:

$$(P+a)v = b(P_o - P), \qquad (2.3.2), \qquad V_{\max} = \frac{(bP_o)}{a}, \qquad (2.3.3),$$

where tension is P and maximum tension P_0. a and b are experimentally derived but a approximates to $P_0/4$ *and* $b = a/P_0$. For a human and animal muscle, in general this has proven to be a reasonable approximation.

The in vitro samples used in these experiments come from a diverse range of mammals, birds and amphibians and, less commonly, humans. Different samples are used to examine different muscle characteristics often without specification of fibre type and with variations in experimental techniques and operating environments. From these data, it is only possible to generalise about a muscle's properties [36]. When analysing and modelling systems of muscles, bones, tendons and ligaments in a limb, during a gait cycle, for example, this level of simplification is necessary due to the complexity of the motion [37]. A large range of models of human motion use modified forms of the Hill model, e.g. Shue and Cargo [38]. Some models attempt to avoid using a muscle model entirely and consider the balancing of forces required to generate the motion, e.g. Gilchrist and Winter [39]. Importantly mechanistic models such as the Hill model say little or nothing about what is going on inside the muscle.

On a shorter length scale models can be found where the sarcomere is simplified: represented by a spring-dampers or force equation. Networks of sarcomere forming myofibrils and fibres can then be studied [40,41]. Such models are supported by the ability to monitor sarcomere length changes in vitro when a fibre or myofibril is artificially stimulated [42]. Models have been developed that focus on the thermodynamics of an individual crossbridge chemical cycle. The results are then extrapolated to the length scale of fibres and bulk muscle against which the output is compared to in vitro data [43,44,45,46].

Many models focus solely on an individual crossbridge's formation, energy release and separation, some of which will be introduced in the description of the model in Chapter 3. Extensions of this analysis of single crossbridges contain representations of multiple crossbridge cycles between actin filaments and myosin cofilaments with some rigid and some compliant components, e.g. the myosin II S2 arm (Section 3.2) [47,48]. The modelling focus is often on the local chemo-mechanical expression and less so the mechanical structure beyond the crossbridge. Statistical extrapolation is

often applied to such models to predict bulk behaviour due to the high number of sarcomere. A model was not found that incorporated the chemo-kinetic aspects of the single crossbridge, the compliance of the actin filament, myosin cofilament and its sub-components and the passive structures within the sarcomere.

In the model described in this project, the individual crossbridge is considered but greater emphasis is put on the mechanical structures of the sarcomere and how it transmits the crossbridge strain energy and influences the interaction of crossbridges.

Chapter 3

3 Half-Sarcomere Sub-Unit Model

3.1 Model Outline

The basic components of the sarcomere unit to be modelled are an actin filament, a composite myosin cofilament and a composite of titin proteins. Figure 1.1.2.A shows a cross-section through the geometry of this group. The myosin cofilament is composed of myosin II proteins (Figure 3.2.1). Their tails combine forming the cofilament stem while extending, on arms, are pairs of globular heads that bind to actin (Figure 2.1.1). The heads protrude from the main stem in a regular, periodic helical pattern, in vertebrate skeletal muscle [49] these are longitudinally separated by 14.3nm and rotated by 120^{o} from the previous pair of heads. The pattern repeats every 42.9nm [50]. Each actin is centred within three myosin cofilaments. The optimum geometric alignment of the cofilaments would present a pair of myosin heads every 14.3nm to the actin. It is possible, therefore, to transform the three-dimensional structure to two-dimensions by combining the three cofilaments into a single cofilament in the model with head spacing of 14.3nm. In the ordered cross-sectional structure of the sarcomere, as each actin is surrounded by three equidistant cofilaments, it is assumed torsional and lateral loads generated between the actin and cofilaments are counter-balanced such that they are negligible. In support of this contracting muscle fibres maintain their striated appearance and actin and myosin cofilaments maintain their parallel alignment [1].

The model has two distinct components which are evaluated in turn at each time step, t_{step}. In the first component, the reaction state of each myosin bond site is evaluated: is the bond site ready to form a crossbridge, is it already in one and if so, does it have strain energy? In the second component, the interactions of those crossbridges are evaluated in terms of a mechanical representation of the system. In the following sections, the model is introduced in stages beginning with the overall structure, then focusing on the different aspects of the individual crossbridge representation and finally the formulation of the equations which describe the mechanical system. How these components are brought together in the model is outlined in Figure 3.8.1 and

Appendix A shows some of the elements graphically with the type of results generated.

3.2 Actin, Myosin Cofilament and Myosin II.

In this section a description of the biological structure of thick (myosin cofilaments) and thin filaments (actin) will be given, together with an evaluation of the importance of these components in terms of characterising the sarcomere's function within the model. The modelling approach will then be described and finally parameter values will be identified.

Myosin cofilaments (thick filaments) are formed from Myosin II proteins, Figure 3.2.1. Myosin II is a hexameric protein of polypeptide chains. Two myosin heavy chains (MHC, c. 200kDa [51]) form a coiled-coil structure. Each MHC terminates in a globular head. The tails of the proteins, the light meromyosin (LMM) section, oligomerise to form the stem of the cofilament. The cofilament is symmetrical about the M-disc and the tails combine at a smooth central region where no heads protrude.

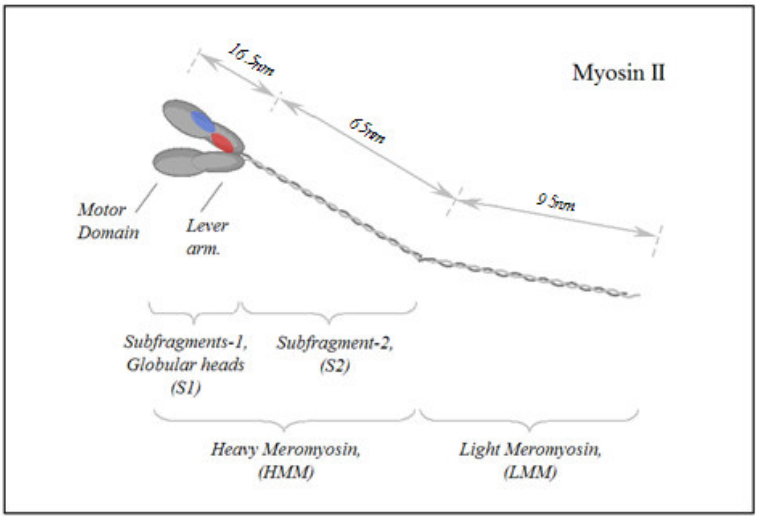

Figure 3.2.1, Schematic of a single myosin II protein. The structure is determined via electron-micrographs and chemical analysis [51]. Via limited hydrolytic reaction (proteolysis) HMM and LMM can be separated. The enzyme papain divides HMM into S1 and S2 subfragments. The regulatory light chain location is highlighted in red and essential light chain in blue on the upper head.

The heavy meromyosin sections (HMM) project from the stem in a helical pattern longitudinally separated by 14.3nm and rotated 120^{o} from the previous HMM [50]. A distinction should be made between the 'lever arm' in each S1 head and the S2

'myosin arm', which protrudes from the cofilament. A head has two myosin light chains (MLC's): a regulatory light chain (RLC, also designated LC2, phosphorylatable [52]) sited in the lever arm near the junction of the heads and an essential light chain (ELC, also known as alkali light chains, isoforms LC1, LC3 [52]) further up the head towards the motor domain. In other species, each head of a pair may differ [15,52] but humans predominantly have common heads of either LC1 or LC3.

Troponin combined with tropomyosin coils around actin to form the thin filament to which actin gives its name. Actin filaments have two forms: skeletal and cardiac. Tropomyosin has an isoform associated with fast fibres and an isoform associated with slow fibres. Troponin and tropomyosins may modify actin-myosin affinity due to their calcium cation bonding [17], a point considered when the chemical cycle is described (see Section 3.3).

Early descriptions of the sarcomere considered these filaments to be rigid [8] but more recent studies (from the early 1990s) indicated significant compliance [53,54] which has led to experiments to measure the component stiffnesses. Kojima *et al's* [55] work indicated that up to 50% of muscle compliance might be due to the actin. This leads to modelling the structure as a linear spring and damper system, Figure 3.2.2 shows a schematic of this. Force and displacement act predominantly in one dimension - longitudinal to the filaments. The coiled-coil structure of myosin and helical actin filaments can be expected to have some torsional components. However, under torsional loading actin breaks more easily (without actomyosin carrying 50% less load, [56]). Due to this comparative weakness, torsion is assumed negligible.

3.2.1 Significance of Components – how much detail to model?

Myosin light chains, Figure 3.2.1, express a diverse range of isoforms, which have been demonstrated to strongly influence force development and motility speeds (contraction rate) of the fibres [15,52,57,58,59]. This influence is exerted by modification of the lever arm flexure rigidity and/or the chemical kinetics of the crossbridge bonding. Regulatory light chains - LC2-fast and LC2-slow have demonstrated a strong influence on motility without modification of the ATPase rate [58, 59] linking them to the flexure rigidity of the lever arm. Much less significant to motility, essential light chains sit closer to the motor domain (Figure 3.2.1), exhibiting

a greater influence on force generation and ATPase rate [15] linking them to actin-myosin affinity and the chemical cycle.

The flexure rigidity of the lever arm in the myosin II head (S1) has been identified as significant to filament motility speeds and less so to force development. The myosin arm (S2) has an unclear contribution to the drag incurred during multiple crossbridge interactions [Huxley, 8]. Variations in actin and associated proteins may influence the filament's mechanical properties. These components are therefore significant in the efficiency of chemo-mechanical energy transfer.

3.2.2 Modelling the Filament and Cofilaments.

The starting point for the modelling carried out in this work was the formulation of a representation of the mechanical components of the Baseline Model of the sarcomere sub-unit, Figure 3.2.2 (Figure 2.1.1 and Appendix A, Figure D, show the actin and myosin components). As crossbridges form and release at different bond sites along the length of the actin filament the relaxed length of the actin filament between crossbridges changes and correspondingly the stiffness between neighbouring crossbridges. To accommodate this, the actin filament's stiffness was viewed as a series of bond-site-to-bond-site lengths, each length being assigned the stiffness k_a. Treating these lengths as springs in series, the crossbridge-to-crossbridge actin filament stiffness could be defined as k_a divided by the number of bond-site-to-bond-site lengths between the crossbridges. A relationship represented by $k_a p_i$ (N/m), where p_i is the dimensionless inverse number of lengths. In Figure 3.2.2, p_{end} refers to the free end of actin. Similarly, for the myosin cofilament: the stiffness between protruding myosin arms (S2), k_{ms} was multiplied by, n_i, where $1/n_i$ is the number of S2-to-S2 lengths. n_1 included the central, smooth section, of the myosin cofilament. Myosin II, S2 and S1 stiffnesses are combined into k_{mi}. Force and displacement at the end of the sarcomere were represented by F_{end} and z_{end}. The system is assumed to be in equilibrium at nodes *a* to *j*. Equations describing the system are given in Section 3.6. Crossbridge properties, k_{bi} and c_{bi} will be discussed in Section 3.5, titin stiffness k_{ta} and k_{tm}, and damping, c, in Section 3.7. z_{actin} and z_t, are the loading of actin's free end and the end of the cofilament.

The system of components operates in an environment which has a very low Reynolds number; subsequently inertia has a negligible influence on the components of this system [60].

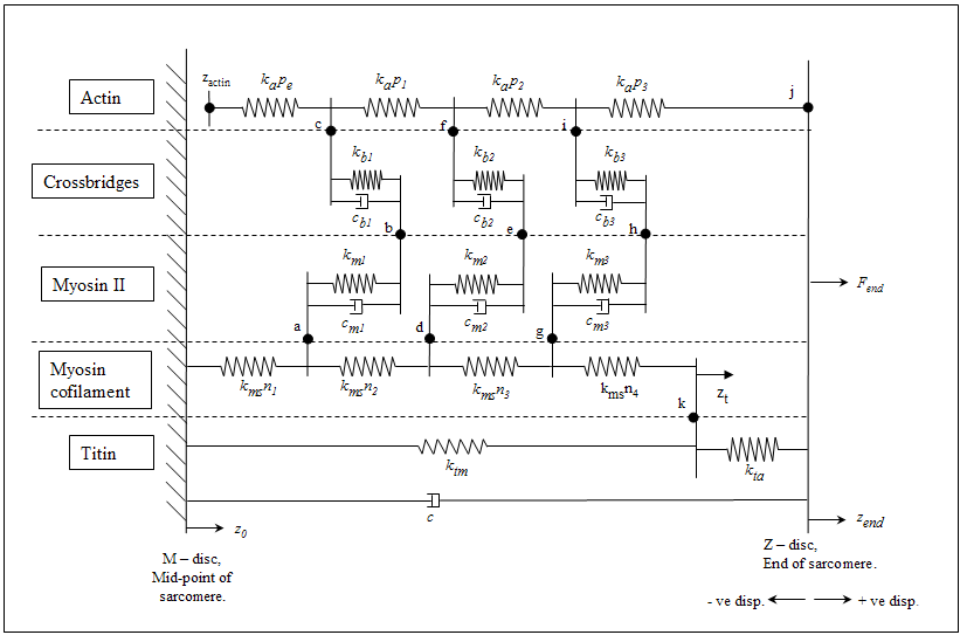

Figure 3.2.2, Spring and damper representation of the sarcomere components represented in the model. Here three levering crossbridges are shown (c-b, f-e, i-h). Another example is shown in Appendix A, diagram E.

Within the duration of a crossbridge, the action of other crossbridges and/or external loading may change the alignment between the actin bond site and the S2-cofilament junction, changing the strain on the crossbridge. This would exhibit itself, in S2 particularly, as transitions between longitudinal stretching, and flexure. In order to encompass potential performance variations due to stiffness in the myosin II, k_{mi}, was represented as a composite of S1 (lever arm) and S2 (myosin arm) stiffnesses, see Figures 3.2.1 and 3.2.2.

In the model, in order to assign a value to k_{mi} the natural length of S2, L_{mrest}, was compared against the distance between the S2-cofilament junction and the myosin bond site, l_m. For the left-hand crossbridge in Figure 3.2.2 the length l_m equalled the distance between node *a* and *b*. A record is maintained in the model, against time, of the actin bond site positions, myosin S2-cofilament positions and crossbridge lengths such that the length l_m can be calculated. As a specific orientation between bond sites is required for crossbridge formation (Section 3.4.1), S1 was assumed to be perpendicular to S2 in the initial stage of crossbridge formation and therefore, did not

contribute to the natural length, $L_{mrest,}$ of the myosin arm. Three scenarios were identified as encompassing the potential position changes that would define k_{mi}:

1) S1 and S2 are compressed below S2's natural length with S1 and S2 acting in series on their compressive stiffnesses (Eq. 3.2.1 a,b).
2) The actin bond site and S2-cofilament junction distance has increased beyond a rest position: S2 is stretched so longitudinal stiffness is active and S1 is in flexure (Eq. 3.2.2a,b).
3) The actin bond site and S2-cofilament junction distance has increased further: S2 is stretched (longitudinal stiffness), S1 is drawn into a rigid state (Eq. 3.2.3 a,b).

The stiffness of S2, k_m, is very low in compression (Appendix B, Table 2, [46]) and relatively high in extension. Scenarios (2) and (3) assign the high, longitudinal, stiffness to k_m. In scenario (1) k_m is assigned the low, compressive, stiffness. Equations for these three scenarios have been derived for the model:

1) $$k_{mi} = \frac{k_m \cdot k_{mh}}{k_m + k_{mh}}, \quad l_m < L_{mrest} \qquad (3.2.1 \text{ a,b})$$

k_m ~ S2 compressive stiff.

2) $$k_{mi} = \frac{k_m \cdot k_{mh}}{k_m + k_{mh}}, \quad L_{mrest} \le l_m < \frac{k_m\left(L_{mrest} + l_{head}\right) + k_{mh} l_{head}}{k_m} \qquad (3.2.2 \text{ a,b})$$

k_m ~ S2 long. stiff.

3) $$k_{mi} = k_m, \quad L_{mrest} \ge \frac{k_m\left(L_{mrest} + l_{head}\right) + k_{mh} l_{head}}{k_m} \qquad (3.2.3 \text{ a,b})$$

k_m ~ S2 long. stiff.

where flexing of the myosin head, S1, is limited to a maximum distance of l_{head} before it becomes rigid. The individual stiffnessess of S1 and S2 are k_{mh} and k_m. The S1 stiffness between pre-, post- and levering (energy release) states could be varied as differences are indicated by in vitro experiments [29] and are examined in Section 3.2.4. The implementation of these equations within the model is shown in Section 3.6, Figure 3.8.1 and Appendix E, Function: ResolveLoad.

Due to the close packing of filaments in the sarcomere, an assumption was made that the myosin arm could not compress beyond the cofilament to S2 junction this is examined further in Section 4.4.7. The low to high stiffness transition incurred at displacements greater than the S2 junction would cause discontinuities in the force output of the model.

3.2.3 Establishing Parameter Values.

Having implemented the mechanistic model shown diagrammatically in Figure 2.1.1 the next step was to determine numerical values for the model parameters. There is reasonable consensus in the literature as to those values which can be measured directly, for example the actin filament and myosin II dimensions and stiffnesses, and the length, flexure and longitudinal stiffness of S2 [10,50,55,61] (Appendix B). Other parameters such as those for the S1 lever arm (k_{mh}, l_{head}) are more difficult to measure and are determined indirectly by analysing the performance of individual crossbridges. This introduces uncertainty in the actual components being measured and the values obtained. In Section 3.2, the strong influence the flexure of the lever arm has on motility was identified and therefore, the importance to the model of understanding the values assigned to k_{mh}, l_{head}. In order to assign values the model was evaluated against single crossbridge experiments from published papers.

There are a number of published experiments examining the stiffness properties of single crossbridges [24,62,63,64,65]. The experiment considered for comparison, Kaya and Higuchi [29], was favoured as cofilaments of myosin were used rather than fragments of myosin, (S1, HMM). This reduced substrate involvement and provided a closer approximation to the muscle environment.

3.2.4 Crossbridge Stiffness Examined by Using the Model.

In the experiments of Kaya and Higuchi [29] an actin filament, marked by detectable quantum dots was suspended between two optical traps. Movement of the traps across reconstituted myosin cofilaments (rabbit skeletal) bound to a substrate allowed single actin-myosin crossbridges to form. In order to emulate this experimental arrangement a single crossbridge was allowed to form in the model, point c of Figure 3.2.3. Titin and damping components associated with the sarcomere were removed. An equal length and therefore stiffness was assigned to the actin on either side of the

crossbridge. The initial tension in the model components was zero. Kaya and Higuchi [29] obtained force and displacement data from the optical traps and displacement from the actin markers in close proximity to the crossbridge. From these data Kaya and Higuchi calculated crossbridge stiffnesses with and without corrections for the cofilament movement and compliance of experimental components. Similarly, the calculations were performed for the model data. A ramp displacement could be applied either individually or simultaneously at nodes d and e of the model. In response to loading, displacements were recorded at nodes a, c, d and e (Figure 3.2.3) and forces at nodes d and e. From these data the force on the crossbridge: $F_c = -(F_d+F_e)$ was calculated. The crossbridge stiffness, k_{cross}, was calculated firstly using the actin movement, z_c, at node *c*, (the observation that would be made in an optical trap experiment): $k_{cross} = (F_d+F_e)/z_c$ and secondly by taking into consideration the cofilaments movement $z_a = (F_d+F_e)/(z_c-z_a)$ at node *a*.

Having inserted the known parameter values into the model the unknown lever arm properties were identified by adjusting their values until the model correlated with the in vitro data.

Before considering the results it should be noted there was a notable structural difference between the published optical trap and model experiments: in the former, the cofilament was bound to a substrate along its length and in the model, the cofilament was anchored at one end. In the optical trap experiment, the cofilament combined with the cofilament to substrate stiffness was measured. In the model, this value was assigned to the cofilament and so the difference in the model was not considered significant.

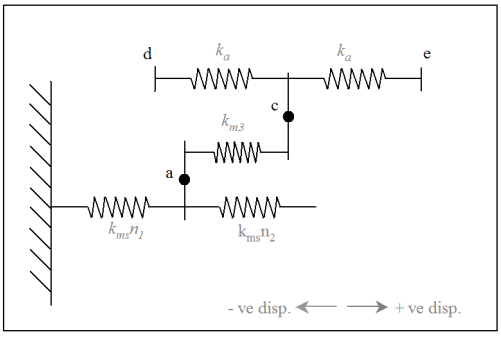

Figure 3.2.3, The mechanical representation of the single crossbridge form of the model.

For comparison with the optical trap experiment [29] the model's fixed parameter values (see also Appendix B) were:

Actin-optical trap to crossbridge stiffness: k_a = 3.5 x 10^{-5}N/m,
Cofilament combined with cofilament to substrate: 9.2 x 10^{-3}N/m,
Myosin arm (S2) rest length: 60nm [50,61],
Myosin arm (S2) longitudinal: k_m = 70 x 10^{-3}N/m
and in flexure k_m ~1x 10^{-5}N/m [61].

The input loading was a ramp displacement of ±300nm applied simultaneously at points *d* and *e* (Figure 3.2.3) in steps of 1.25nm (note there is no damping active so timing is not pertinent in the model).

3.2.5 Crossbridge Stiffness Results

A comparison between crossbridge displacement and stiffness was made at two points: firstly, the peak positive force measured by Kaya and Higuchi [29], which corresponded to the maximum positive extension of the crossbridge.

The optical trap experiment and this version of the model could displace the crossbridge -80 to +10nm and –90 to +75nm respectively. An assumption was imposed on the model that due to the ordered structure of the sarcomere it would not be possible for the myosin arm (S2) to be bent or compressed beyond its natural length, here taken to be 60nm [11,51]. This assumption is examined in more detail in Section 4.4.7. At –50nm the arm is nearing maximum compression before transitioning past the S2-cofilament junction with the convention that at 0nm displacement the crossbridge and S2 are unstrained. Between -50 to 0nm the force-displacement was linear transitioning to a second linear value above 0nm. This transition was non-linear but rapid and so the modelled approximation was an immediate change between the two linear states using Equations 3.2.1, 3.2.2 and 3.2.3. Kaya and Higuchi [29] modified the chemical concentrations used in the experiments in order to study crossbridge stiffness in a pre-lever state (increased ADP) and in a post-lever state (in the absence of nucleotides: ATP) where the lever state is the release of strain energy into the system (see Section 3.3 where the chemical cycle is described).

Model and optical trap experiments are compared in Table 3.2.1 and post-lever data is shown in Figure 3.2.4. At the peak positive optical trap load of 9.5pN, result (2) for post-lever and result (5) for pre-lever compare the model and optical trap output. Here, the lever arm stiffness, k_{mh}, was optimised to align the model crossbridge stiffness

with that of the optical trap experiment. Comparison was made between the results where cofilament movement had been taken into consideration. For the combined S2 and lever arm stiffness, k_{mi}, to match the optical trap stiffness of 2.9*p*N/*n*m, k_{mh} had to be set to 3.03 pN/nm, for a stiffness of 2.6 pN/nm, k_{mh} = 2.7pN/nm. Under a compression of –50nm, results (3) and (6) show the crossbridge stiffness drops to ~0.02pN/nm: optical trap and ~0.01pN/nm in the model. An error was not given on the optical trap data.

Under the positive load, the crossbridge was elongated. In the model Equation 3.2.2.a defines the crossbridge stiffness, k_{mi}. As $k_{mh} << k_m$, S2's longitudinal stiffness, the lever arm, k_{mh}, dominated the relationship. Under large compressions Equation 3.2.1.a defined the stiffness of the crossbridge. Due to the relative magnitude of S2 in flexure (k_m = 0.01 pN/nm) compared to the lever arm, k_{mh}, S2 dominated the crossbridge stiffness. This change in the model's dominant stiffness was comparable to the optical trap results. Results (6) and (7) show increasing k_m to 0.02 pN/nm increased the model crossbridge stiffness to 0.02 pN/nm, a closer alignment with the optical trap result.

The model could be set to emulate the experimental data under compression and extension if the results compared were those that took account of cofilament-substrate movement. Where the crossbridge movement alone was taken into consideration the discrepancy between the model and optical trap stiffness increased, for example result (1), Table 3.2.1 2.2pN/nm and 2pN/nm respectively. This is not a large variation for this type of experiment (see discussion). The optical trap experiment and the model have a cofilament element but the in vitro data have an additional actin component not accounted for in the model but adjusted for in the optical trap results. Therefore, the model parameters have been set such that the model output matches against the modified form of data. The parameter values obtained are examined in the following discussion of Section 3.2.6.

The extremes of crossbridge displacement in the model were greater than those measured by Kaya and Higuchi [29] but so too were the force levels and there may have been a physical constraint in the optical trap experiments in applying the higher level of force.

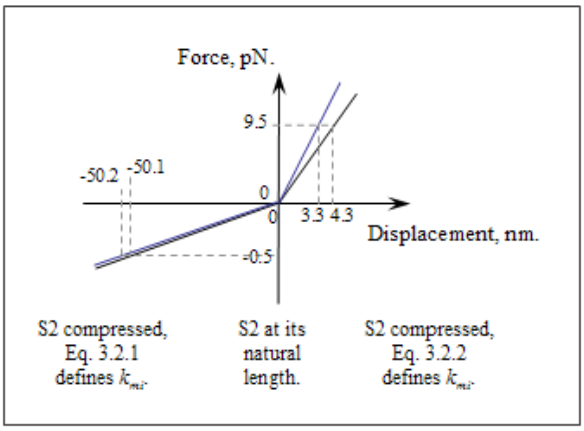

Figure 3.2.4,Crossbridge displacement for post-lever data, model generated results.k_{mh}=3.03pN/nm. Blue line: crossbridge displacement minus cofilament displacement. Numbered points indicate values compared to in vitro test data.

Table 3.2.1, Model comparison against key crossbridge optical trap experiment data from [29].(a)The crossbridge stiffness calculated using crossbridge-cofilament movement,(b)The crossbridge stiffness taking into account the cofilament-substrate and experimental stiffnesses,(c)Calculation of displacement based on force and optical trap modified stiffness.

	Model Generated Results.					Test Data Stiff. from [29]		Est.(c) disp. [29].	
	Force on crossbridge, (pN)	Crossbridge displacement, (nm)	Crossbridge minus cofilament disp., (nm)	Crossbridge stiffness, (pN/nm)	Crossbridge stiffness,(a) (displacement minus cofil.), (pN/nm)	Observed C'bridge stiffness, (pN/nm).	Modified(b) C'bridge stiffness, (pN/nm).	C'bridge disp., (nm)	C'bridge disp.minus cofil disp, (nm)
	Model input: Post-lever k_{mh} = 3.03 pN/nm, k_m = 70 pN/nm					Post-lever			
(1)	8.494	3.852	2.929	2.205	2.900	~2	~2.9	4.247	2.929
(2)	9.497	4.307	3.275	2.205	2.900	~2	~2.9	4.749	3.275
(3)	-0.500	-50.176	-50.122	0.010	0.010		~0.02		-24.980
	Model input: Pre-lever k_{mh} = 2.70 pN/nm, k_m = 70 pN/nm					Pre-lever			
(4)	8.493	4.098	3.267	2.073	2.600	~1.8	~2.6	4.719	3.267
(5)	9.495	4.581	3.652	2.073	2.600			5.275	3.652
	Model input: k_{mh} = 2.70 pN/nm, km = 0.01 pN/nm								
(6)	-0.497	-49.967	-49.918	0.010	0.010		~0.02		-24.870
	Model input: k_{mh} = 2.70 pN/nm, km = 0.02 pN/nm								
(7)	-0.996	-50.242	-49.957	0.020	0.020		~0.02		-49.777

3.2.6 Discussion and Comparison with Other Experimental Sources.

Values for the S1 lever arm stiffness, k_{mh}, estimated to fit the in vitro data using the model were 2.7 and 3.03pN/nm in the pre- and post-levering states, respectively. Typical values obtained from experiments where this fragment has been studied in isolation, are 0.13, 0.6, 0.48, 1.79pN/nm [62,64,65]. The wide range of values from similar experiments indicates the difficulty in measuring these components. In other experimental studies the HMM fragment have also been considered with typical

stiffness values of 0.65, 0.7pN/nm [62] being obtained compared to those of 2.6 and 2.9pN/nm measured by Kaya and Higuchi [29].

Fast and slow isoforms of the regulatory light chain (LC2) are known to influence flexure rigidity in the lever arm which may explain variation in the reported experimental results as the isoform is not readily identifiable in a single crossbridge. Electrophoresis of myosin fragments in solution is required to identify isoforms at this scale and the solution usually contains a mixture of isoforms. In addition, the crossbridge may be in a levering state (releasing strain energy) rather than pre- or post-levering (examined in Section 3.5).

Kaya and Higuchi*'s* [29] study used a cofilament bound to a substrate. From their results the cofilament-substrate movement had a large influence on the observed crossbridge displacement, for example at 9.5pN the cofilament movement accounts for 24% of the apparent crossbridge movement and if not accounted for reduces the apparent crossbridge stiffness. Kaya and Higuchi's [29] test data were selected as appropriate for parameterising the model described in this thesis as it used a cofilament. The cofilament provided a larger fragment to substrate interface which would be less likely to interfere with the crossbridge and provide a more natural alignment of myosin to actin rather than the random scatter of S1 and HMM fragments (Figure 3.2.1) previously used by experimenters in this field. Using the model described in this thesis, the significance of the stiffness of the substrate-fragment interface on the apparent crossbridge stiffness was identified.

The influence of the cofilament-substrate stiffness on the apparent crossbridge stiffness, that is the movement of the central crossbridge without consideration of the cofilament movement, was clearly seen in the model and is shown in Figure 3.2.5. Experimentally the apparent stiffness would be measured and the actual stiffness derived by analysing the experimental apparatus. Greater drops in cofilament-substrate stiffness, as would be expected with smaller myosin fragments, lead to a greater apparent drop in crossbridge stiffness. This offered a possible explanation as to the range of reported values previously mentioned. The observed crossbridge stiffness 2pN/nm is 69% of the compensated value, 2.9pN/nm, in Kaya and Higuchi's [29] case experiment and 73% in the model.

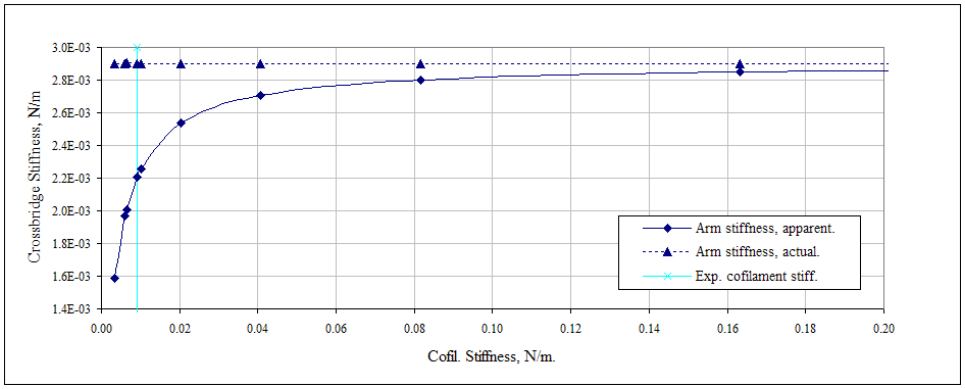

Figure 3.2.5, Crossbridge stiffness relative to cofilament stiffness under extension in the model. Model settings: k_m =70pN/nm k_{mh} = 3.03pN/nm load = 9.5pN. To prevent transition to the very stiff scenario 3, l_{head} = 50nm. Apparent stiffness is the crossbridge's movement without consideration of cofilament movement. The actual arm stiffness plot takes into consideration the cofilament's movement, this stiffness corresponds to that derived from Equation 3.2.3 a,b. Exp. cofilament stiffness is the estimated in vitro cofilament-substrate stiffness.

Although, there is confidence in the S2 longitudinal stiffness (70pN/nm), which has been measured directly as an individual component [51,61] it does raise the question as to why it has not been observed in optical trap crossbridge experiments. To maximise the actin filament's movement during a lever event myosin's movement should be minimal, so a higher resisting stiffness would be most important. It seems reasonable to assume that the S1 component has a finite flexure length, l_{head}, where it may appear effectively rigid and transition occurs to the S2 longitudinal stiffness, Equation 3.2.3a. The crossbridge itself may separate as the load increases before that extreme distortion of the S1 component but that would limit a crossbridge's load bearing capabilities. Alternatively, the applied forces in the optical trap experiments may have been inadequate.

In the model, a linear approximation of the crossbridge arm stiffness leads to a point change where, if discontinuities are to be avoided, force and displacement are equal for the two stiffness values. This transition point, T_p, between the stiffnesses specified by Equations 3.2.2a and 3.2.3a was derived and found to be dependent on l_{head}:

$$l_{head} = \frac{k_m \cdot T_p}{(k_m + k_{mh})}, \qquad (3.2.4),$$

where $T_P + L_{mrest} = l_m$. If a stiffness transition point occurs it must be above c. 9.5 – 10pN [29] as below this transition no rapid increase in stiffness was observed. Taking these force levels divided by the crossbridge stiffnesses from Table 3.2.1 the transition

points, T_p, were identified and by applying them to Equation 3.2.4 minimum values were determined for l_{head} for pre- and post-lever states:

For per-lever displacement

10pN / 2.6pN/nm = 3.85nm, S1 flexure l_{head} = 3.71nm.

9.5pN / 2.6pN/nm = 3.65nm, S1 flexure l_{head} = 3.52nm.

For post-lever displacement

10pN / 2.9pN/nm = 3.45nm, S1 flexure l_{head} = 3.31nm.

9.5pN / 2.9pN/nm = 3.28nm, S1 flexure l_{head} = 3.15nm.

A potential maximum, excluding any elastic extension, was taken from the length of S1: 16.5nm [51].

3.2.7 Myosin Cofilament Stiffness.

Although the dimensions and stiffness of myosin II components and the dimensions of the myosin cofilament have been measured, the cofilament's stiffness was not found in the literature. The myosin cofilament stiffness was therefore deduced from the estimated division of compliance (stiffness^{-1}) in fibres. A study of frog muscle fibre gives the distribution: actin 42%, myosin 27%, and crossbridges 30%. A second study [66] gives 55% actin under transient loads and 44% under isometric loading (fibre type unspecified). An actin filament stiffness of 53*p*N/*n*m [37] per 1μm length lead to a cofilament stiffness, k_{ms}, of 4.610N/m + 62% per 14.3 nm length, this was for the distance between S2 myosin arms [10]. The value used was the minimum but several magnitudes greater than the stiffness of actin, titin and mysoin II components. Note the repeat longitudinal alignment of S2's is 42.9nm and the model's cofilament represents actin's interaction with three myosin cofilaments, see Section 3.1.

3.2.8 Summary of Parameter Values.

By comparing the predicted values from the model with the measured values from Kaya and Higuchi [29], under low extension (resistance to normal levering direction) the results obtained from the model have shown that S1 stiffness was of greater significance than S2 longitudinal stiffness. If the lever event occurred under low extension, S1, the lever arm, would dictate the efficiency with which strain energy

from the lever event was divided between actin and myosin linking to its known influence on motility speeds.

Under compression, S2 flexure stiffness was of greater significance than that of S1, the benefits of this when multiple crossbridges interact are examined in Section 4.6.3. No distinction could be made between compressed and extended lever arm stiffnessess. More compliant pre-lever than post-lever stiffness values, may be part of the efficiency mechanism of overlapping crossbridge events (Chapter 4).

From this study, the initial values were established for S1 pre- and post-lever stiffness (k_{mh}), pre- and post-lever maximum flexure (l_{head}) and myosin model cofilament stiffness (k_{ms}). The following values were extracted from the literature: S2 bending and longitudinal stiffness (k_m) [46], actin stiffness (k_a) [55], S2 length and distance S2 to S2 junctions with cofilament (M_{head}) [49,50]. These values are tabulated in Appendix B. The contribution of substrate stiffness, S2 and S1 lever arm stiffnesses to filament movement is examined in Sections 4.6.3 and 4.6.5.

3.2.9 Are Two Heads Better than One?

As pointed out by Huxley in 1990 [60], the two heads on each myosin II are generally ignored and each myosin arm is only considered in terms of having only one head as only one can form a crossbridge at a time. There is some evidence in smooth muscle that the heads may cooperate in a single crossbridge to enhance movement [67] but none has been presented for skeletal muscle. In the Baseline Model each myosin is considered to have only one head. The option of two heads has been incorporated into the model. The second head follows its own reaction path and if it is in a more favourable state to form a crossbridge it is effectively swapped with the first, expediting the recovery of bond sites after crossbridge formation. How this influences force-velocity characteristics is considered in Section 4.

3.3 Chemical-Mechanical Cycle.

In the previous sections, the mechanical characteristics of the structure of the half sarcomere have been described. In this and subsequent sections the conversion of energy provided by chemical reactions to a mechanical output are described. In 1957, based on his own experiments and those of many others, Huxley [8] proposed that the

expression of energy (ATP) stored in the myosin head could be approximated as the release of tension in a spring: termed the power stroke model. Since this initial interpretation, the chemical to mechanical energy conversion at a crossbridge has been considerably refined by other workers as will now be summarised. The implementation of these characteristics into the Baseline Model is then described in Sections 3.4, 3.5 and 3.6.

3.3.1 Significant Characteristics: chemical to mechanical reaction cycle.

Excitation of a muscle fibre's motor nerve initiates a sequence of ion imbalances, through the nerve and into the muscle fibre stimulating the release of calcium ions from their reservoir in the terminal cisternea ('end sacs'). These are located at specific junctions on the sarcomere. Released into the sarcomere the calcium cations bind to troponin, a protein which wraps around the actin filaments in a helical path blocking myosin's access to the actin bond sites. By binding to troponin the calcium, cations deform it, opening actin-binding sites and leaving them receptive to interactions with myosin. Hence, this increase in the concentration of calcium cations in the sarcomere initiates the crossbridge chemical to mechanical cycle that drives the fibre's contraction.

The overall crossbridge reaction cycle requires one actin bond site (A), one myosin bond site (M) and one adenosine triphosphate molecule (ATP). Force is generated as an output together with one molecule of adenosine diphosphate (ADP) and one γ-phosphate (Pi) [1,68]:

$$A + M + ATP \rightarrow A + M + ADP + Pi + Force \qquad (3.3.1).$$

Lymn-Taylor [69] analysed the biochemical sequence of events in a crossbridge attachment/detachment cycle and proposed a four-phase chemical-mechanical relationship known as the Lymn-Taylor actomyosin ATPase hydrolysis mechanism [68]. In more recent studies based on x-ray crystallographic analysis of individual skeletal muscle mysoin, actin and ATP binding structures Rayment and Holden [51] proposed a swinging lever arm hypothesis based on small structural changes in the myosin head during ATP hydrolysis driving larger conformation changes (changes in structural arrangement).

It is not feasible to physically measure all of the stages of the actin-myosin hydrolysis cycle directly. Determining the path and reaction rates of the cycle requires the interpretation of data from thermodynamic analysis, directly measured reaction rates (for example those form the myosin hydrolysis cycle [49,70]) and the mechanical behaviour of muscle fibres.

Various techniques have been used to identify reaction parameters and directions. These include stopped-flow apparatus [49] where homogeneous solutions of components in controlled concentrations are rapidly mixed and the products are monitored by fluorescence changes. An alternative approach uses quenched-flow apparatus where acids are used to halt the reaction and ADP and ATP concentrations are monitored. Isotopes of O^{18} have also been used to label and monitor γ-phosphate. State flow models are required for analysing branched systems. From these data the chemical scheme has been developed in Figure 3.3.1 taken from the summary given by *Howard* [10]. The chemical reaction approaches described are limited as it is not possible to impose strain on the reaction or the geometric alignment provided by the sarcomere.

Drawing on the results from these experimental techniques, the current consensus (see below) as to the sequence of events in a crossbridge cycle can be summarised and is illustrated in Figure 3.3.1. In this figure, in order to relate the chemical and mechanical components of muscle activation, the mechanical stages (taken from a number of sources) have been sketched in parallel to the chemical cycle.

In the initial state:

A myosin head is strongly bound to an actin bond site. The head is in a rigor conformation: a large cleft in the head is open (1.3 x 1.3 nm), a narrow cleft between the head and neck is closed.

Phase 1, 'Unbinding':

An ATP molecule binds to myosin catalysing its release from actin.

Phase 2, 'Recovery stroke':

The ATP is hydrolysed on the free myosin. Freed from the actin the narrow cleft in myosin is probably opened (but this detail has not yet been clearly identified experimentally) by the ATP's γ-phosphate. The large cleft closes around ADP forming a meta-stable conformation.

Phase 3, 'Binding':

The strained myosin-ADP head rebinds (stereospecifically), probably in multiple stages to actin.

Phase 4, 'Working stroke':

Myosin sites bind strongly to actin sites and to γ-phosphate but not at the same time so the γ-phosphate may be forced out [10]. γ-phosphate's release is associated with closing of the narrow cleft and initiation of the power stroke, strengthening the bond between actin and myosin. ADP's release is associated with the large cleft opening and the expression of mechanical work followed by a return to the initial rigor conformation. Note that in smooth muscle ADP release triggers the strain release but in skeletal muscle the same, pre-strain, conformation has been found with and without ADP [10,70]. Delays between ADP release and strain expression have also been demonstrated in some instances in single crossbridge experiments [71] so the point of strain release is not clear.

Post strain release:

Actin and myosin bond sites are returned to the initial state ready to complete another cycle.

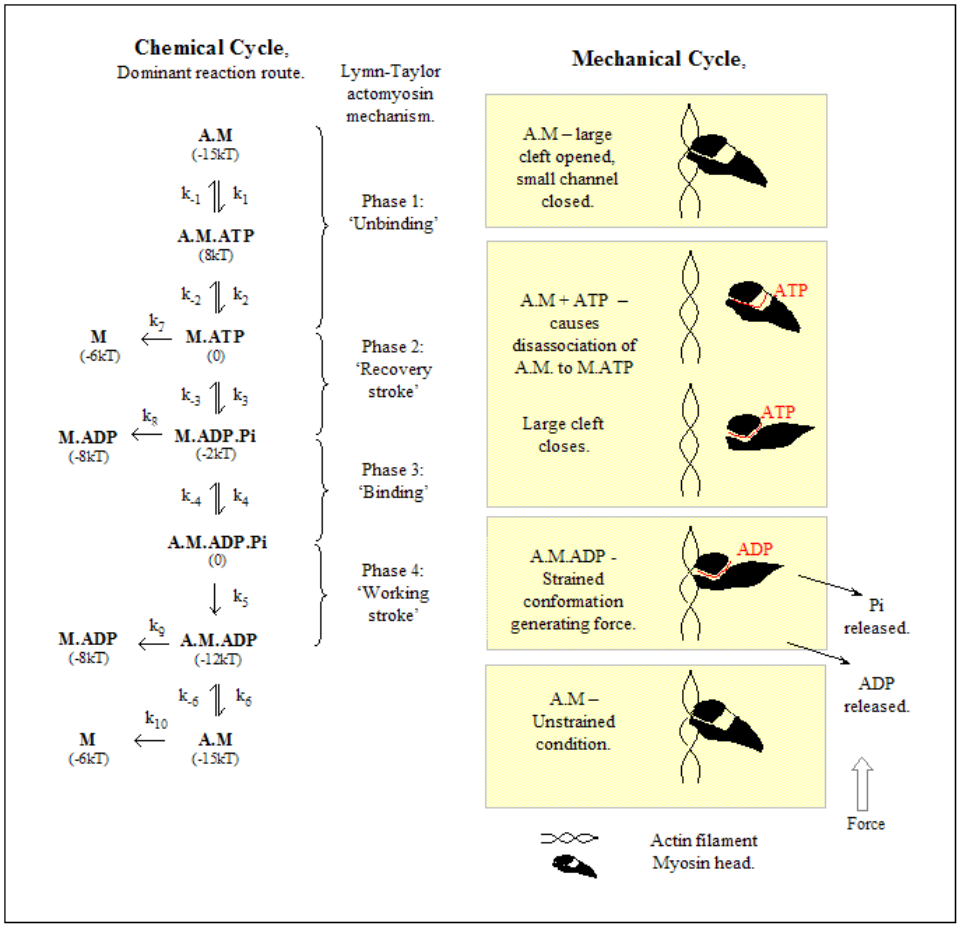

Figure 3.3.1, Summary of chemical and mechanical cycles and their interdependency. Information sourced from: [10(p210,p235),51,72]. A~actin, M~myosin, ATP~adenosine triphosphate, ADP~ adenosine diphosphate, Pi~γphosphate and k_i ~ reaction rate. Bracketed numbers e.g. (15kT) refer to the free energy of the chemical state, where k is Boltzmann's constant and T, temperature. Free energies assume [ATP] = 4nM, [Pi]=2mM, [ADP]=20μM and [A]= 1mM. Force, indicates the force imposed on the actin filament.

3.3.2 Modelling Reaction Rates: concentration and strain dependency.

Whether or not the cycle begins (actin binds to myosin) is dependent on the relative position of bond sites, (considered in Section 3.4). Once initiated the crossbridge's progression will be dependent on the chemical reaction rates, the direction and timing of which will be a function of temperature, chemical concentrations, pH levels and mechanical strain.

The following relationships, specifically Equations 3.3.3 and 3.3.7, were used to represent temperature, concentration and strain dependent reactions in the model described in this thesis. In the model a record was kept at each time step, t_{step}, of the

concentrations of: Ca^{++}, ADP, ATP and Pi (γ-phosphate) (see Appendix E, Function: ReactionRate and Figure 3.8.1).

A mathematical relationship, a rate equation, can be formulated linking concentrations of chemicals (A, B) and products (C, D) via reaction rates (k_1 and k_{-1}). Equation 3.3.2 is an example of a second order reaction [10].

$$mA + nB \underset{k_{-1}}{\overset{k_1}{\rightleftharpoons}} pC + qD, \qquad (3.3.2).$$

The reaction rate, r, is given by:

$$r = k_1(T,F)\cdot[A]^{n^1}[B]^{m^1}, \qquad (3.3.3),$$

where k_1 is the reaction rate coefficient and is a function of temperature, T, and applied force, F. [A] relates to the concentration of reactant A, n^1 and m^1 are the stoichiometric coefficients of reactants in the elementary step of the reaction (elementary in that the reaction can not be further reduced into sub-reactions). In the model each reaction step is considered individually and is 'one-to-one' i.e. one myosin bound actin with one ATP produces one actin and one myosin bound to ATP so $n^1 = m^1 = 1$. Similar relationships can be defined for the reverse reactions.

The reaction rate coefficient was related to temperature via the Arrhenius equation:

$$k_i(T) = A_f \exp\left[-\frac{\Delta G_{ai}}{kT}\right], \qquad (3.3.4),\ \Delta G_{ai} = G_a - G_i, \qquad (3.3.5),$$

where A_f is a frequency factor, G_a is the free energy of the reactions activated state, G_i the free energy of the initial state (free energy: energy free to perform non-volume changing work), G_{ai} the final state's free energy, T temperature and k, Boltzmann's constant. The activation energy is the minimum energy required for a chemical reaction to begin can be thought of as a potential energy threshold value. A_f and ($\Delta G_{ai}/k$) are obtained experimentally. Equation 3.3.4 relates to the rate per particle, the per mol. value is the gas constant, R divided by Avogadro's constant, N_A. The term free energy is used in preference to Gibbs free energy as the potential energy from mechanical forces is assumed to exist.

Force can change the energy of a system. If, for the case of actin binding to myosin, a rigid protein structure is assumed and a displacement associated with the molecular transition: a characteristic bond length Δx_{a1} (determined empirically [73]), the Arrhenius equation can be modified in order to relate the reaction rate at zero tension, k_i^0 , to the rate under tension [10 (p75-89)]:

$$k_i(T,F,x) = A_f \exp\left[\frac{-\Delta G_{ai} - F\Delta x_{ai}}{kT}\right], \qquad (3.3.6),$$

$$k_i(T,F,x) = k_i^0 \exp\left[\frac{F\Delta x_{ai}}{kT}\right], \qquad (3.3.7).$$

There are theories that elaborate on the meaning of Δx_{a1}, these are considered when the head ratchet models (mechanical representation of the crossbridge) are examined in Section 3.5.1. In this model Δx_{a1} is treated as a constant, x_{a1}.

In addition to the primary reaction path (see Figure 3.3.1), rupturing of the crossbridge is considered in order to deal with rapid transient loads. Equation 3.3.7 is the Bell model [74] for bond dissociation under loading. Evans and Ritchie [75], in an extension of Kramer's theory for reaction kinetics, modified this representation to consider the dissociation in terms of a loading rate, r_f, instead of a fixed load, F:

$$f^* = \frac{kT}{x_{ai}} \ln\left(\frac{x_{ai}}{k_i^0 kT}\right) + \frac{kT}{x_{ai}} \ln(r_f), \qquad (3.3.8),$$

where f^* represents the load at which breakage will most commonly occur. This theoretical model suggests a single bond may have multiple sequential stages or energy barriers to overcome before separation occurs. These two representations are implemented in the model: the forward and reverse progression through the primary reaction path is regulated by the static load representation and re-evaluated if strain changes, and crossbridge rupture, a breaking of the cycle, is considered in terms of the load rate.

The secondary reaction paths indicated by k_7 to k_{10} (Figure 3.3.1) are not evaluated as part of the normal crossbridge cycle. In order to recycle the myosin involved in ruptured crossbridges, consideration of additional reaction paths is required:

$$\mathbf{M.ADP} \xrightarrow{k_{11}} \mathbf{M + ADP}, \quad \text{and} \quad \mathbf{M + ATP} \xrightarrow{k_{12}} \mathbf{M.ATP}.$$

These reaction paths have been measured directly [49] and are included in Table 3.3.1.

3.3.3 Initial Reaction Parameters for the Baseline Model.

Howard [10] has collated data for the cycle shown in Figure 3.1 for rabbit skeletal muscle. There are probably subtle differences between species but the most complete set of data available is for the rabbit. These are shown in Table 3.3.1. The measurement difficulties are highlighted by Howard [10] and it is noted that some values varied by a factor of ten between different laboratories. The values are a composite of data. Some values are determined by halting the reaction between concentrations of fragments of actin and myosin in vitro solution and measuring the change in concentrations. The concentrations of S1 and myofibril fragments are studied at approximately physiological strength. Other values are determined by extrapolations from concentration models and energy transitions [4,10]. The influence of the structure of the sarcomere is not considered. The actin filament movement may influence the initial stereospecific bonding. The inverses of these coefficients are used as initial, strain-free, reaction durations in the Baseline Model. These values, k_i^0 (s^{-1}), are refined and strain dependent values are introduced, via Equation 3.3.7, in Chapter 4 as filament motility and isometric force development are examined.

Howard [10] assigned no value to k_{-5}. A number of studies [10,76,77,78,79] have reported that increased phosphate concentrations appear to have no effect on the contractile speed of striated muscle but under isometric loading, the level of force is reduced. This indicates k_{-5} is a feasible strain dependent step.

Table 3.3.1, Baseline reaction coefficients rabbit skeletal muscle taken from a summary of published experimental data by Howard [10(p235)]. (a) k_{12} a dissociation constant is used for convenience of units, M represents molar. Temperature ~20°C. '…roughly physiological ionic strength.' These rates are used in the model for the strain free, reaction value, $k_i^0(s^{-1})$, the inverse of which gives the reaction duration in the model (s).

Reaction Constant	Reaction Coefficient (s^{-1})	Reaction Constant	Reaction Coefficient (s^{-1})	Reaction Constant	Reaction Coefficient (s^{-1})	Reaction Constant	Reaction Coefficient (s^{-1})
k_1	20 000	k_{-1}	2 000	k_2	2 000	k_{-2}	0.4
k_3	100	k_{-3}	10	k_4	30	k_{-4}	300
k_5	$\geq 10^4$			k_6	10^3	k_{-6}	100
k_7	$\sim 10^{-4}$	k_8	0.1	k_9	0.2	k_{10}	1
k_{11}	2	k_{12}	$2\mu M^{-1}$ (a)				

Parameters which define the strain dependency of reactions are considered in Chapter 4. The load rate dependent rupture parameters are taken from the work of Guo and Guilford [73]. Guo and Guilford [73] investigated rupture characteristics using an optical trap to draw lengths of actin across a HMM coated bead (rabbit skeletal actomyosin). The effects of applying linearly increasing and step loads to crossbridges in post-lever (A.M., rigor) and pre-lever (A.M.ADP) states were measured. High ADP concentrations prevented the reaction cycle from proceeding to the strain release (levering) stage and low ATP concentrations inhibited the separation of the crossbridge; holding it in a post-lever state. Guo and Guilford [73] observed two distinct linearities for each of the pre- and post-lever states, interpreting each pair as distinct energy barriers (inner and outer) to be overcome for rupture to occur (see Equation 3.3.8 definition). Guo and Guilford used Equation 3.3.8 to fit the test data and identify the parameters x_{ai} and k_i^0 for each linear region. The energy barrier to be overcome was dependent on load rate (Figure 3.3.2). Large errors in the low energy barrier values were measured and no data was available to relate behaviour to temperature.

In the Baseline Model the load rate was compared to Equation 3.3.8 incorporating Guo and Guilford's parameter values. Crossbridges in excess of the load rate were then removed. To determine whether the model should be compared to the inner or outer parameter values the transition point between the two linearities was calculated (Figure 3.3.2). The point at which inner and outer parameters generated the same rupture force for a common load rate in Equation 3.3.8, for use in the model, is given by Equation 3.3.9.

$$\text{Transition} = \exp\left(\left(\frac{x_{R1}x_{R2}}{x_{R1}-x_{R2}}\right)\left(\frac{1}{x_{R1}}\ln\left(\frac{x_{R1}}{k_{R1}^{o}kT}\right)-\frac{1}{x_{R2}}\ln\left(\frac{x_{R2}}{k_{R2}^{o}kT}\right)\right)\right), \quad (3.3.9),$$

where x_{R1}, $k_{R1}{}^{o}$ indicate the inner energy barrier and x_{R2}, $k_{R2}{}^{o}$ the outer.

The rupture data were specific to the states A.M.ADP and A.M. where concentrations restricted the reaction to either reversing or rupturing. Additional states may be encountered in the Baseline Model: A.M.ADP.Pi, are grouped into pre-lever for model evaluation and A.M.ATP and levering into post-lever.

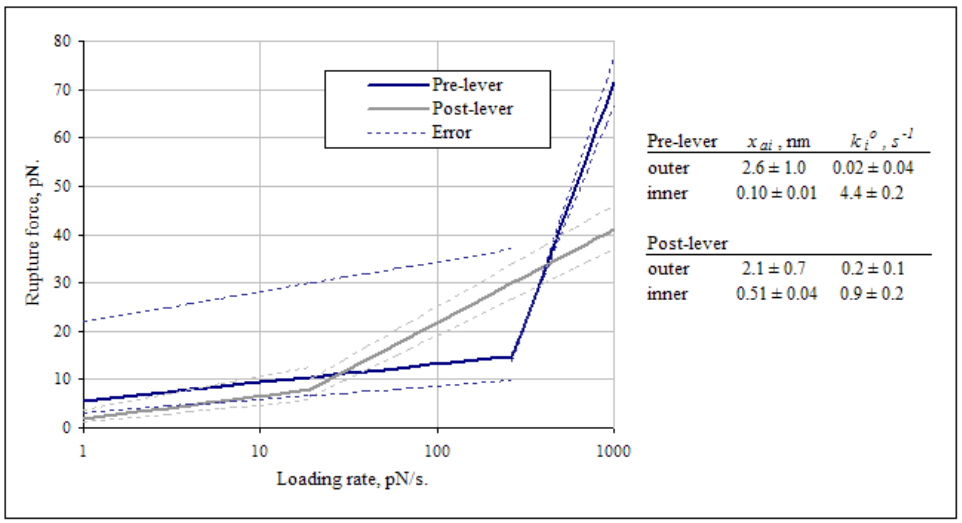

Pre-lever	x_{ai}, nm	$k_i{}^{o}$, s^{-1}
outer	2.6 ± 1.0	0.02 ± 0.04
inner	0.10 ± 0.01	4.4 ± 0.2
Post-lever		
outer	2.1 ± 0.7	0.2 ± 0.1
inner	0.51 ± 0.04	0.9 ± 0.2

Figure 3.3.2, Bell parameters for rupture calculations from Guo and Guilford [73]. The parameter values are applied to Equation 3.3.9. The inner energy barrier refers to the lower gradient region of the plot. The error values were generated by applying the extremes of Guo and Guilford's error estimates to Equation 3.3.9.

3.4 Determining Whether Crossbridge Formation Will Occur.

The formation of a crossbridge is dependent on actin and myosin bond sites being in a chemically receptive state, this was examined in Section 3.3. In addition, as will be considered next, the relative positions and relative velocities of bond sites influence crossbridge formation.

3.4.1 Significant Characteristics.

Actin has a polarity due to the asymmetry of its monomers [10 (p126)]. As an actin filament moves forward, an actin site will favourably bind to a myosin site that is in advance of its position. Thus, the actin filament dictates its direction of motion. This was initially demonstrated experimentally by tracking myosin coated beads travelling across bundles of actin in vitro [25] and later in filament motility studies where actin filaments followed roughly linear paths across a random distribution of myosin fragments bound to a nitrocellulose surface [28].

Binding is stereospecific [10], that is, a specific orientation and position are required between the two sites. In motility studies actin filaments have been observed to move in one direction to the edge of a surface turn around and continue moving across a random distribution of HMM fragments. From this it has been interpreted that the myosin head can swivel 180^{o} [80]. This may be significant in highly compressed sarcomere where actin filaments overlap.

Along with these demonstrations of the significance of physical proximity and orientation, there are indications that the relative speed of bond sites is also important. A decrease in stiffness has been observed in muscle fibres as contraction speed increases [81], this leads to the assumption that fewer crossbridges form or are sustained as relative site-to-site speed increases.

3.4.2 Modelling the Criteria for Crossbridge Formation.

Huxley's model [8] of crossbridge formation presents the theory of a 'window-of-opportunity' in which the myosin arms, buffeted by Brownian motion, may connect with an actin site. This can be formulated as [10]:

$$\frac{\partial p_{on}(x,t)}{\partial t} = k_{on}(x)p_{off}(x,t) - k_{off}(x)p_{on}(x,t) + v\frac{\partial p_{on}}{\partial x}(x,t), \qquad (3.4.1),$$

where x is the displacement 'window-of-opportunity', k_{on} and k_{off} are simplified reaction rates for the reaction stages within a crossbridge when it has formed, 'on' or when the bond sites are unattached, 'off', time t, probability p and v is actin filament speed. Huxley's model was not used directly in the Baseline Model but it brings

together the criteria used in the model. The criteria for a crossbridge to form in the model were: the correct reaction state, relative position and relative speed.

To accommodate stereospecific behaviour within the model, myosin S2's were assumed to be at their rest length, S1 is perpendicular to S2 and the bond sites are at the tip of the head. During contraction actin moves to the left in the model's convention, Figure 2.1.1, the bond site must be within a given spatial range, z_{range} , (similar to Huxley's window of opportunity, x) to the right of the myosin site or have travelled to the left, across the myosin bond site in the previous time step, t_{step}. The maximum speed with which the sites pass and may still bond was denoted by v_{cross}.

A further refinement of the relative speed was introduced into the Baseline Model as an inactive option for further investigation (see Section 4.4.8). This refinement was a weighting factor applied such that a relative speed of v_{cross} has zero probability of bonding; a speed of zero has a hundred percent probability if all other criteria for crossbridge formation are met. As an electrostatic attraction, an inverse square rule could have been used to define a capture range, z_{range}, but by associating the interaction with strain, more disparate bonds will have greater load and higher risk of rupture or rapid dissipation through the strain dependent reaction rates. The relative speed of crossbridge bond sites, $v_{cross,}$ and the bond site-to-site displacement, z_{range}, will be examined in terms of filament motility in Chapter 4.

Having determined a means via reaction state (Section 3.3), relative position and speed (Section 3.4) to define the formation of a crossbridge (see Appendix A, frame 3), in the next section how that crossbridge expresses strain energy into the filament system is considered.

3.5 Crossbridge Levering Mechanism: mechanical output.

3.5.1 Characteristics of Components

As previously described in Section 3.3, there is currently a reasonable understanding of the set of chemical reactions associated with an individual crossbridge levering

event. The mechanism by which the motor domain of the myosin II head stores energy and then releases it is not currently clear. Two prominent reaction rate theories, those of Eyring and Kramer, have been proposed to describe the protein conformation change in more detail [10].

Eyring's theory leads to an approximation of the conformation change as a localised diffusion stimulated chemical change initiating the release of a strained condition allowing it to relax and conveying that strain as force and displacement into the actin-myosin crossbridge. Huxley [8] back in 1957 proposed the Kramer theory or 'thermal ratchet method' to describe the mechanism. In this theory, diffusion drives the conformation change, when enough energy has accumulated to reach the transition state a localised reaction locks the system into place. If strain in the filament opposes the diffusion, the theory reverts to the Eyring representation. These theories can be considered elaborations of the frequency factor, A_f in the Arrhenius equation (Section 3.3).

Both theories have been considered in terms of theoretical crossbridge models [8,82]. The Eyring theory is more pertinent to the breakage of single bonds as the initial trigger of events is a single event so may not apply to the multiple parts of a conformation change. The Kramer theory relies heavily on the comparatively slow process of diffusion and the time constant for the process indicates a limit on the efficiency of ATP conversion to strain energy of fifty percent [10 (p88)] which aligns with estimates of 50-60% thermodynamic efficiency of muscle [10,22,76,83].

Huxley and Simmons 1971 [84] explored the kinetics of the process in terms of experimental data and modelled the data as a sequence of energy barriers where strain is released in stages rather than a single lever event.

3.5.2 Modelling

Section 3.5.1 focused on the fine detail of the crossbridge reaction thermodynamics: how fast the myosin II head can recover strain energy before forming a new crossbridge and how that energy is subsequently released. For the purposes of the model described in this thesis, these processes can be represented in terms of their effects. The key behaviours are the limitation of the detachment time for the recharge of strain energy in the myosin head and the release of that energy as force and

displacement, where maximum force corresponds to zero displacement and maximum displacement corresponds to zero force. In the pre-lever crossbridge state, actin and myosin bond sites are coincident. The release of myosin's strain energy causes these initial positions to be offset (Appendix A, Diagram G).

In the model described in this thesis force development was represented as an elastic component denoted by k_b in parallel with a velocity dependent dashpot c_b. The dashpot provides a drag factor in order to inhibit the instantaneous release of energy into the model. This spring-damper interpretation of the crossbridge lever event is akin to a Kelvin-Voigt representation [85] for creep. The general equations for a spring and damper in parallel were then modified, for use in the model, to match the observed extremes of crossbridge behaviour. The applied force, F_{bridge}, was limited by the displacement between actin and myosin bond sites, z, and the maximum lever distance, b_{max}. The resulting equations (3.5.1 and 3.5.2) show that if zero displacement, $z = 0$, occurs between actin and myosin bond sites no conformation change has taken place, the force generated is at a maximum. At maximum displacement, $z = b_{max}$, the conformation change has relaxed and the force drops to zero, $F_{bridge} = 0$, (see Figure 3.5.2). The implementation of Equation 3.5.1 is explained in Section 3.6.

$$F_{bridge} = (b_{\max} - z)k_b = c_b \frac{dz}{dt} + k_b \cdot z, \qquad (3.5.1),$$

$$z(t) = b_{\max}\left(1 - \exp\left(-\frac{k_b}{c_b}t\right)\right), \qquad (3.5.2),$$

$$U = \left[\frac{1}{2}k_b (b_{\max} - z)^2\right]_{z_1}^{z_2}, \qquad (3.5.3),$$

where U is the strain energy into the system. Equation 3.5.2 represents the relationship between time and displacement only if no external force is applied. Time from the initial release of crossbridge strain energy is denoted by t and the time constant is therefore:

$$\tau = \frac{c_b}{k_b}, \qquad (3.5.4).$$

Figure 3.5.1 shows the schematic representation of a single crossbridge between nodes c and b. Maximum force and lever displacements are assumed constants, as they are generated by a conformation change in the motor domain. The drag factor represents a

characteristic of the reaction process/s in the motor domain and so may be concentration and temperature dependent, which is considered in, Section 3.3. By assuming non-levering crossbridges have a high stiffness that is variable between pre- and post-levering states and assigning a zero drag coefficient, the bond-bond strain at non-levering crossbridges can be analysed. It has been demonstrated [31] that the maximum force per crossbridge is not temperature dependent but temperature increases the number of crossbridge linkage events, over time, along a filament. Therefore, the maximum force from a single crossbridge is temperature independent.

This is a simplified model of the crossbridge event. A multiple stage lever event and a Kramer style model of the thermodynamics of the crossbridge (a refinement of the frequency factor A_f in Equation 3.3.6) will be a complexity that will need to be considered in future model refinements.

3.5.3 Model Evaluation: isometric loading of crossbridge.

In order to evaluate the levering model and associated parameter values the Baseline Model was modified to emulate elements of Takaji *et al's* [63] investigation into crossbridge force responses to dynamic loads using substrate bound rabbit HMM fragments and actin filaments held between optical traps. Individual crossbridges were studied as they levered under low external loading and with the detected force fed back to the crossbridge in order to replicate an isometric load. In an isometric muscle contraction force develops without a change in displacement.

The Baseline Model was constrained to form a single crossbridge, overall damping and titin components were removed. The mechanical structure of this model is shown in Figure 3.5.1 (a). In Takaji *et al*'s [63] experiment corrective displacement (integral gain) was applied at the left optical trap, motor (M), in response to left trap movement, transducer (T). Maintaining the actin's length, in this way, was aimed at raising the dynamic stiffness presented to the myosin and reducing the actin's influence on the experiment. The stiffness of the actin and the optical trap were considered to be in series and represented by k_a. Model cofilament, k_{ms}, values approximated the HMM to substrate stiffness. As S2 was the component bound to the surface, not LMM (see Figure 3.2.2) this potentially influenced the value of k_m . The levering crossbridge representation is between nodes b and c of Figure 3.5.1 (a).

In order to gauge the magnitude and rate of isometric loading Takaji *et al* [63] determined the feedback gain for a recovery of $\tau_{½}$ equal to 1ms by applying a square wave perturbation to a bead-actin-bead arrangement. In order to replicate this the modified Baseline Model of Figure 3.5.1(a) was further refined (Figure 3.5.1(b)). Model cofilament stiffness, k_{ms} , was set high, so effectively rigid, k_m and k_a were assigned the stiffness of actin in series with an optical trap. A step displacement was applied between c and b and the displacement of T monitored and corrected for at M.

For the purposes of studying the levering parameters in isolation, the levering event was considered from the initiation of force and displacement. The completion of the event where the reaction cycle moved on or the crossbridge disengaged is considered in Section 3.3. For clarity, this allowed reaction rate behaviour to be set aside.

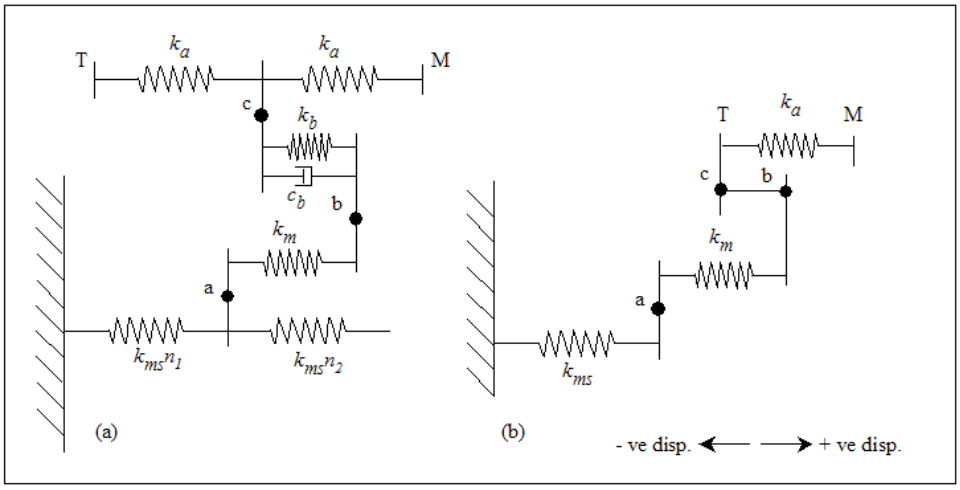

Figures 3.5.1, (a) Schematic of modified Baseline Model set-up for single crossbridge levering experiment. Schematic (b) shows the version of model (a) used to calculate feedback gain. T indicates the transducer position in Takaji et al's experiment and M the motor.

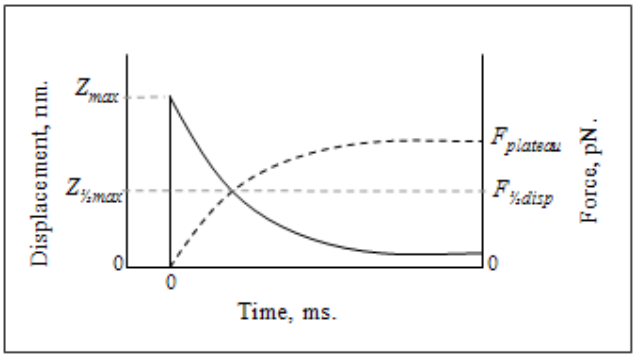

Figure 3.5.2, Sketch of force and displacement of a single crossbridge under isometric loading. Values for z_{max}, $z_{½max}$, $F_{plateau}$ and $F_{½disp}$ are examined experimentally.

The ensemble averaged responses for $\tau_{½}$ = 1ms for attachments longer than 5ms from Takaji *et al* [63] were examined at two distinct points. Point one: initial maximum displacement (z_{max}) (see Figure 5.3.2) and associated forces at T and M. The lever distance of the crossbridge could be approximated to this value once the experimental compliance and feedback have been taken into consideration. Point two: force on the crossbridge at half maximum displacement ($F_{½disp}$ and $z_{½max}$) and time of occurrence. At small displacements and forces, the significance of experimental noise increases. For these data when displacement is high force is very low, when force is high displacement is very low, hence a mid-point is examined. In the model forces at T and M, and displacements at nodes a, b, c, T and M were measured for comparison with the optical trap responses at T and M. From these two distinct points a plateau force and crossbridge stiffness were extrapolated:

$$F_{½disp}/(\ z_{max}/(\ z_{max} - z_{½max})) \quad \text{and} \quad F_{½disp}/(z_{max} - z_{½max}) \text{ respectively.}$$

The parameter values required to model the single crossbridge levering event were: k_{mh}, k_{ms}, k_m, k_a, c_b, k_b, b_{max} and l_{head}. These were simplified to five key parameters (Table 3.5.1) as will be explained. Actin stiffness, k_a (0.1776N/m bond-site-to-bond-site [55,86, Section 3.2]), modelled in series with the optical trap stiffness (0.066pN/nm measured by Takaji *et al* [63]) was negligible in comparison to the trap stiffness. Substrate stiffness to HMM stiffness, represented here by k_{ms}, was not known and an initial value of 9.2pN/nm was used based on the study in Section 3.2. Due to the reduced interface of HMM to the substrate this value would be considered a maximum. k_{ms}, k_{mh} and k_m act in series with k_m under extension. k_m = 70pN/nm and k_{mh} (during levering) ~ 2.7 pN/nm (from Section 3.2.7). Due to these relative magnitudes k_m values were not significant, so were not considered to be variable. Due to the structure of the model and the relative magnitudes of k_{ms} and k_{mh} their individual values could not be distinguished in the results so k_{mh} was considered to be variable and k_{ms} to be constant. Maximum head flexure, l_{head}, was set at 3.4nm (Section 3.2) a length at which it was not expected to influence the results. The lever distance, b_{max} was considered in the 7 to 8nm range in alignment with findings from more recent optical trap studies [29,63].

A response surface model was generated in order to systematically and efficiently examine the interaction of the parameters and their influence on the Matlab model output. The response surface model was defined by a set of parameter values (Table 3.5.1) and the corresponding responses generated by the Matlab model. The response

surface model was then processed in a standard statistical software package, MiniTab, which had inbuilt functions that identified the best-fit parameters to achieve target outputs and could instantly display the effect on responses to parameter variations. A central composite (Box-Wilson) circumscribed experimental design and analysis was selected to generate the response surface model. Other composite designs were considered but the estimation of coefficients would have been less precise and coverage of the design space (parameter levels) would have been less effective and provide less information about any non-linear behaviour [87,88].

The mathematical structure of the design dictated a fifty-two run, full factorial set of experiments with each of the five parameters evaluated at five different values (levels) to highlight any curvature in the response, Table 3.5.1. The outer range of values for each parameter were defined by the mathematical structure of the central composite design. The response surface model took the form of a second order quadratic equation which approximated the output of the spring-damper model in response to the input parameters [87,88]. MiniTab was used to determine the coefficients of the equation. The deviation of the response surface model predictions from the Matlab spring-damper model was gauged using the adjusted coefficient of determination (adj. R-squared), at > 99.9% the response surface model provided a good representation of the spring-damper model [87,88].

The mechanical work performed per crossbridge was limited by the energy released from one ATP in the cellular environment, $\approx 100 \times 10^{-21}$ Joules [10]. Muscle thermodynamic efficiency has been estimated at 50-60% [10,11,12], defined in terms of the mechanical work performed per crossbridge. The energy limitation in combination with the peak force observations of 15pN by Takaji *et al* [63] were used to define the range of values for k_b. Preliminary, unloaded runs of the model indicated c_b to be less than 0.16 pN/μm/s. Muscle contraction speeds are typically 6 to 7 μm/s [10] while actin filaments moving across a substrate scattered with myosin fragments appear to move more quickly: 8 to 9 μm/s, [16,28,52,89,90,91]. An individual crossbridge levering event must proceed rapidly enough to generate this speed limiting c_b.

The spring-damper Matlab model was run with time steps of 10^{-5}s, a rate rapid enough to capture the characteristics of the force and displacement development, but sampling for and the application of feedback was applied at 5×10^{-5}s in order to correspond with the 20kHz test data from Takaji *et al* [63].

Table 3.5.1, Parameters and values used to define the Box-Wilson response surface model.

Parameter	*Units*	*Value*				
b_{max}	nm	6.31	7.0	7.50	8.0	8.69
c_b	pN/μm/s	0.01	0.04	0.082	0.122	0.163
k_b	pN/nm	1.657	1.933	2.133	2.333	2.609
k_{mh}	pN/nm	1.511	2.200	2.700	3.200	3.889
Op' Trap	10^{-5}N/m	4.697	5.800	6.600	7.400	8.503

3.5.4 Results

Using the response surface model individual parameter values could be rapidly changed (within the maximum and minimum levels) and responses immediately calculated. This allowed a systematic search of the parameter space, varying each in turn to find a 'best fit' to the test data.

In order to determine the parameter values which best fit the test data, the surface model boundaries were constrained by fixing the optical trap tension to that given by Takaji *et al's* [63]: 0.66 pN/μm, and fixing the maximum crossbridge strain energy to 60 x 10^{-21}J, in effect making k_b dependent on b_{max}. c_b was initially set to a minimum in the model (0.04 pN/μm/s) as its influence was limited to the force levels at maximum displacement.

From the discussion in Section 3.5.3 and Figure 3.5.2 the following targets were selected from test data obtained experimentally by Takaji *et al's* [63] from substrate bound rabbit HMM:

(1) Peak displacement (-7.02 ± 0.06nm).

(2) Peak force: the plateau force in the model is 8.53pN/nm lower than the 9 ± 0.02pN from the linear extrapolation of points between full and mid-displacement but as Figure 3.5.4 shows the behaviour is not linear. The extrapolated values provide a useful guide to the rate of change between full and mid-displacement. As does the crossbridge stiffness (1.3 ± 0.02nm).

(3) Motor force at half displacement (4.52 ± 0.003pN), which should approximate to the crossbridge force.

(4) Force at maximum displacement on left and right optical traps: -0.421 ± 0.003pN and 0.627 ± 0.003pN).

(5) Time to reach half-maximum displacement: 10ms. In Takaji *et al's* [63] experiments despite feedback being set at $\tau_{½}$ = 1ms the time at which half

maximum displacement was recorded for the ensemble averaged data was 10ms.

Table 3.5.3 summarises the values of k_{mh} required to achieve key targets with changing values of b_{max}, where the value of k_b is set by the maximum crossbridge strain energy and b_{max}. The parameter values b_{max} = 7.9nm, k_b = 1.923 pN/nm, k_{mh} = 3.530 pN/nm provided the 'best fit' to the target values. The results of feeding the central composite model results into the model of Figure 3.5.1(a) are shown in record (1), Table 3.5.2. Maximum crossbridge displacement, target (1), at 7.01nm and motor force at half displacement, target (3), at 4.52pN matched, within error boundaries, Takaji *et al's* [63] data while the extrapolated peak force, target (2), at 9.03pN was slightly out of range. However, to achieve half-maximum displacement the model took 19ms (target (5) 10ms). The feedback amplitude gain used was 0.68. This value was determined by applying a step input of 7.27nm to the modified model shown in Figure 3.5.1(b) in order to emulate the method performed by Takaji *et al*. The time of half-maximum displacement dropped to 10m (record (2) , Table 3.5.2) with minimal effect on other outputs if the amplitude feedback gain was increased to 1.3 ($\tau_{½}$ = 0.52ms in the feedback model, Figure 3.5.1(b)).

A set of parameters was not found that aligned the model output with the forces on the optical traps at maximum displacement (record (1), Table 3.5.2). The left trap force was high at -0.462pN while the right trap was low, 0.498pN. By modifying the lever damping, c_b, the balance of force on the optical traps could be modified (record (2)-(5), Table 3.5.2) but not without shifting other results away from their target values.

By using the response surface model in the way described a fit to the majority of the test data targets was found. The data at key points against target are shown in record (2) of Table 3.5.2 and the spring-damper model output is plotted in Figure 3.5.3 and 4. The parameter values determined: b_{max} = 7.9nm, k_b = 1.92 pN/nm, k_{mh} (levering) = 3.53 pN/nm, optical trap stiffness = 0.66 pN/μm and c_b = 0.04 pN/μm/s with a feedback amplitude gain set to 1.3. Sensitivity of the system to a five percent variation in these parameter values and with b_{max} = 7.8 to 8.0 nm are shown in record (6)-(15) of Table 3.5.2. Figure 3.5.3, and Figure 3.5.4 show force levels are slightly more sensitive to the changing parameters than the displacement. The small changes in the output indicated a stable set of parameter values.

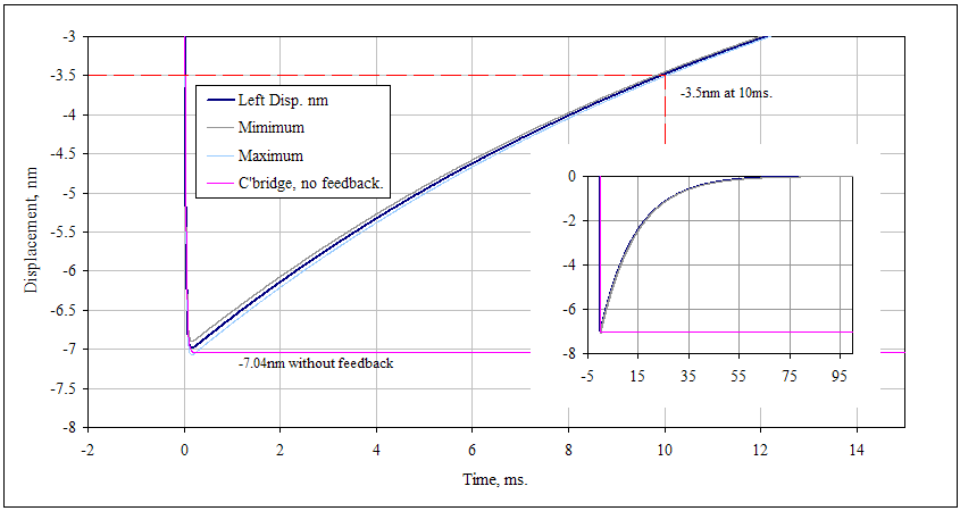

Figure 3.5.3, Spring-damper model generated crossbridge levering displacement: free release and release under isometric loading. Results generated from modified Baseline Model, Figure 3.5.1(a).

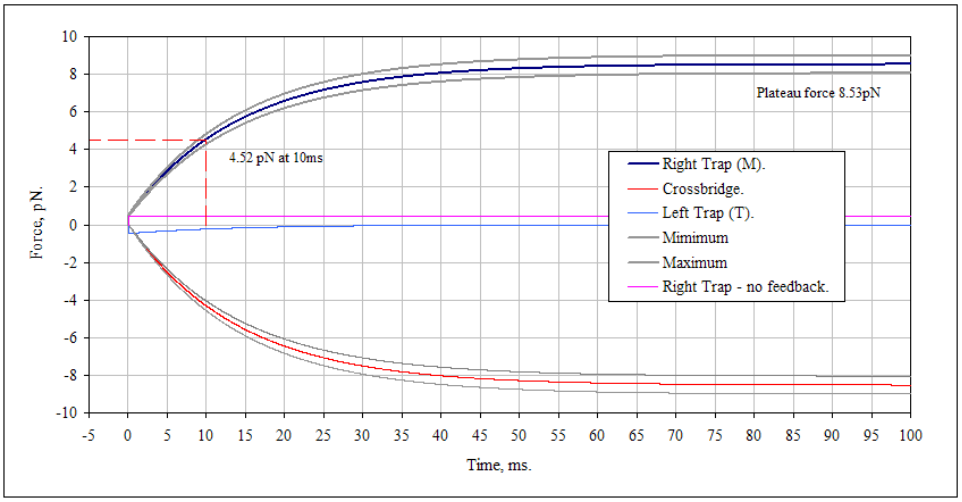

Figure 3.5.4, Spring-damper model generated crossbridge levering force, free release and release under isometric loading. Results generated from modified Baseline Model, Figure 3.5.1(a). The restoring force on the right trap (M) is applied (+ve) to the right as the crossbridge pushes to the left (-ve) generating a low load on the left trap (T). Right Trap – no feedback: is the right trap response when the crossbridge lever is not opposed by loading at the right trap.

Table 3.5.2, Isometric loading of a single crossbridge: comparison of spring-damper model to optical trap data targets (bottom of table) from [63]. Results generated from modified Baseline Model, Figure 3.5.1(a). (a) Crossbridge displacement including cofilament substrate movement: node c to b in Figure 3.5.1(a). (b) At onset of crossbridge lever displacement right trap average: 7.46 ± 0.06nm and 0.627±0.004pN, left trap: 7.02 ± 0.06nm and -0.421 ± 0.003pN.

		Peak Disp. (nm) and associated force. [b]					Marker point, mid-displacement.					Right (M) trap.	Linear extrap.	
		Time (ms)	Actin disp. at C'bridge, (nm)	C'bridge disp., (nm)[a]	Force left optical trap (pN)	Force right optical trap (pN)	Time, (msec)	Left trap, Actin disp. at C'bridge, (nm)	C'bridge disp., (nm)[a]	Force, right trap (pN)	C'bridge force (pN)	Peak force (at 0.25secs) (pN)	Ex'polated Peak force reached (pN)	C'bridge Stiff., (pN/nm)
	Feedback amplitude:													
(1)	0.680	0.32	-7.01	-7.11	-0.462	0.498	19.06	-3.50	-4.02	4.52	-4.29	8.53	9.03	1.29
(2)	1.300	0.30	-6.99	-7.09	-0.461	0.517	10.06	-3.50	-4.02	4.52	-4.29	8.53	9.06	1.30
	Variation in cb (pN/μm/s) with feedback amplitude 1.3:													
(2)	0.04	0.30	-6.99	-7.09	-0.461	0.517	10.06	-3.50	-4.02	4.52	-4.29	8.53	9.06	1.30
(3)	0.06	0.35	-6.96	-7.07	-0.459	0.541	10.07	-3.50	-4.02	4.52	-4.29	8.53	9.10	1.31
(4)	0.08	0.40	-6.94	-7.05	-0.458	0.565	10.08	-3.50	-4.02	4.52	-4.29	8.53	9.13	1.32
(5)	0.12	0.49	-6.90	-7.01	-0.455	0.605	10.10	-3.50	-4.02	4.53	-4.30	8.53	9.19	1.33
	Parameter sensitivty:													
(2)		0.30	-6.99	-7.09	-0.461	0.517	10.06	-3.50	-4.02	4.52	-4.29	8.53	9.06	1.30
(6)	Min.	0.31	-6.90	-7.00	-0.432	0.491	9.95	-3.50	-3.98	4.22	-4.00	8.05	8.57	1.24
(7)	Max.	0.30	-7.07	-7.18	-0.490	0.550	10.17	-3.50	-4.05	4.83	-4.59	9.01	9.56	1.35
(8)	b_{max} = 7.8nm	0.30	-6.90	-7.00	-0.455	0.511	9.88	-3.50	-4.01	4.41	-4.18	8.42	8.96	1.30
(9)	b_{max} = 8.0nm	0.30	-7.07	-7.18	-0.467	0.524	10.24	-3.50	-4.03	4.63	-4.40	8.64	9.16	1.30
(10)	k_b -5%	0.31	-6.96	-7.07	-0.459	0.521	9.77	-3.50	-4.00	4.39	-4.16	8.28	8.82	1.27
(11)	k_b +5%	0.30	-7.01	-7.12	-0.462	0.519	10.35	-3.50	-4.03	4.65	-4.42	8.76	9.29	1.33
(12)	k_{mh} -5%	0.30	-6.97	-7.08	-0.460	0.516	9.90	-3.50	-4.01	4.45	-4.22	8.39	8.93	1.28
(13)	k_{mh} +5%	0.30	-7.00	-7.10	-0.462	0.518	10.22	-3.50	-4.02	4.59	-4.36	8.65	9.19	1.31
(14)	*trap stiff.* -5%	0.30	-7.03	-7.13	-0.440	0.494	10.61	-3.50	-4.02	4.53	-4.32	8.53	9.03	1.29
(15)	*trap stiff.* +5%	0.30	-6.95	-7.06	-0.481	0.540	9.57	-3.50	-4.02	4.51	-4.27	8.53	9.09	1.31
	Targets:		-7.02 ± 0.06		-0.421 ± 0.003	0.627 ± 0.004	10ms	-3.50 ± 0.03		4.52 ± 0.003			-9.0 ± 0.02	1.3 ± 0.02

Table 3.5.3, Identification of k_{mh} stiffness values during levering (S1) in pN/nm against target values in response surface model.

	Target (3)	Target (1)	Target (2)	Target (2)
Levering distance, b_{Max} (nm)	Mid. displace. Tension, right trap (pN)	Peak disp. (nm).	Crossbridge Stiff., (pN/nm)	Extrapol'ed Peak tension reached (pN)
7.6	3.89	not achieved	3.0 to 3.35	3.41 to 3.4
7.8	3.65	not achieved	3.28 to 3.76	3.445 to 3.465
7.9	3.53	2.9 to > 4	3.45 to 3.975	3.47 to 3.53
8	3.42	2.4 to 3.5	3.68 to > 4	3.485 to 3.55
8.2	3.23	not achieved	3.45 to 3.975	3.52 to 3.59

3.5.5 Discussion

In Takaji *et al*'s data the feedback gain for $\tau_{½}$ = 1ms generated a half-maximal displacement at 10ms. In the model, setting feedback gain for $\tau_{½}$ = 1ms resulted in the half-maximal displacement at 19ms, the feedback gain had to be almost doubled ($\tau_{½}$ = 0.52ms in the feedback model) to achieve 10ms. The response surface model showed some indications as to why these discrepancies occurred.

The optical trap stiffness had a negligible influence on the calculation of feedback but did influence the mid-displacement time target in the response surface model. Increasing the optical trap stiffness reduced the time as did reducing k_{mh}, k_b and b_{max}. The loading applied via the optical trap is also opposed by the lever stiffnesses, k_{mh} and k_b. Also working against the optical trap is the cofilament stiffness the behaviour of which would follow the trend of k_{mh}. By changing the balance of compliance between the cofilament, lever arm and optical trap the half-maximal displacement time is modified. Levering stiffnesses k_{mh} and k_b are not present when setting the feedback level.

Modifying optical trap, k_{mh}, k_b and b_{max} values within the response surface model boundaries significantly compromised the ability to align with other targets while failing to bring the time down lower than ~ 16ms. At mid-displacement 12.8% of the crossbridge displacement was transferred to the cofilament and at initial maximum displacement 1.5%, result (2), Table 3.5.2. Dropping k_{mh}, while lowering the time of $\tau_{½,}$ would confer greater displacement to the substrate, reducing the movement of actin and the apparent lever distance. The difference in response times, therefore, seems attributable to the setting of the feedback gain and the compliance used for it. This could be pursued further using the model, but was not deemed useful to the over all project.

Within the response surface model, the optical trap stiffness also influenced the magnitude of the forces at maximum displacement, a state where they are in equilibrium with the cofilament/substrate stiffness. The damping of the lever arm increases the force on the right trap as it slows the lever release so the right trap has to work against greater strain energy in the crossbridge with small losses in displacement results (2)-(5), Table 3.5.2. Increasing the feedback gain has a similar influence. The difference between the model and in vitro forces may be due to a variation in performance between the motor and transducer in Takaji *et al's* [63] experiment compared to the symmetry of loading in the model or a potential variation in force profile at the end of the lever movement.

In the model, the crossbridge length is greater than the displacement of the actin bond site. To distinguish between these two lengths the crossbridge length at its maximum is the lever distance denoted by b_{max} and the actin bond displacement, the working distance denoted z. The difference in length may be due to the deformation of the myosin component (see Section 3.2.6). Most experiments have attempted to correct

for this as a known experimental error and it may contribute to the broad range of displacements reported for individual events: from 5.5nm and 15nm [32,53,64,65,92]. Studies that are more recent give values in the 6-10nm range, for example Kaya and Higuchi [29] determined a working stroke mean of 7.6nm peaking at 8nm. The b_{max} = 7.9nm specified from the model fits comfortably within this more recent range of values (see Appendix B, Table 3).

Equation 3.5.1 with k_b = 1.923 pN/nm and b_{max} = 7.9nm gave a peak force of 15.2pN consistent with the peak forces observed by Takaji et al [63] of 15pN (although with a few outlying 17pN events). The model's plateau force under isometric loading was 8.53pN which is comparable to the upper end of values measured elsewhere in related optical trap experiments: 0.8 to 7pN [30,31,64,65,71] where these author's were inclined to consider their measurements lower estimates due to compliance in their experimental set-ups.

The speed of movement of the actin can be used to indicate if the crossbridge is releasing quickly enough, i.e. to determine whether c_b is small enough while the k_b component of the time constant (Section 3.5.2) has been set by the peak force and b_{max}. Typical muscle contraction speeds are 6 to 7 µm/s [10]. Actin filaments moving across a substrate scattered with myosin fragments appear to move more quickly: 8 to 9 µm/s, [16,28,52,89,90,91]. An individual crossbridge's displacement of actin, z (the working distance), divided by the time myosin remains bound to actin must achieve these velocities as no other means of increased speed presents itself. The duration of that attachment is dependent on the time the crossbridge spends releasing strain energy (levering actin), t_{lever}, and the time the crossbridge is present before and after levering, t_{dwell}.

$$\dot{x} = \frac{z}{t_{lever} + t_{dwell}}, \qquad (3.5.8),$$

From result (2), Table 3.5.2, z = 6.99nm, t_{lever} = 0.3ms the crossbridge speed is 23.3µm/s. The crossbridge is levering rapidly enough with some time remaining for attachment and release of the crossbridge t_{dwell}.

The S1 head stiffness during levering was determined as k_{mh} = 3.530 pN/nm and is of a similar order to values established for the S1 head stiffness post- and pre-lever in Section 3.2.4 of 2.7 and 3.03pN/nm respectively. It is important to note, the

cofilament stiffnesses, k_{ms} and k_{mh} act in series in this version of the model. If k_{mh} is reduced, k_{ms} must be increased to maintain the same output. The substrate-cofilament stiffness used here was taken from Section 3.2.6 and was for a cofilament attached to a substrate but in this instance a smaller fragment was bound to the substrate giving a smaller contact area leading to a lower stiffness. So it follows that k_{ms}, in this analysis, was set high and therefore k_{mh} is a lower estimate.

The crossbridge stiffness 1.3pN/nm during levering dropped due to the additional in series compliance of k_b, which was previously found to be 2.6 and 2.9pN/nm pre- and post-lever (Section 3.2.4). This lower value aligns with crossbridge values from other experimenters, e.g. 0.13, 0.6, 0.48, 1.79pN/nm [62,64,65]. The damping component, c_b, applies 0.21% of the total force on the crossbridge so should have minimal influence on the crossbridge stiffness.

b_{max}, k_b, k_{mh} and c_b represent behaviours in the motor domain and S1 region of the myosin II fragment. Therefore, they can all be considered open to modification when considering the isoforms of myosin II.

3.5.6 Summary of Parameter Values.

The model lever arm representation has been compared to a single crossbridge levering event under isometric loading. Comparable results have been generated indicating that the model is in good agreement with in vitro data. Values have been determined for the following parameters that are consistent with other published data.

b_{max},	Maximum lever displacement:	7.9nm,
k_b,	Elastic component of levering:	1.92 pN/nm,
k_{mh},	S1 stiffness during levering, lower estimate:	3.53 pN/nm,
c_b,	Viscous damping component of levering:	0.04 pN/μm/s,

Sensitivity of the system to a five percent variation in the parameters k_b, k_{mh}, c_b, and $b_{max} \pm 0.1$nm was ~2% for maximum displacement of actin and ~7% for the force at half-maximum displacement.

3.5.7 Isometric Loading: levering crossbridges held in equilibrium.

In Section 3.5.2, the modelling of the crossbridge levering mechanism as a spring and damper system was introduced. Parameters were identified in Section 3.5.4 that demonstrated the model was representative of the in vitro measured initial stages of isometric loading in a single crossbridge. Beyond the point at which the crossbridge reached equilibrium with the applied load the model diverged from the in vitro data.

In Takagi *et al's* [63] single crossbridge optical trap experiments, crossbridges which reached equilibrium with the isometric load ($\tau_{½}$ = 1ms feedback amplitude gain, see Section 3.5.5) were short-lived, lasting much less than 0.01ms with the rare event lasting 0.9ms. Reducing feedback resulted in the duration of the longer-lived events increasing but the peak isometric force dropping. However, in the model once equilibrium with the external force was achieved the crossbridge was sustained indefinitely and varying feedback simply changed the time to reach the equilibrium force. Here the cause of these differences and an adaptation to the model is considered to accommodate this behaviour.

In the model described in this chapter, after the release of an ADP (Figure 3.3.1, Section 3.3.1), the crossbridge enters the levering stage where, in the mechanical representation of the filaments (see Figure 3.2.2), it is represented as a spring-damper system. The spring and damper are initially compressed, so have stored strain energy, which applies force and displacement on the actin bond site and myosin S1. If the crossbridge releases all of its strain energy, after a minimum time duration, it can progress through the final reaction stage where the actin and myosin bond sites have a fixed separation (b_{max}, see Section 3.5.2) and the attachment cycle can be completed by ATP separating the crossbridge bond sites. If the crossbridge cannot release any strain energy it may be returned to a pre-lever state where the bond sites are coincident and the strain energy in the myosin is stored but not able to release into the filament system. Under isometric loading the single levering crossbridge, in the mechanical spring-damper interpretation, is unable to release all of its strain energy and therefore cannot progress forward through the reaction stages and be released, nor can it recover the strain energy it has already expressed in counteracting the isometric load and return to a pre-lever state. For the lever event to complete in the forward direction the isometric force must be lowered or the crossbridge obtain more energy by some

means. A third path to release would be for the crossbridge to diffuse away, sacrificing the remaining strain energy.

If the lever cycle has released most of its strain energy a very small amount of external force will allow the crossbridge to complete the lever cycle. A random movement due to Brownian motion could be a source of sufficient energy. Using the equipartition rule and data taken from Veigel *et al* [92] an estimate was made of the mean force on an optical trap of $(4.568 \times 10^{-3})(KT)^{0.5}$ N, where T equals 296.15^0 K (23^0C) [92], randomly applied within time blocks of *1*/200Hz. Applied to the model, with a crossbridge in equilibrium with the optical trap stiffness, lever completions of random duration were achieved. Although, it is a normal scenario for crossbridges to be constantly jostled in this way, due to the low level of energy imparted, this was not incorporated as a standard Baseline Model component.

In the absence of an external energy change if the bonds in the levering crossbridge disconnect, releasing the crossbridge, they cannot part based on force alone as the crossbridge has carried higher forces than the isometric load at the beginning of the lever event. The interpretation here is that the separation is force and time dependent. Guo and Guilford [73] demonstrated, experimentally, this property in pre- and post-lever crossbridges.

Takagi *et al* [63] measured maximum attachment times against isometric loading in single crossbridge optical trap experiments. In Takagi *et al's* results it was observed that a levering crossbridge under isometric load had a greater chance of lasting for longer if the force on it was low, yet there was still a chance it would be short lived. These data were used to apply a force-time characteristic into the levering stage of the model described in this chapter. In order to do this, a curve was fitted to Takagi *et al's* data recorded many crossbridges samples to establish a maximum attachment time, S_{time}, in response to an isometric force on the crossbridge, F_s.

$$S_{time} = A_p \exp(-1.30 \times 10^{12} F_s), \qquad (3.5.9),$$

where A_p is a constant (s/N). If a levering crossbridge in the model had not completed its lever process or reversed after the minimum reaction duration (k_6, Table 3.3.1), the chance of the crossbridge remaining attached was evaluated (Figure 3.8.1 and Appendix E, Function:HeadProcessing). To generate a normalised weighting curve,

Equation 3.5.9 was divided by A_p. The force dependent attachment time was therefore scaled between 0 and 1.

$$\text{Normalised weighting} = \exp(-1.30 \times 10^{12} F_s), \qquad (3.5.10).$$

A pseudorandom number in the interval 0 to 1 was generated using Matlab; if higher than the weighting the crossbridge was released, if lower the crossbridge persisted for another time period, t_A (a multiple of the model time steps, t_{step}), after which the crossbridge was revaluated. So crossbridges with low loads have a greater chance of enduring a 'roll-of-the-dice' but how often the crossbridge is tested in this way also changes its maximum survival time: t_A, divided by the maximum survival time dictates the overall probability of the crossbridges survival. To align with Takagi *et al*'*s* maximum survival times t_A equal to 4ms was used in the model. While sustained in this way the crossbridge could still respond to changes in external loading.

The process described was applied to 10^5 randomly generated forces, which represented 10^5 isometrically loaded crossbridges; the resultant survival times are plotted in Figure 3.5.5. By applying this approach to the model the duration of the crossbridges, which would have remained indefinitely in the previous isometric study, (Section 3.5.3) with a load of 8.52pN, would have a range of durations comparable to those observed by Takagi *et al*. The approach was applied thousands of times to a force of 8.52pN and the distribution of survival times of the events are shown in Figure 3.4.6. 90% of events were short lived, completed within 4ms, with 1 in 6.25 x 10^4 crossbridges staying attached for 40ms. For comparison 0.5pN events, which tend to last longer are also plotted. At low force levels in the model, the longest duration was 944ms at 0.127pN, this is much longer than the results measured by Takagi *et al* but, as previously discussed, Brownian noise may provide enough energy to move such crossbridges to completion.

While this aspect of the model allows levering crossbridges held in equilibrium to be removed there are still characteristics of the levering process that have not been clearly determined. Takagi *et al* observed that reducing the feedback on an isometrically loaded crossbridge reduced the peak force and delayed the time to reach that force. In the original model, with reduced feedback, this did not occur the peak force was not reduced merely the time to reach it. The modification in this section may explain this characteristic. Increased feedback force reduces the probability of sustaining attachment but also increases the speed at which the peak force is reached.

Lower feedback forces are more likely to be sustained but they will take much longer to reach higher force levels and in that time be lost reducing the apparent peak force. The influence of this crossbridge modification is observed and considered in Chapter 4.

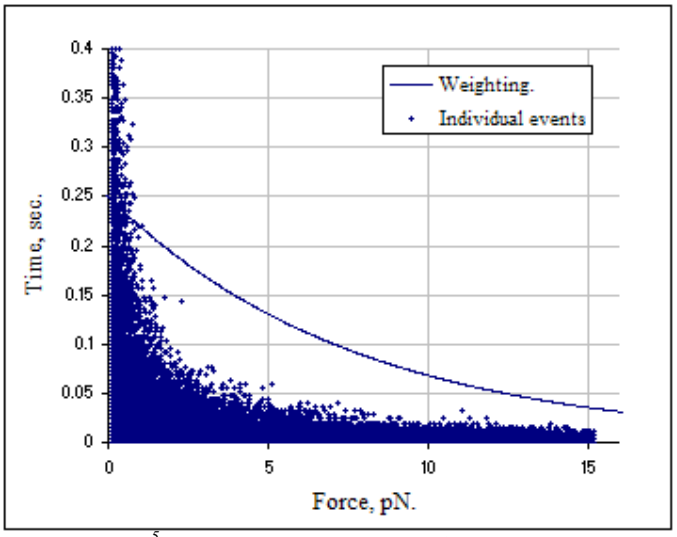

Figure 3.5.5, Duration of 10^5 randomly generated forces between 0-15pN applied to Equation 3.5.10 to represent crossbridges in isometric loading during levering. Release of crossbridges evaluated every t_A=4ms after the initial reaction period (k_6 had elapsed). The weighting curve is plotted at 25%.

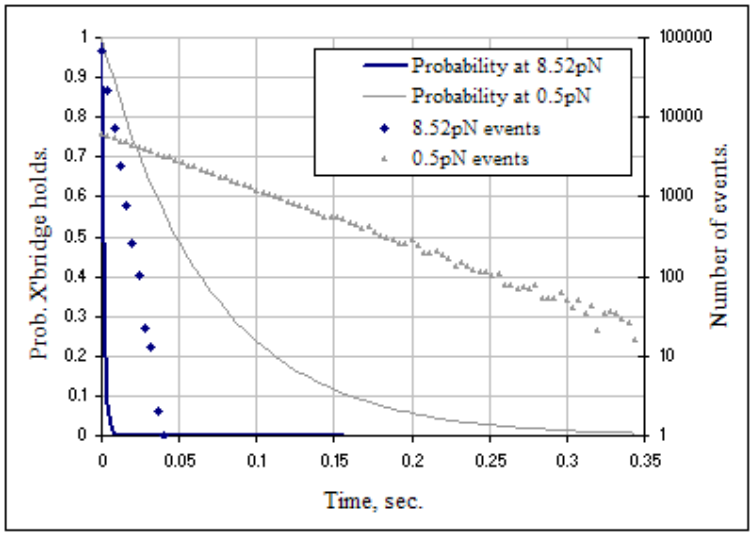

Figure 3.5.6, Results extracted from Figure 3.5.5, for forces of 8.52pN and 0.5pN. The length of time events are sustained for the 8.52pN and 0.5pN forces when the weighting approach was applied. The probability lines indicate the chance of an individual event at the given force level surviving over time.

3.6 Equation Formulation to Resolve Filament Forces.

The model is evaluated in distinct time steps, t_{step}. Once the reaction state of the crossbridges and bond sites have been determined in the model, it is necessary to calculate their mechanical interaction in the sarcomere: that is the combined effect of strain energy generated by the crossbridges and external loading on the actin and myosin cofilaments. The formulation of the equations of the mechanical representation of the sarcomere fragment is shown below by considering the scenario of a three-crossbridge system, see Figure 3.6.1.

The M-disc is treated as having a fixed position. Loads can be applied to the model at the Z-disc in terms of a time dependent force or displacement. The resultant force and displacement of the Z-disc are denoted by F_{end} and z_{end} respectively for the time step, t_{step}. A viscous drag component has been included in the sarcomere as a speed dependent dash-pot (lower case c). k_{tm} and k_{ta} denote the stiffness of the titin molecule that is in parallel with the myosin cofilament and from the end of the myosin cofilament to the Z-disc, see Section 3.7.

A record is maintained at each time step of the position of each actin bond site (c, f, i in Figure 3.6.1), myosin S2-to-cofilament position (a, d, g in Figure 3.6.1) and the position of the ends of the filaments (z_{actin}, j, k in Figure 3.6.1). The reaction state of each bond site is also recorded together with the displacement due to levering, which may have already occurred in previous time steps of the crossbridge causing the spatial off-set of the actin and myosin bond sites (e.g. c and b in Figure 3.6.1). Therefore, at the onset of the time step, t_{step}, the actin filament and myosin cofilament stiffnesses between crossbridges, $k_a p_i$ and $k_{ms} n_i$ respectively, can be determined (Section 3.2.2). The myosin arm stiffnesses, k_{mi}, are calculated from Equations 3.2.1, 3.2.2 and 3.2.3. The crossbridges are represented by stiffness k_{bi} and damping c_{bi} (Section 3.5.2) between the myosin bond sites b, e, h and actin bond sites c, f and i.

An equation can be written balancing each node, a to k in Figure 3.6.1 to generate a set of equations which, when solved, give the displacements within the system and the force and displacement of the Z-disc over the time step, t_{step}. The chemical state of the bond sites can then be evaluated for the next time step. The set of equations builds up in a systematic pattern as the number of crossbridges increases and can be rapidly reformulated each new time step.

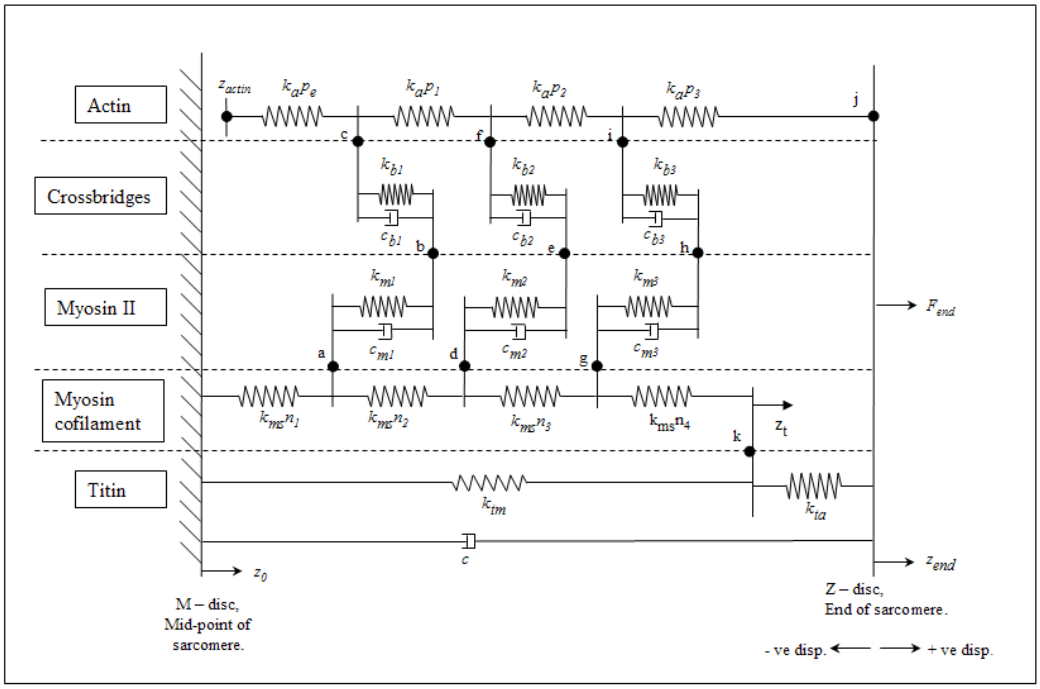

Figure 3.6.1, Schematic of spring-damper representation of model. Three crossbridges are shown in a levering state.

The displacement of each node is denoted by z_a , z_b , … where positive displacement is towards the Z-disc. The displacement of each node is taken relative to its position at the onset of the time step, t_{step}, so prior loads which have built up in the system must be included as preloads in the calculations.

The preloads in the myosin cofilament (crossbridge-to-crossbridge) are denoted by d_{mi} k_{ms} n_i, where d_{mi} is the previous displacement of the ith spring with stiffness k_{ms} n_i. Similarly, d_{mai} k_{mi} is the preload in the myosin arm, d_{ai} $k_a p_i$ the actin filament crossbridge to crossbridge preload, d_e k_a p_e the preload in the left end of actin and d_{ta} k_{ts} and d_{tm} k_{tm} are the preloads in titin protein parallel to actin and titin parallel to myosin. F_{end} is the force at the Z-disc which can be defined as an input.

As an example, the formulation of the equation for node i will be examined. Node i :

$$k_a.p_3\left(z_{end}-z_i+d_{a3}\right)+\frac{c_{b3}}{t_{step}}\left(z_h-z_i\right)=k_{b3}\left(b_3-\left(z_h-z_i\right)\right)+k_a.p_2\left(z_i-z_f+d_{a2}\right),$$

(3.6.1).

In Figure 3.6.2 the displacements, z_i and spring forces T_i on node i are sketched and from these the four component equations, 3.6.1 (i – iv), can be written.

$$T_l=k_a p_2\left(z_i-z_f+d_{a2}\right), \qquad \text{(3.6.1,(i))}, \qquad T_d=c_{b3}\left(\frac{z_h-z_i}{t_{step}}\right), \qquad \text{(3.6.1,(iv))},$$

$$T_r = k_a p_3 \left(z_{end} - z_i + d_{a3} \right), \quad \text{(3.6.1,(ii))}, \qquad T_r + T_d = T_l + T_f, \quad \text{(3.6.1,(v))},$$

$$T_f = k_{b3} \left(b_3 - \left(z_h - z_i \right) \right), \quad \text{(3.6.1,(iii))}.$$

T_l and T_r are the tensions in the actin filament left and right respectively. T_f is the force due to the strain energy released from the myosin bond site as it relaxes and T_d is the damping force which is opposing the energy release (Section 3.5.2). At the onset of t_{step}, if levering begins in this time step; node *i* and *h* are considered coincident, the initial force pushing these nodes apart is $b_{max}\, k_{bi}$ (Equation 3.5.1). If the crossbridge has partially levered in previous time steps the force remaining is $b_i\, k_{bi}$, where *i* is the designation of the crossbridge, $i = 3$ in this example, and some of the strain energy or preload from the crossbridge (b_{max} - b_i) has already been released into the system and has been recorded in the model by the position of actin and myosin bond sites relative to the M-disc. If a crossbridge is in a pre-lever state it is not releasing strain energy so node *i* and *h* would be coincident; b_i would be set to zero and k_{bi} made relatively stiff compared to the rest of the system in order to maintain that alignment. If the crossbridge was in a post-lever state node *i* and *h* would be off-set by b_{max} and to maintain this offset k_{bi} would, again, be made relatively stiff.

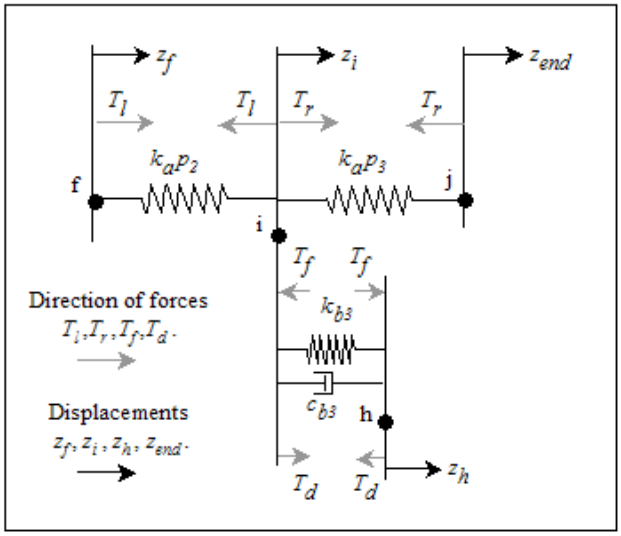

Figure 3.6.2, Schematic of the loads on node i from the three crossbridge system shown in Figure 3.6.1.

In order to test this representation of the crossbridge and the formulation of the equation sets the model was run with simple scenarios of one, two or three crossbridges offset in time. The plotted outputs could then be verified against a logical expectation of behaviour.

Below are further example equations from the set of eleven that were determined for a system with three crossbridges, shown in Figure 3.6.1:

Balanced forces at node c, (3.6.2 a, b):

$$\begin{cases} l_{ae} - l_{a1} \geq 0 & k_a.p_1\left(z_f - z_c + d_{a1}\right) + \dfrac{c_{b1}}{t_{step}}\left(z_b - z_c\right) = k_{b1}\left(b_1 - \left(z_b - z_c\right)\right), \\ l_{ae} - l_{a1} < 0 & k_a.p_1\left(z_f - z_c + d_{a1}\right) + \dfrac{c_{b1}}{t_{step}}\left(z_b - z_c\right) = \\ & \qquad k_{b1}\left(b_1 - \left(z_b - z_c\right)\right) + k_a.p_e\left(z_c - z_0 + d_e\right) \end{cases}$$

node g, (3.6.3):

$$k_{ms} \cdot n_4\left(z_t - z_g + d_{m4}\right) + k_{m3}\left(z_h - z_g + d_{ma3}\right) + \frac{c_{m3}}{t_{step}}\left(z_h - z_g\right) = k_{ms}.n_3\left(z_g - z_d + d_{m3}\right),$$

node h, (3.6.4):

$$k_{m3}\left(z_h - z_g + d_{ma3}\right) + \frac{c_{m3}}{t_{step}}\left(z_h - z_g\right) + \frac{c_{b3}}{t_{step}}\left(z_h - z_i\right) = k_{b3}\left(b_3 - \left(z_h - z_i\right)\right),$$

node j, (3.6.5):

$$k_a.p_3\left(z_{end} - z_i + d_{a3}\right) + k_{ta}\left(z_{end} - z_t + d_{ta}\right) + \frac{c}{t_{step}}.z_{end} = F_{end},$$

node k, (3.6.6):

$$k_{ms}.n_4\left(z_t - z_g + d_{m4}\right) + k_{tm}\left(z_t + d_{tm}\right) = k_{ta}\left(z_{end} - z_t + d_{ta}\right).$$

The positions of the left-hand end of the actin filament and the right-hand end of the cofilament at node k in Figure 3.6.1 require special consideration. The M-disc is the mid-point of the myosin cofilament, a line of symmetry in the sarcomere. As the sarcomere contracts and draws the free end of actin, z_{actin}, across the M-disc it will come into conflict with the actin filament being drawn in the opposite direction, on the other half-of the sarcomere, see Figure 1.1.2, c and Figure 2.1.1. At node *c*, Equation 3.6.2, the natural length of z_{actin} to the first actin connection, here c, is l_{ae} and the M-disc to the first actin connection is l_a. When l_{ae} is less than l_a, $k_a.p_e\left(z_c - z_0 + d_e\right)$ represents the extra load on actin.

When loading is such that the Z-disc is coincident with the end of the cofilament, node *k* and *j* are coincident: $z_{end} = z_t$, simplifying point *k*, Equation 3.6.6. A preload of $d_{ta} = -l_{ta}$ where l_{ta} is the natural length of titin protein parallel to the actin filament is required. Preloads are used to avoid discontinuities when transitioning between states

during individual time steps. In the titin instance $d_{ta} = (z_t - z_{end} + 2d_{ta} + l_{ta})$ and z_t equals or does not equal z_{end} depending on whether the final state of titin is completely compressed or not. In the actin case: $d_e = -l_{ae} + l_{a1} + z_c$. In the transitions between loaded to unloaded states $k_a.p_e\,(z_c - z_o)$ is removed from the node c equation and when transitioning between unloaded to loaded equation c is unmodified.

The components of the equations are organised into a stiffness and damping matrix [**A**], a matrix of displacements [**Z**] and a matrix of constants [**B**]. These are solved (using Matlab) to determine the unknown displacements at the key points in the structure, nodes a-j in Figure 3.6.1 for example:

$$[Z] = [A]^{-1}[B] \qquad (3.6.7).$$

If a displacement is applied at the end of the sarcomere (z_{end}), the matrices need to be reformulated to accommodate the extra information.

As the structure of the model is known, internal tensions can be calculated from the node movements and the force on the end of the sarcomere, should a displacement be imposed on it. If crossbridges are excessively loaded (Section 3.3.3), the model is re-evaluated with the most overloaded crossbridge removed until none are over-strained. If there is a rapid change in the myosin arm length and consequently its stiffness (Section 3.2.2), the model is re-evaluated over shorter time steps to capture the change.

The resultant displacements are used to re-plot the position of the filaments via their bond sites and record any remaining crossbridge strain energy. The generation of these data marks the end of a model time step, t_{step}, the beginning being the evaluation of the state of the bond sites see Appendix A. Over a number of model time cycles the tension in and movement of the actin filament can be plotted against time, Appendix A, Figure F. In more detailed plots the interaction and state of individual crossbridges can be plotted, Appendix A, Diagram G.

3.7 Titin - Passive Force.

3.7.1 Significant Characteristics.

Within the sarcomere several proteins have been identified which appear [1] to maintain structural order. The polypeptide titin is the dominant component in maintaining this structure and defining the rest length of the sarcomere. Titin has been associated with passive forces in the muscle, creep and hysteresis [93]. Passive forces are an important part of normal muscle function [1]. There are six titin's per myosin cofilament, running from Z-disc to Z-disc. Titin binds to the myosin cofilament along its length. Whilst in isolation titin has uniform stiffness along its length [93] this binding causes titin parallel to myosin to appear inextensible in comparison with that in line with actin. When stressed for extended periods, titin detaches bonds from the end of the myosin cofilament increasing the length of the more compliant component parallel to actin. The number of sarcomere in line appears to modify to maintain the preferred operating length of the individual sarcomere.

Burkholder and Lieber have collated experimental test data [1,9] for the operating lengths of sarcomere in a variety of species and muscle types with myosin and actin lengths. Measurements suggest [9, Fig.2] that some human muscles operate over small length changes and others over very large length changes. The operating length influences the range and rate of force change as sarcomere length changes. This is highlighted in the force-length profile generated by Gordon *et al* [94] and shown in Figure 3.7.1. The key features of which have been interpreted in the following manner: E to D actin-myosin progressively overlap increased number of crossbridges and therefore force, D to C actin crosses smooth mid-section of myosin, no additional crossbridges available, C to B ends of actin come into conflict, B to A actin filaments

overlap and disrupt crossbridge formation.

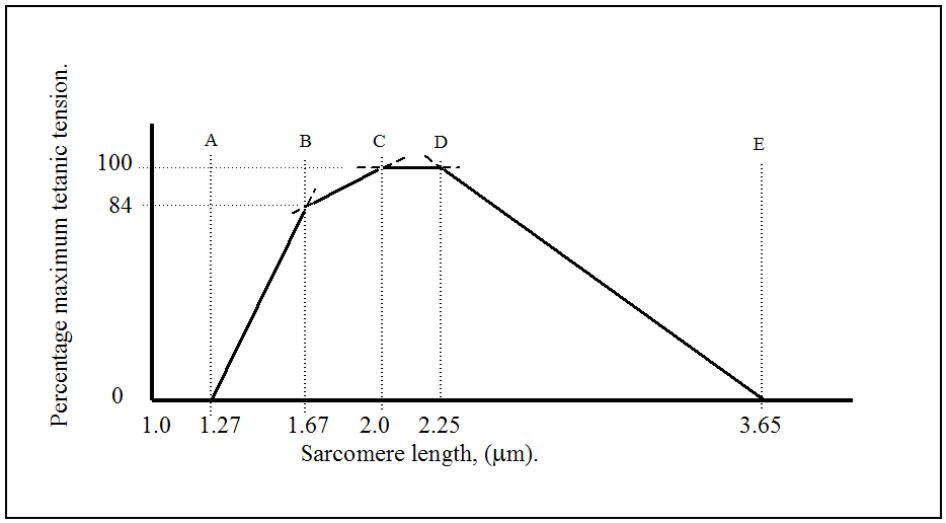

Figure 3.7.1, Force tension curve measured by Gordon, Huxley et al. values taken from their paper [94].

Consequently, the natural length of titin varies between muscles. The myosin cofilament is reasonably consistent in length 1.6µm [9]. Actin ranges between 0.95-1.27µm for human muscle, (1.9µm has been measured for the specialised muscles of the hummingbird). The most common actin length observed is 1µm. In addition to variations across muscle types, experimental variation is high, for the same muscle a factor of two variation, e.g. flexor carpi ulnaris, controlling flexure and abduction of the hand). Two examples of the types of value anticipated: gastrocnemius (calf) minimum to maximum sarcomere length 1.01 – 4.41µm, temporalis (jaw) 2.20 – 3.80µm. It is therefore difficult to specify a natural length without being muscle specific.

3.7.2 Modelling Titin in the Sarcomere.

In the model, a single connection is assumed between the end of the titin protein and the end of the myosin cofilament (point k in Figure 3.6.1). The stiffness assigned to titin in alignment with myosin is denoted by k_{tm} and that parallel to actin as k_{ta}.

In its simplest form, the model would have no crossbridges, this provides an opportunity to evaluate the remaining parameters in isolation. The remaining significant parameters are the stiffnesses of titin (k_{tm}, k_{ta}), myosin cofilament stiffness, the damping component and the natural length of the sarcomere. The equations describing this system are given by:

$$\begin{cases} l_{ae} - l_{a1} \geq 0 \\ l_{ae} - l_{a1} < 0 \end{cases}$$

$$k_{ta}\left(z_{end} - z_t + d_{ta}\right) + \frac{c}{t_{step}}.z_{end} = F\,, \qquad (3.7.1),$$

$$k_a \cdot p_e\left(z_c - z_0 + d_e\right) + k_{ta}\left(z_{end} - z_t + d_{ta}\right) + \frac{c}{t_{step}}.z_{end} = F \qquad (3.7.2),$$

$$k_{ms}.n_1\left(z_t + d_{m1}\right) + k_{tm}\left(z_t + d_m\right) = k_{ta}\left(z_{end} - z_t + d_a\right), \qquad (3.7.3).$$

3.7.3 Parameter Values.

In order to assign stiffness values to titin, the results of the examination of titin in rabbit muscle fibres by Wang *et al* [93] were considered. They determined the natural length of the sample sarcomere to be 2.2µm; under extension tension increased up to a yield point of 3.8µm. At 5.7µm extension a further drop in stiffness occurred. From their analysis, above 4.5µm extensions the network around the sarcomere (components not modelled) increasingly contributed to the myofibril's overall stiffness.

This provides enough information to approximate the stiffness of titin. The given yield tension per cofilament estimated from a myofibril cross-section [93] was 1.53 x 10^{-10}N over a displacement of 1.3µm. With six titin polypeptides per myosin a stiffness of 5.89 x 10^{-5} N/m for k_{ta} in the model was derived. Titin parallel to myosin was taken as relatively inextensible and so k_{tm} was set equal to k_{ta} due to the relatively high myosin cofilament stiffness.

There are indications (rabbit studies) that fast and slow isoforms of titin exist due to variations in resting tensions [17]. This may be a result of attachment methods as the Z-disc decreases in thickness (an additional passive component not considered in this level of modelling) in faster fibre types [95].

3.8 Summary of Chapter 3

In this chapter the structure and function of the half-sarcomere has been presented in parallel to a description of the model of a half-sarcomere fragment. A representation

has been given of the key structural components of the sarcomere: titin proteins which maintain structural order and actin filaments and myosin cofilaments which interact to generate and transmit contractile force to the ends of the sarcomere. Particular focus has been placed on the characteristics of individual crossbridges, specifically the chemical cycle, the geometric alignment for bonding and the generation of mechanical output. How these components are brought together in the Matlab model is outlined in Figure 3.8.1 and the key sub-components are shown in Appendix E.

The model has a large number of parameters, tabulated in Appendix B. In the published literature, there is a high degree of confidence attached to some values, e.g. the longitudinal myosin arm stiffness, whilst other values are not easily measured and so are imprecise or cannot, as yet, be measured. By restricting the model to a single crossbridge and pre-, post- or levering states the modelling mechanisms and parameters could be tested against in vitro single crossbridge experiments. By this method, stiffness parameters were assigned to the myosin S1 component and those defining the energy release of the crossbridge with good alignment to the in vitro data.

In the next Chapter, the individual components of the model are bought together at the filament/sarcomere scale. The interaction of crossbridges and external loading will allow parameters such as the strain dependency of reaction rates, which have not, as yet, been assigned values in the model to be evaluated and the model to be tested against a different set of in vitro data.

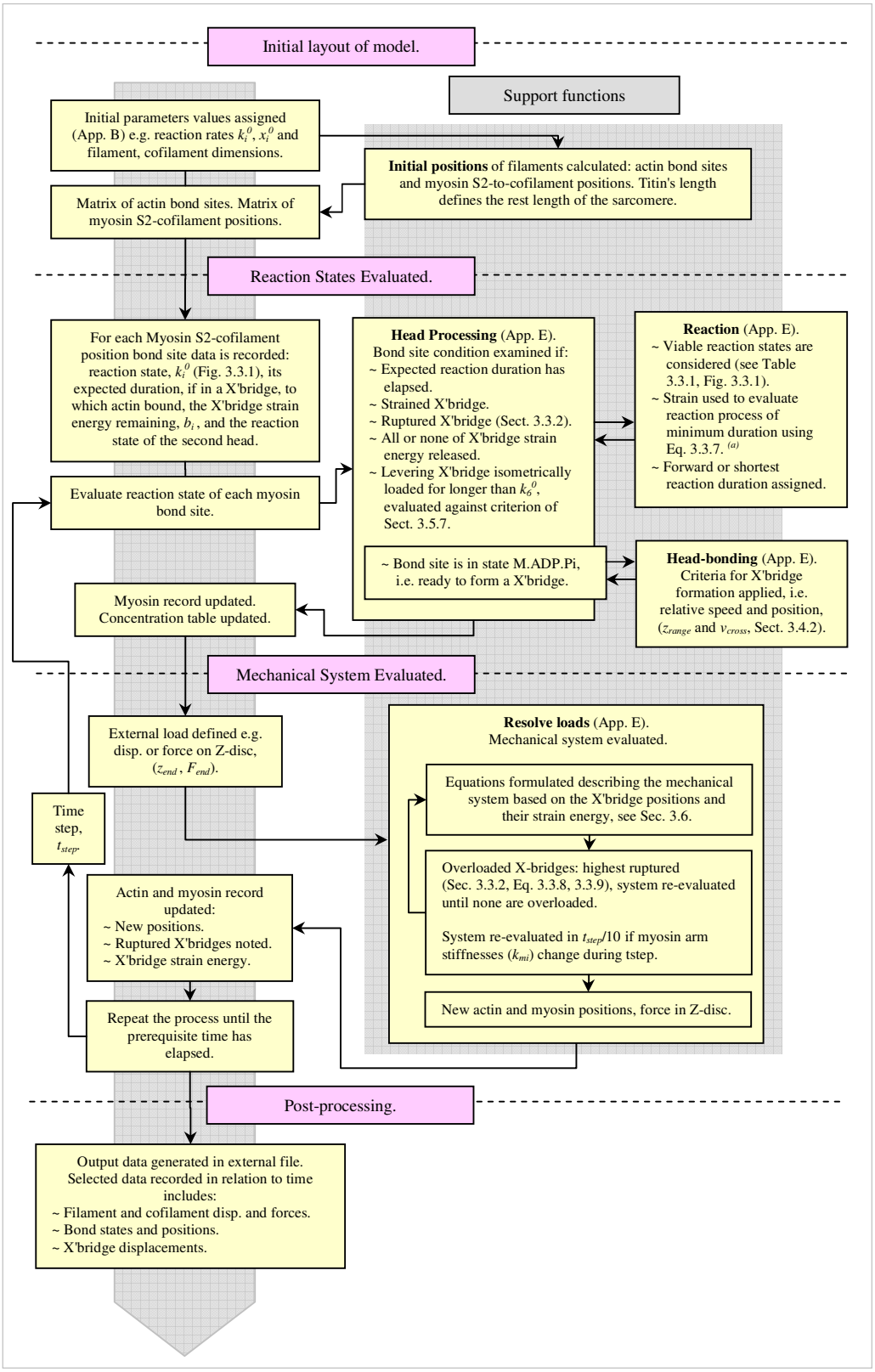

Figure 3.8.1, Schematic of the processes used in the Matlab model. Individual schematics of functions HeadProcessing, ReactionRate and ResolveLoads are given in more detail in Appendix E. (a) Equation 3.3.7 has concentration and temperature components which were not explored in the Baseline Model. For examples of output data see Figures 4.4.8, 4.4.7 and 4.7.6.

Chapter 4

4 Filament Motility and Force Generation

4.1 Introduction

In Chapter 3, the Baseline Model has been described in stages where particular focus was placed on modelling and defining the parameters of a single crossbridge. The contraction and force generation of the half-sarcomere filaments requires the combined input of multiple crossbridges. Some parameters are dependent on the interaction of those crossbridges, e.g. strain dependent reaction durations and others may help define it, e.g. the compliance of myosin II, S2, in compression. Therefore, within this chapter, the interaction of multiple crossbridges between a single actin filament and a myosin filament are considered in a series of numerical experiments that relate to two extremes of muscle action: a concentric contraction (low load high displacement) and an isometric contraction (high load, no displacement). In a concentric contraction, the energy from the crossbridges translates to longitudinal displacement of the actin filaments across the myosin cofilaments. This corresponds to a shortening of the sarcomere the base contractile unit of the muscle where M- and Z-discs are drawn together (Figure 2.1.1). An isometric contraction sees the discs unable to move and the crossbridge energy is expressed as force.

The reported speed of filament movement [10,59,91] is inconsistent with the short lever distance and long attachment times of individual crossbridges as discussed in Section 3.3.2. Therefore the initial investigation in this chapter focuses on the pre-lever reaction process as it dominates the crossbridge attachment time. The strain dependent duration of the pre-lever state, the criteria for crossbridge formation and crossbridge release due to spatial restrictions were investigated. The results from this study are then compared against the results from two in vitro experiments reported in the literature in order to evaluate the overall performance of the model. Isometric loading is considered in relation to strained pre-lever reaction rates. Finally, the sensitivity of the parameters is explored and considered in terms of isoforms and fibre types.

4.2 Experimental Method for the Study of Filament Motility and Force.

For these investigations, the Baseline Model of the half-sarcomere sub-fragment was used (Section 3.2.2). The model was composed of a composite myosin cofilament, half an actin filament and a composite titin protein, all aligned and acting in parallel (see Appendix A, Figures A and D). In order to compare the model to published motility data (Section 2.2), where an actin filament traverses myosin cofilaments and fragments bound to a substrate, the model was modified. In the model, the left hand end of the actin filament was allowed to move freely, the M-disc did not impede its movement (see Figure 2.1.1).

The parameter values identified in Chapter 3 (tabulated in Appendix B, Table 1-4) were used in the Baseline Model with the following exceptions, clarifications and additions:

- Actin filament half-length: 1μm (Identified in Section 3.7.4).
- Myosin cofilament length: 1.6μm (Identified in Section 3.7.4).
- Myosin smooth mid-section: 0.2μm [50].
- Actin bond-site-to-actin-bond-site length, A_{head}, 38.5nm [50].
- Sarcomere damping, c, was set to zero as the component is not present in motility studies (Section 2.2).
- The default stiffness assigned to the protein titin was: parallel to actin 6 x 10^{-7}N/m/s and parallel to the myosin cofilament 6 x 10^{-7}N/m/s (k_{ta} and k_{tm} respectively). For comparison with biological motility data both values were set low compared to the values previously assigned to them (Section 3.7.1). k_{tm} is low compared to the myosin cofilament stiffness to remove its influence as titin is not present in the motility studies. k_{ta} is assigned a lower magnitude to minimalise the restoring force on the actin filament, effectively the load resisting the actin filament's displacement.
- The length assigned to the titin protein was 3.85 x 10^{-7}m. This length positioned the actin filament such that two initial crossbridges formed with approximately ten actin bond sites overhanging the myosin cofilament to the right.
- The range of electrostatic attraction, z_{range} (Section 3.4) the distance between bond sites below which they are considered for crossbridge formation: 2.2x10^{-22}m. In preliminary models, this parameter caused small actin filament displacements as actin and myosin bond sites were drawn into alignment. In

some instances, the accumulated effect on the actin filament's displacement without the input of levering crossbridges was quite significant. The small value used allowed crossbridges to form but minimised that displacement input.

- The maximum relative speed of crossbridge bond sites, v_{cross} , (Section 3.4) above which the sites will not form a crossbridge was initially set at 10m/s, a value far greater than the maximum filament motility speeds in order to remove its influence. Its significance is examined in Section 4.4.8.
- Temperature = 310^{o} Kelvin based on a normal human body temperature (37^{o}C). Temperature is treated as a constant and is not explored.
- Chemical concentrations have not been studied within this project. The input of ATP and expulsion of phosphate and ADP are recorded but the availability and removal of by-products is not constrained. The remaining parameters were set to those defined in the previous chapter.
- The unstrained reaction rates, k_i^0, are taken from Table 3.3.1. These rates are per second for multiple events in solution. The duration of a reaction stage is taken as the inverse of these values.

4.3 Filament Motility: strain independent reaction values.

In the parameter values extracted from the published in vitro data a commonly recognised [10] inconsistancy was observed. A single crossbridge displacement is ~7.9nm, the attachment time of a crossbridge according to ATPase assays (Section 3.3, Table 3.3.1) is ~34ms which gives a maximum velocity of about 0.23μm/s when in vitro experiments have shown unloaded filaments travel at speeds up to ~8μm/s [59,90,91] and muscle contraction's speeds are of the order 6-7 μm/s [10].

From the work described in Section 3.5, the lever distance is consistent with that from other work therefore the slow crossbridge duration was studied using the model described in this thesis. The crossbridge forms in reaction stage k_4, where M.ADP.Pi binds to actin forming the crossbridge (Figure 3.3.1) where a myosin bond site finds and binds to an actin bond site. The strain independent duration of this is ~33ms obtained from in vitro solutions of actin and myosin fragments (Section 3.3.3). In the sarcomere where the movement of the actin filament presents its bond sites to the myosin bond sites in a systematic way the time taken to find a pairing would be

shorter than random fragments in the 3-d space of an in vitro solution. Therefore, as an apparently dominant component of the attached time, the pre-lever reaction k_4 was examined by reducing its duration (increasing its reaction rate). As the reactions were strain independent they could not go into reverse.

In Figure 4.3.1 model data for the displacement against time of the right hand end of the actin filament are plotted for different durations of reaction stage k_4. The filament moved in steps, which settled, over time, into a pattern that roughly repeated (Figure 4.3.1 inset). The step duration decreased as pre-lever times decreased, increasing the filament's speed. As k_4's duration decreased below ~2.5ms the filament displacement became unstable: after a short distance no new crossbridges formed to replace those that had released and with no crossbridges remaining the restoring force of titin drew the filament back to its initial position.

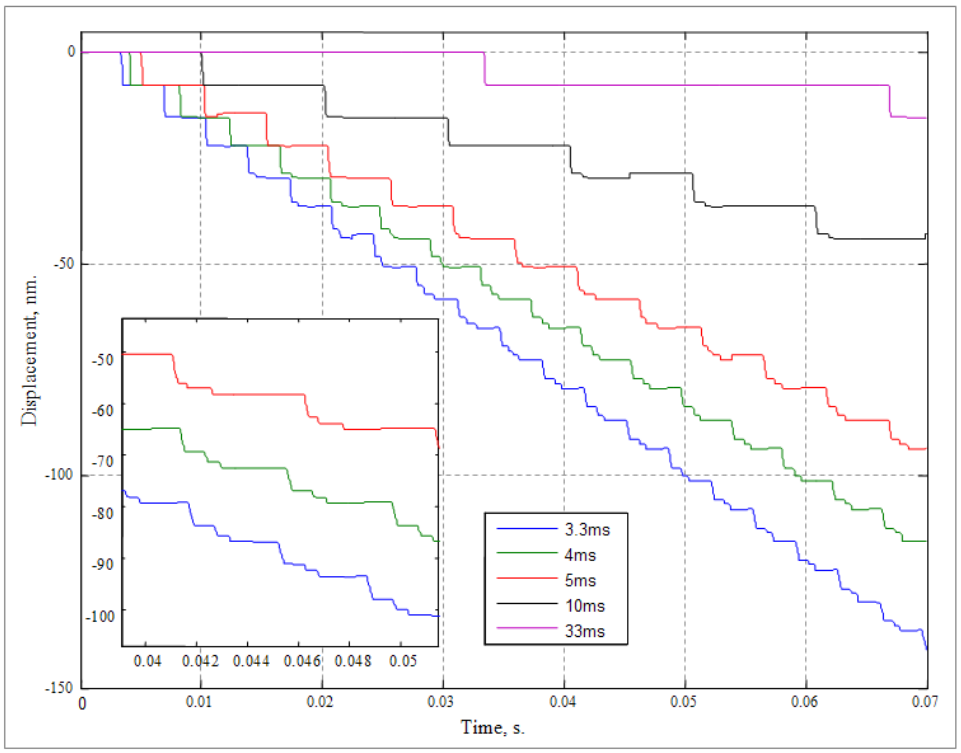

Figure 4.3.1, Results from the Baseline Model; displacement of the right-hand end of the actin filament over time showing the influence of the pre-lever reaction's duration. The inset window shows an enlargement of the 40 to 50 msec of movement, k_{ta} set at 0.06 x 10^{-5}N/m.

In order to consider the involvement of k_4 in the filament movement the repeat pattern of behaviour was examined in more detail. Figure 4.3.2 plots the position and reaction state of each bond site and crossbridge against time for k_4=300s^{-1} (3.3ms duration) (filament speed = 2µm/s) between 38-52ms after the model has started (the displacement is shown in the inset of Figure 4.3.2). To understand the contribution of

the reaction stages to the overall movement the position and reaction state of each of the bond sites and crossbridges were plotted against time. The *x*-axis aligns longitudinally with the actin filament. Diagrams B and the enlargement C show the longitudinal positions of the actin (solid grey lines) and myosin (blue dashed lines) bond sites (*x*-axis) against time (*y*-axis) as bonds are created and broken. B shows the full length of the actin and myosin filaments. Zero on the *x*-axis aligns with the M-disc. Each bond site is colour coded depending on its reaction state (D). The final positions of the bond sites on the actin filament are shown as black crosses on a black line representing the actin filament's final position (B).

Figure 4.3.2 C shows multiple crossbridges lever at the same time e.g. (2) and (3) having the displacement of a single crossbridge in this low load situation. Distortion of the myosin cofilament was minimal as it is stiff compared to the actin filament and myosin arms. With a long pre-lever duration a crossbridge can travel a large distance as the actin filament is moved on by other crossbridges before it expresses its strain energy. Its lever distance then becomes ineffectual in propelling the actin forward and puts energy into straightening the myosin arm it is attached to (E). During the crossbridge the blue-dashed line indicates the relaxed arm, S1-S2, position this allows the displacement of the crossbridge from its initial formation to be seen. Figure 4.3.2, C shows all of the crossbridges losing movement in this way with (1), (4) losing the majority of forward displacement.

Similar plots showed that as the pre-lever was shortened below ~2.5ms the duration of the levering stage, k_6, (Figure 3.3.1) came to dominate the attachment cycle and the crossbridges went into equilibrium with the forces in the actin filament. The pattern and timing of the release of these crossbridges became dependent on the probability and chance model described in Section 3.5.7.

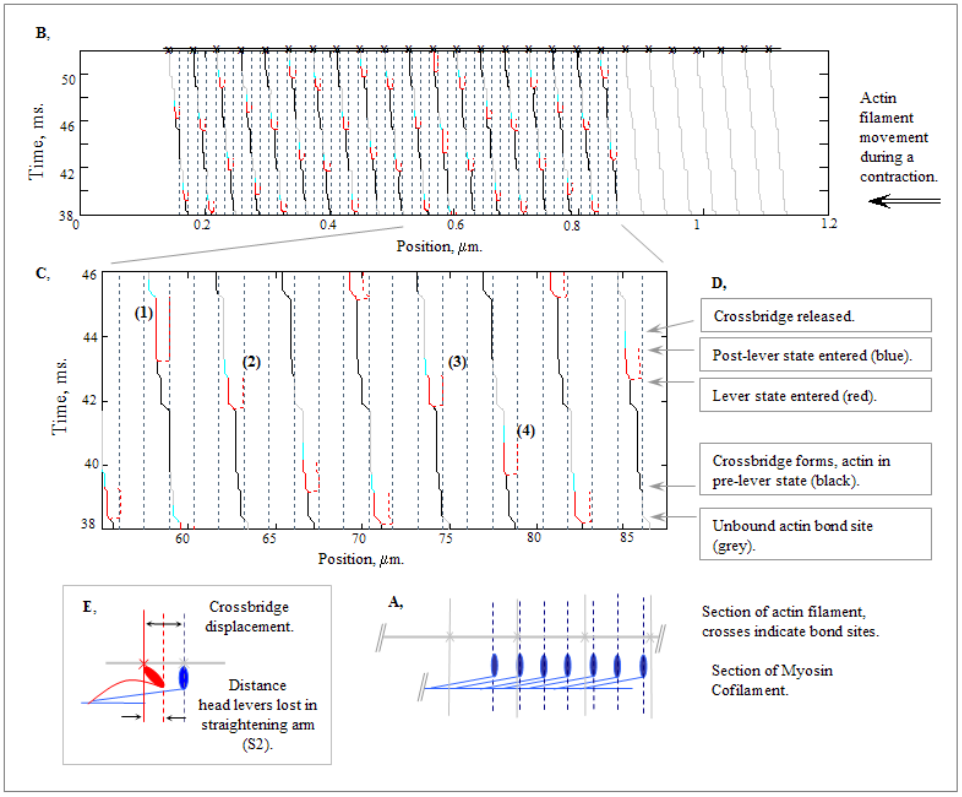

Figure 4.3.2, The position and reaction state of individual crossbridges during the repeat cycle of behaviour observed in Figure 4.3.1. $k_4 = 300s^{-1}$ (3.3ms duration). Reaction states: actin site unbound (grey), pre-lever (black), levering (red), post-lever (blue). Myosin bond sites (dashed blue) marks the S2-S1 junction if the arm was relaxed this allows the crossbridge displacement from its natural position to be gauged (E). The distance between the red and dashed red markers indicates the lever distance of the crossbridge (E).

4.3.1 Motility with Strain Independent Reactions: conclusions.

As discussed in Section 4.1 the pre-lever reaction time has a dominant influence on filament speed. If shortened a modest amount the speed increased (2μm/s, k_4= $300s^{-1}$ (3.3ms duration)) but if over shortened the persistence of movement was lost, the actin filament stopped moving forward and the restoring force of titin returned it to its start point. Stability may not be necessary in a sarcomere where multiple filaments work together but observations made during in vitro motility [91] studies show filaments of 1μm length can maintain movement with much higher speeds (6-7μm/s). The overall filament displacement generated per crossbridge seemed inefficient: crossbridges levered together and travelled long distances in pre-lever states potentially straining against the forward movement of other crossbridges and losing their lever input to straightening their myosin arm. To investigate these characteristics further and better match the observed data, strain dependent pre-lever reactions were applied to the

Baseline Model. These had the potential to provide long strain free times consistent with in vitro reaction data but short attachment times during motility.

The unattached reaction cycle (Section 3.3.3) will not be considered at this time; an assumption is made that the in vitro measurements of individual fragments in solution in this strain free state are representative of those in the sarcomere. In addition, the system has been modelled with two heads per myosin arm (Section 3.2.9). As the first myosin bond site releases from a crossbridge the second myosin head has had time to go through the unattached reaction stages and was then available to bond.

4.4 Filament Motility: strain dependent pre-lever reaction rates.

In this section the question posed in Section 4.3 was pursued: how to reconcile filament speed, lever distance and a long crossbridge attachment time. In Section 4.3, it was shown that shortening the pre-lever time increased speed but over-shortening failed to sustain movement. Taking the Baseline Model as described in Section 4.2 for the strain independent pre-lever study of Section 4.3, a study was performed of the strain dependent pre-lever time's influence on filament motility and the efficiency of crossbridge usage within that movement.

4.4.1 Experimental Set-Up.

In order to reduce the number of parameters influencing the pre-lever reaction the model configuration was simplified. The pre-lever reaction incorporates two reaction stages, the initial binding k_4 and k_{-4} (unstrained values of $30s^{-1}$ (33.3ms duration) and $300s^{-1}$ (3.3ms duration) respectively) and the release of a γ-phosphate, k_5, ($\geq 10^4$ s^{-1}) after which the release of ADP initiates the onset of levering, reaction k_6, (Section 3.3, Figure 3.3.1). The phosphate release stage, k_5, was treated as a strain independent linkage step due to its short duration and the evidence that it does not influence motility if chemical concentrations are held constant (Section 3.3). The value of k_{-5} was set equal to that of k_5. In solution, k_{-5} is not considered a viable path but in some in vitro experiments it appears to occur (Section 3.3). Here it is assumed a path of short duration; its presence allows the levering crossbridge to reverse into a pre-lever state and release without rupturing. If a crossbridge formed, the reaction automatically

cycled through k_5 to the lever reaction stage (k_6). If the lever reaction stage was reversed (k_{-6}), the system cycled though k_{-5} and returned to k_4/k_{-4} (Figure 3.3.1).

Simplifying the pre-lever reaction cycle in this way reduced the strain dependent reaction parameters to the reaction rates at zero tension, k_4^0 and k_{-4}^0, with units s^{-1}, and the characteristic bond lengths x_4 and x_{-4}, which have fixed values that shape the strain dependency of the reaction equation. The strain dependent reaction, Equation 3.3.7 in Section 3.3.2 specified for the forward pre-lever reaction is:

$$k_4 = k_4^0 \exp\left[\frac{Fx_4}{kT}\right], \qquad (4.4.1).$$

4.4.2 Parameter Values and Performance Gauges.

Consideration of potential positive crossbridge properties and the strain free reaction times guided the range of values examined for k_4^0, k_{-4}^0, x_4 and x_{-4}, and the results measured. In the Baseline Model, the reaction direction was selected by the shortest reaction time. The shortest time was used as an indication of the easiest path to follow. If other points of evaluation were equal, the forward reaction would be selected. In the Baseline Model in the filament's initial, relaxed state, the strain on the first crossbridges to form was zero. To avoid losing those crossbridges and consequently failing to get the filament moving, forward and reverse pre-lever reactions (k_4 and k_{-4}) were assigned the same zero strain values.

In Section 4.3 a similar pattern of behaviour developed for k_4^0 reaction rates that had a duration lower than 33ms (the in vitro value) but greater than 2.5ms and as the sarcomere system is a 1-d structure rather than a 3-d solution of fragments (Section 4.3) $k_4^0 = k_{-4}^0 = 100s^{-1}$ (10ms duration) was used in the strain dependent study. This shortened the model processing time, as many iterations were required. Filament motion was monitored for 0.1s as for a value of $k_4^0 = 100s^{-1}$ the strain independent movement settled into the repeat pattern of behaviour shown in Figure 4.3.1 within this period of time. Filament motility was evaluated as the displacement over time of the right-hand end of the actin filament.

Multiple crossbridges levering together during low load filament displacement and large movements of pre-lever crossbridges (Section 4.3) is inefficient in terms of the

use of energy (ATP) therefore this was considered in the strain dependent reaction study. Efficiency was quantified as the mean displacement per ADP released into the system calculated from by the total filament displacement divided by the total number of ADP molecules released. ADP rather than ATP was used as ADP marks the onset of the lever event, the inputting of strain energy into the system, avoiding issues with failing to capture the whole reaction cycle, e.g. loss of crossbridges post-lever but pre-ATP release. Comparably in vitro motility assays are commonly halted and phosphate, which precedes the ADP release, concentrations are used to quantify the ATPase rate [91,96].

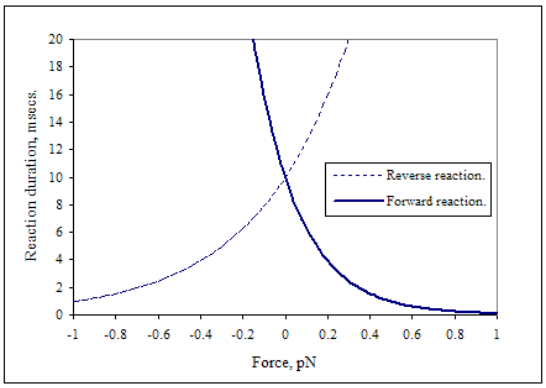

Figure 4.4.1, Dependency of pre-lever reaction duration (the inverse of the reaction rates k_4 and k_{-4} s^{-1}) on the force applied to the crossbridge. Positive force opposes the crossbridge lever and contraction direction. The model favours the reaction path of shortest duration. The forward reaction, k_4, solid line, is favoured when the load is positive as it is of short duration in comparison to the reverse reaction, k_{-4}, dashed line. Under negative loading the reverse reaction is favoured.

To counter a positive load on a filament, one opposing contraction, increasing the number of crossbridges releasing strain energy (levering) would be desirable. Assigning a positive value to x_4 in Equation 4.4.1 increases the reaction rate of k_4 (s^{-1}) and therefore reduces the reaction duration (s), shown in Figure 4.4.1, transitioning crossbridges into the levering state (k_6) more quickly. Alternatively, if the force on a crossbridge is negative the crossbridge is being pushed in the direction of, and potentially hampering, the contraction. Such pre-lever movement would reduce the effectiveness of the levering crossbridge (Section 4.3). In the model the reaction path of shortest duration is favoured. By applying a negative value to x_{-4} the reverse pre-lever time can be rapidly reduced such that it becomes more favourable than the forward reaction and the crossbridge is released, Figure 4.4.1. k_4^0 and k_{-4}^0 having unstrained values of 30 and 300 s^{-1} respectively indicated the magnitude of x_{-4} should be larger than x_4 to generate a shorter attachment time at lower strains. Based on these observations and the initial results from the Baseline Model the range of values

examined using the Baseline Model were 0 to 80nm for the forward reaction, x_4, and 0 to –125nm for the reverse reaction, x_{-4}.

4.4.3 Motility: results of the pre-lever parameter study.

A selection of displacement results from the Baseline Model are plotted in Figure 4.4.7. For each result of this type the overall filament speed and efficiency was recorded (matrices 1 and 2 of Appendix C). Trends in these data will be reviewed followed by a more detailed examination of individual results to understand the underlying crossbridge movements.

Figure 4.4.2 plots filament speed in response to the modification of forward and reverse pre-lever reaction's durations by varying the parameters x_4 (forward) and x_{-4} (reverse), see Sections 3.3.2 and 4.4.1. Increasing x_4 (highlighted in Figures 4.4.3) increased filament speed. As the value of x_4 increased, the optimum value of x_{-4} decreased as can be seen in Figure 4.4.2 by a diagonal ridge of higher speeds. The benefits of increasing the forward reaction plateaued at x_4 ~100nm (Figure 4.4.3). Figure 4.4.2 also highlights speed was more sensitive to the forward reaction.

These trends in x_4 and x_{-4} to achieve higher filament speeds correspond to shortening the forward pre-lever reaction time and proportionally lengthening the reverse reaction time (k_4 and k_{-4} respectively). The positively loaded crossbridges lever more quickly and negatively loaded crossbridges take a longer time to release. Filament speeds increased from a strain independent 0.65μm/s to 1.24μm/s ($k_4^0 = 100s^{-1}$ (10ms duration), x_4 = 100nm, x_{-4} = -50nm).

In Figure 4.4.5 and 4.4.6 the influence of x_4 and x_{-4} on the displacement per ADP released, efficiency, is plotted. x_4 is the dominant factor; efficiency rises with x_4 and appears to plateaux at 60nm and decreases with a decrease in x_{-4}. Peak values of 1.55nm/ADP with x_4 = 40nm and x_{-4} = 0nm were an improvement on the strain independent rate of 0.9nm/ADP.

Anomalous points in the efficiency data were identified at x_{-4} = -125nm, x_4 = (0,5,10,15,25)nm (inset of Figure 4.4.5). Comparison of these results to those at x_{-4} = -100nm showed a greater number of pauses in motion, reduced numbers of concurrent crossbridges and a greater tendency for the filaments to slip and be drawn backwards

by the restoring force of the titin. This indicated levering events were poorly distributed in time and the low number of crossbridges, although putting more into the filament movement had reduced the stability of motility. Increasing x_4 above 25nm appeared to stabilise the movement.

During the experiment, two issues were identified. As x_4 was set higher than 30nm the model showed an effect best described as 'scissoring' of crossbridges. A crossbridge moved so far to the left before releasing that the myosin bond site to its right bound to the actin bond site to its left. The release of these crossbridges caused the equation sets in the model to be incorrectly formulated. Initial model assumptions were that the close packing of the actin myosin filaments in the sarcomere, deduced from x-ray crystallographic data, would inhibit this degree of movement. However there was no constraint in the model to prevent this occurrence. Actin filaments interacting with a myosin cofilament on a single basis may have more room to allow for this behaviour. Here a model rule was introduced that should a crossbridge travel more than a percentage of the distance between actin bond sites it was broken, forced away by the limited space. For the reaction study, this percentage was set at 95%. The effect of this value is examined in Section 4.4.7.

Not all filaments maintained movement. When the number of crossbridges dropped to zero the actin filament returned to its initial position under the restoring force of titin. These runs were repeated without slippage occurring.

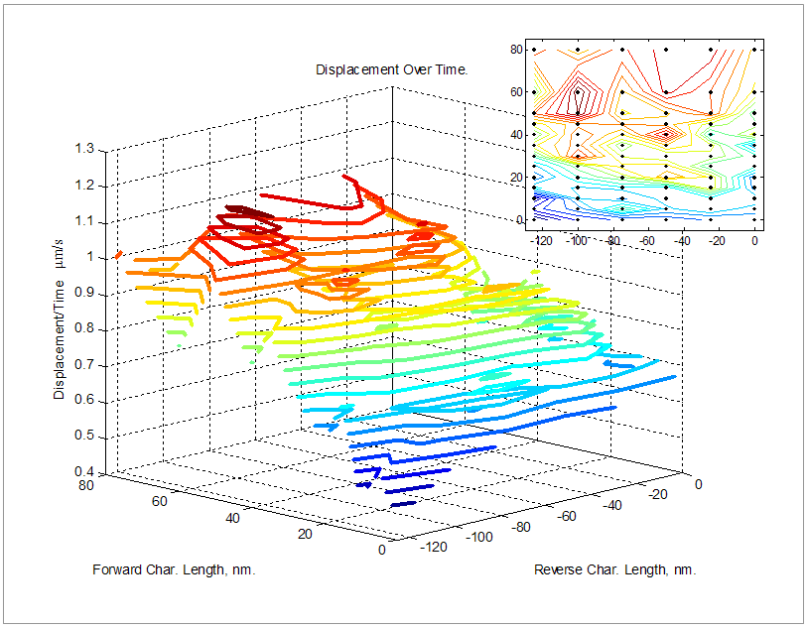

Figure 4.4.2, Displacement over time in response to variation in pre-lever reaction character lengths, x_4 and x_{-4}. Note the model convention is negative movement is contractile here contraction has been plotted as a positive.

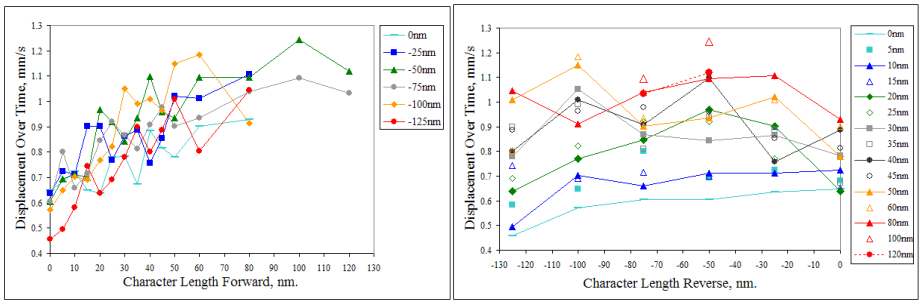

Figure 4.4.3 (left), and Figure 4.4.4 (right), Trend in displacement over time with variation in pre-lever forward reaction and pre-lever reverse reaction. Note the model convention is negative movement is contractile here contraction has been plotted as a positive.

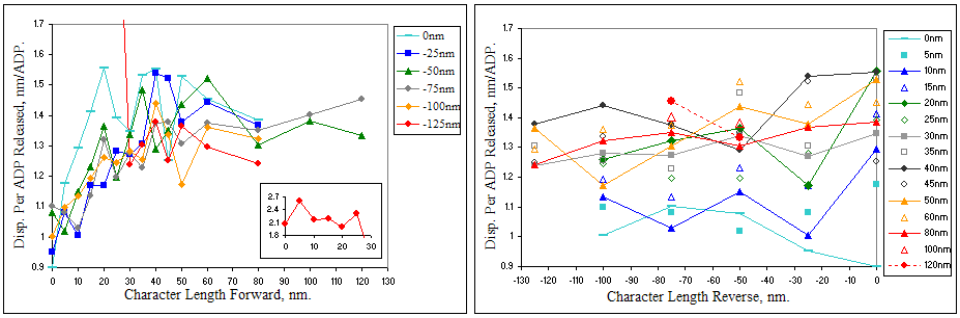

Figure 4.4.5 (left), and Figure 4.4.6 (right), Trend in displacement per ADP released with variation in pre-lever forward reaction and pre-lever reverse reaction. Note anomalous group of points not plotted in Figure 4.4.6.

4.4.4 Examination of Crossbridge Interactions.

To understand the impact of the parameter changes of Section 4.4.3 the filament movements with strain independent reactions and strain dependent reactions for a faster filament (blue and black lines respectively in Figure 4.4.7) were studied in detail by plotting the crossbridge behaviour between 0.08 and 0.1s (Figure 4.4.8).

In Figure 4.4.8 upper, the long strain independent pre-lever times can be seen (black) followed by the lever events (red) inputing strain energy into the system at similar times. The expression of this is the rhythmic filament movement seen in Figure 4.4.8 (blue line). In comparison, the strain dependent result has an uneven distribution of movements. Examination of the crossbridges (Figure 4.4.8 lower) shows a wide distribution in the duration of pre-lever times (black) and a greater distribution in the timing of lever events (red).

In Figure 4.4.8 lower crossbridges of short duration are grouped predominantly in the centre of the filament where, in the preceding time period, the number of crossbridges was sparse. To the right, the constrained end of actin, the crossbridges are of long duration. To the left, towards the free end of the actin filament, the crossbridges are, again, longer in duration. Consideration of the strain in the filament explains this distribution. As the filament moves to the right, tension builds up in the left end as the protein titin resists movement. To the right the filament is pushing against the far right crossbridges putting the filament into compression. Both characteristics will extend the pre-lever reaction time but combined they create a net load to the right on the centre of the filament accelerating the forward pre-lever reaction (Figure 4.4.1). Crossbridges to the left are in the pre-lever state longer than 10ms (k_4=100s^{-1}), e.g. actin site 17 was > 15ms indicating the pre-lever state is drifting between forward and reverse reactions. The load due to the titin and the resisting opposing crossbridges to the left of the filament only impose a low strain so the reaction direction will be sensitive to changes in the direction of loading (Figure 4.4.1). In Section 4.4.9 the profile of crossbridge attachment times are examined.

Three samples of filament movement with strain dependent reactions (Figure 4.4.7 from black line: insets A, B and C), were examined in terms of the crossbridge behaviour (Figure 4.4.8 lower) in order to identify some of the benefits and losses due to the strain sensitivity.

The levering of site 4 at ~0.0913s is opposed by three crossbridges to its left but the lever only has to work against the low stiffness of the myosin arms so they are pushed to the left when site 4 releases its strain energy. A movement of 6.18nm goes into the forward filament movement and the remainder straightens site 4's myosin arm: it has moved since it formed. Before this lever completes sites 7 and later 10 contribute 1.04nm and 1.02nm displacement respectively combining to give the displacement step of 8.23nm shown in Figure 4.4.7, A. Much of site 7 and 10's potential displacement is lost when site 4 lever moves them to the left before they lever. In Figure 4.4.7, C at ~0.0973s the filament slips backwards as crossbridges at actin sites 11 and 16 are released. The backward slip is limited by crossbridges at actin sites 7 and 10, which in pre-lever, slip back to their initial formation position were the myosin arm is fully extended and therefore its stiffness is high, limiting further movement to the right. The long pre-lever states and longitudinal stiffness of the myosin arms are seen to stabilise the filament's movement against the restoring force.

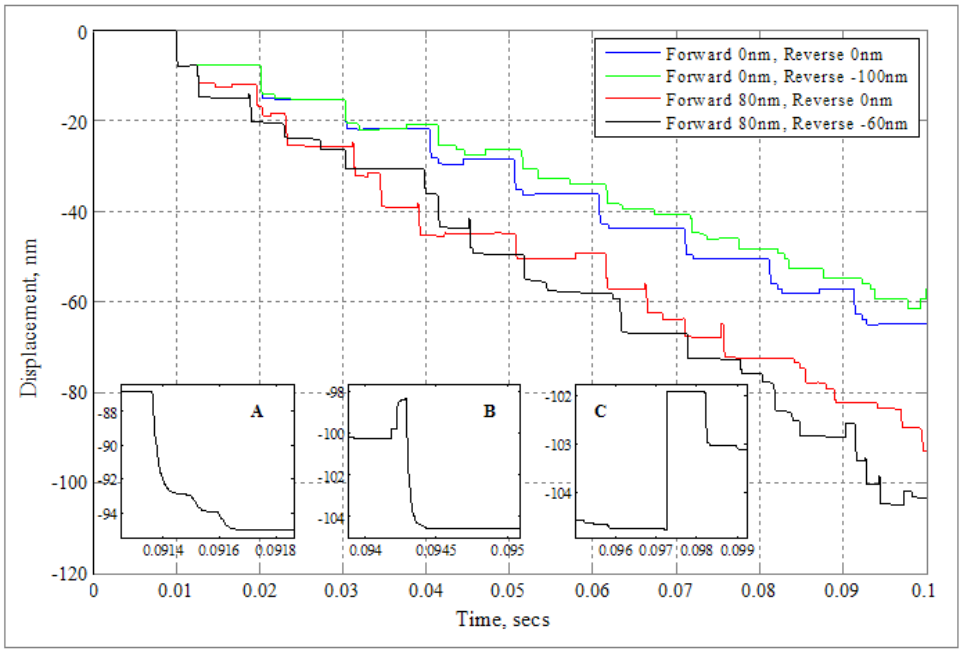

Figure 4.4.7, Displacement over time of the right-hand end (Z-disc) of an actin filament for a selection of pre-lever reaction settings (x_4 and x_{-4}). The Forward 80nm, Reverse –60nm path is shown enlarged in the inset plots A-C. Negative displacement as actin moves to the right. Displacements over time: 0.725, 0.648, 1.052, 1.062 μm/s.

In Figure 4.4.7, B, a backward slip occurs in the plot of the right-hand (Z-disc) end of the actin filament. The mid-section of the actin filament is in compression. When actin sites 9 and 12 release (Figure 4.4.8) the actin filament is able to release some of that compressive force by moving towards the right, which has less resistance than the left,

resulting in a backward movement of the Z-disc end of the actin filament. The levering of site 8 recovers this lost displacement 1.91nm and moves the filament on 4.28nm (totalling 6.19nm). Site 13 levers at the same time but has travelled so far while attached it contributes nothing to the movement. Crossbridges at actin sites 13 and 15 release before levering this potentially saves energy particularly as site 15 clearly moves so far to the right its levering would not propel the filament forward, movement would be lost in straightening its myosin arm.

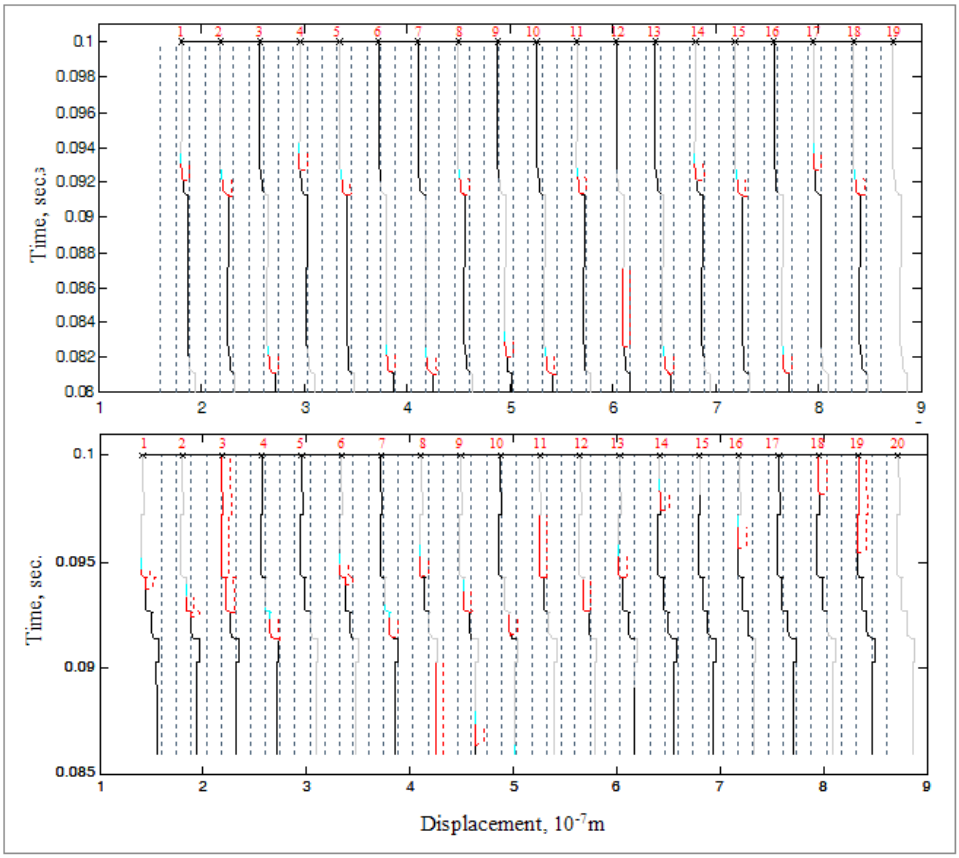

Figure 4.4.8, Crossbridge behaviour during displacement over time as shown in Figure 4.4.7. The top plot shows the strain independent run 0.08 to 0.1s and the bottom the crossbridge movements between 0.086 and 0.1s for the strain dependent pre-lever reaction rates set with character lengths of forward 80nm and reverse –60nm.Actin bond sites are identified by the red numbers. For a key to this plot see Figure 4.3.2. All of the myosin bond sites are plotted but further actin bond sites, to those shown, are present towards the right.

4.4.5 Random Variation in the Model.

To avoid the stagnation of levering crossbridges that were unable to progress to completion or reverse, a means of release was incorporated in the Baseline Model (Section 3.5.7). This model property has both a random time and strain dependent component in order to emulate in vitro observations. Examples of the release of these

levering crossbridges can be seen in Figure 4.4.8 indicated by the absence of the post-lever reaction (blue). In the upper plot one levering crossbridge diffuses away whilst four levering crossbridges diffuse away in the lower diagram. Multiple model results with fixed initial parameter values show this characteristic had a significant influence on motility. In Table 4.4.1, multiple model runs with two sets of parameters were considered. The increased range of values between result sets (3) and (4) indicated the lever component became more significant as the rate of displacement increased. Efficiency maintained a similar range of behaviour.

Table 4.4.1, Variation in individual results: the mean values of multiple runs with common parameter values. $k_4^0 = k_{-4}^0 = 100s^{-1}$ (10ms duration).

		Peak Force (pN)			Impulse to Peak Force (10^{-14} Ns)			ADP Released to Peak			Time to Peak Force (m)			Disp'ment 0 to 0.1s (nm)			Disp/ADP Released 0 to 0.1s (nm/ADP)		
		Mean	Max.	Min.	Mean	Max.	Min.	Mean	Max.	Min.	Mean	Max.	Min.	Mean	Max.	Min.	Mean	Max.	Min.
(1)	Every third myosin bond site blocked. x_{-4} = -60nm, x_4 = 80nm. Five runs.	14.54	20.79 + 43.0%	9.24 -36.4%	2.49	4.16 + 66.9%	0.82 -67.1%	5.2	7 + 34.6%	3 - 42.3%	8.46	10.92 + 29.1%	2.8 -67.3%	93.7	97.8 + 4.3%	86.5 -7.8%	1.85	1.69 + 6.5%	1.58 -8.6%
(2)	All sites available. x_{-4} = -75nm, x_4 - 10nm. Four runs.	14.34	18.76 + 30.8%	6.81 -52.5%	3.30	5.19 + 57.2%	1.63 -50.7%	5.3	7 + 33.3%	4 - 23.8%	8.91	12.33 + 38.4%	4.79 -46.2%	64.0	68.1 + 6.45%	61.5 -3.8%	1.57	1.62 + 2.89%	1.48 -5.95%
(3)	Every third myosin bond site blocked. x_{-4} = -75nm, x_4 = 10nm. Four runs.	26.05	30.20 + 16.0%	23.59 -9.4%	3.19	6.07 + 90.0%	1.86 -41.9%	8.0	10 + 25.0%	6 - 25.0%	4.59	6.66 + 45.0%	3.23 -29.6%	71.9	75.8 + 5.4%	66.8 -7.0%	1.12	1.19 + 6.2%	1.07 -5.1%
(4)	All sites available. x_{-4} = -60nm, x_4 = 80nm. Five runs.													98.7	106.2 +7.57	87.9 -10.5	1.36	1.44 +5.8%	1.26 -7.2%
(5)	x_{-4} = -50nm, x_4 = 80nm.	8.65			1.18			7			3.85			109.6			1.31		
	x_{-4} = -75nm, x_4 = 80nm.	9.59			2.85			7			6.48			104.0			1.35		
	x_{-4} = -50nm, x_4 = 60nm.	32.49			2.09			5			1.20			109.6			1.52		
	x_{-4} = -75nm, x_4 = 60nm.	19.59			2.35			7			2.11			93.4			1.37		

4.4.6 Changing the Zero-Strain Pre-lever Reaction Rate.

The in vitro measurement of k_4^0 is given as $30s^{-1}$ (33ms duration) (Section 3.3.3). To investigate this value it was compared against $k_4^0 = 100s^{-1}$ (10ms duration) using strain dependent values for x_4 and x_{-4} which had previously been identified in this section to give a high speed and continuous attachment when $k_4^0 = 100s^{-1}$.

Two results were generated for $k_4^0 = 100s^{-1}$, in the first the filament was allowed to travel for 0.1s (Figure 4.4.9, black) and in the second (pale blue) the model time was extended to 0.3s. Good agreement can be seen in the 0.1s region for both analyses. In the second case, at 0.179s, the filament lost all crossbridge attachments and the

restoring force of titin returned it to its initial position where it began to move with fresh crossbridges. With a strain dependent $k_4^0 = 30s^{-1}$ reaction rate, the speed of filament movement compared to a strain independent reaction rate (0.20µm/s) increased (0.54µm/s and 0.57µm/s) but did not move as rapidly as filaments with the same parameter values as a strain dependent k_4^0 equal to $100s^{-1}$ (1.06µm/s and 1.22µm/s). Longer pauses in movement were observed with $k_4^0 = 30s^{-1}$. The most rapid period of movement, 0.06 to 0.1s, in the selection of results in Figure 4.4.9 was for $k_4^0 = 30s^{-1}$ (red line). The efficiency of ATP usage improved with the strain dependent results for $k_4^0 = 30s^{-1}$: strain independent 0.94 nm/ADP to strain dependent 1.50nm/ADP (green) and 1.30nm/ADP (red). This was a similar level of efficiency to $k_4^0 = 100s^{-1}$ (1.26nm/ADP (black) and 1.41nm/ADP (pale blue)).

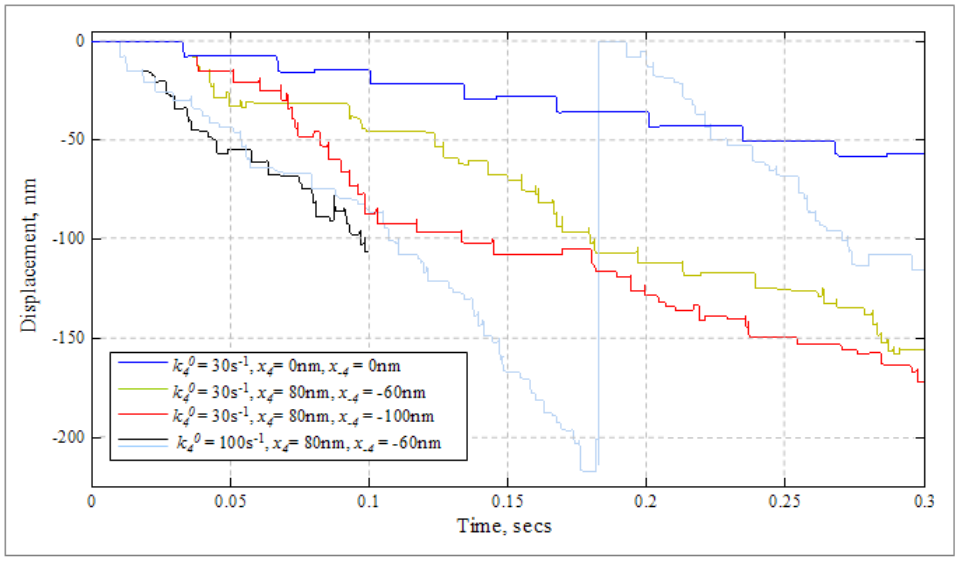

Figure 4.4.9, Displacement over time of the right-hand end of actin (Z-disc) for an increased pre-lever zero strain rate. k_4^0 equals k_{-4}^0. Two results are plotted for $k_4^0 = 100s^{-1}$ the first study (black) maintained movement for 0.01s, and for comparison, the filament in the second study (pale blue) maintained movement for 0.3s before releasing all crossbridges and returning to its start position.

4.4.7 Packing Restrictions: influence on filament motility.

In Section 4.4.3 it was found necessary to restrict the displacement of crossbridges in the direction of contraction in order to prevent them becoming entangled with one another, disrupting the geometry representing the filaments in the model. If a crossbridge travelled more than 95% of the distance between two adjacent actin bond sites, the crossbridge was disconnected.

Electron micrographs of a myofibril [2,10,50] indicate a spacing between filaments in the ordered cross-section of the sarcomere (Figure 2.1.1, A) of ~20nm filament centre-to-centre; the diameter of the myosin cofilament and actin filaments being ~11nm and ~5nm respectively. There must be enough space in this tightly packed structure to allow the myosin head with a length of ~16.5nm [2] to bond stereospecifically to actin (Section 3.3.1). This geometry means a myosin head must travel at least 42.9nm before it encounters the next head. This in turn restricts the space in which the arm could compress or bend considerably increasing its apparent stiffness and the strain on the crossbridge.

Taking the baseline parameters and Baseline Model arrangement from Section 4.3 the influence of the maximum crossbridge travel before imposed separation was examined in terms of filament speed and efficiency (with $k_4^0 = 100s^{-1}$, $x_4 = 100$nm and $x_{-4} = -50$nm). The responses were plotted against the maximum crossbridge displacement as a fraction of the actin bond site spacing (36.6nm).

In Section 4.4.4 the benefits of having a compliant arm opposing the direction of contraction were identified and the toleration of too much crossbridge movement made its strain release ineffectual in terms of displacement. Efficiency improved as the displacement fraction decreased, almost doubling at 0.25 (9.21nm, Figure 4.4.10) demonstrating the benefits of removing crossbridges which travel more than the lever distance (7.9nm). The statistical trend is shown in Figure 4.4.11.

The variation in the speed results (Figure 4.4.11) indicates there may be coupling between parameters at some settings. In Section 4.6 this type of oscillatory parameter sensitivity is considered further. Neither a linear nor a quadratic trend was statistically identified although visually there appeared to be an increase at 0.3-0.35 lengths. This suggested the packing restriction would have to be tight in order for it to exhibit an influence.

In a sarcomere, there would potentially be less space between the filaments than for an individual filament moving over substrate bound myosin in vitro. Therefore, this parameter may be more significant in the sarcomere than in an in vitro motility study. As a muscle contracts, the overlap between filaments increases restricting the space available perpendicular to the filaments so a packing restriction may be sarcomere length dependent.

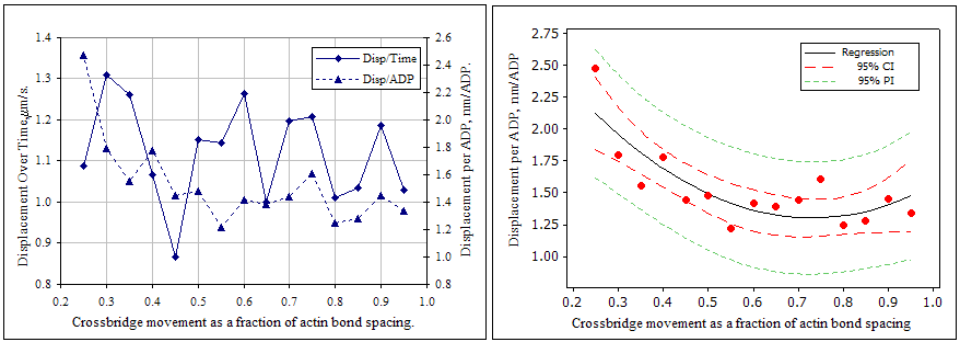

Figure 4.4.10 (left) and Figure 4.4.11 (right), Displacement over time and displacement per ADP plotted against the distance the crossbridge is allowed to travel before being removed. Quadratic regression of displacement per ADP, (right-hand plot) performed in MiniTab, (R.Sq (adj)=62.6%) p value 0.011.

4.4.8 Motility: v_{cross} the relative speed of bond sites.

In Section 3.4.1, the assumption was made that the speed at which actin and myosin bond sites pass one another may influence the chance of those sites forming a crossbridge. The maximum relative speed above which a crossbridge would not be allowed to form was assigned v_{cross} and defined as the relative displacement of the two sites over the previous time step, t_{step} (Figure 3.8.1, Appendix E, Function: HeadBonding). In this part of the work the speed and efficiency (nm/ADP) responses of the Baseline Model as described in Section 4.3 with $k_4^0 = 100s^{-1}$, $x_4 = 100$nm and $x_{-4} = -50$nm were examined for varying v_{cross}.

Sources of filament movement and therefore bond site realignment and potential new crossbridge formation could be due to external loading of the filament e.g. passive loading, but in this study the focus was on an unloaded filament's movement. Therefore, v_{cross} became a selection criterion for when new crossbridges form in relation to those that are currently generating movement. At the onset of levering, where strain energy is high, the unconstrained displacement of the crossbridge is rapid (see Figure 3.5.2, Section 3.5.3), since, as its energy declines the rate of displacement rapidly drops. A high v_{cross} value will allow new crossbridges to form earlier in the initial crossbridge's movement where as a low v_{cross} will limit formation to later in the lever release when strain energy is low. These characteristics are demonstrated in the model results.

In Figure 4.4.12 the displacement and duration of movement for a filament with varying v_{cross} is plotted. Below v_{cross} = ~18µm/s the filaments form no new crossbridges after the initial crossbridges have levered. The short duration of filament

movements with low v_{cross} values distorts the filament's speeds and efficiencies plotted in Figure 4.4.13. Overall, increasing v_{cross} increased filament speed and the number of concurrent crossbridges while reducing the efficiency (Figure 4.4.13). Above 150μm/s the values observed are comparable to v_{cross} = 10m/s, the default model value, (~1μm/s, ~1.4nm/ADP and ~ 11 concurrent crossbridges). Between v_{cross} = 65 to 75μm/s there is a shift in the mean number of crossbridges (1.62 and 4.37 respectively) marking a transition between using a few crossbridges efficiently and more less efficiently (6.2nm/ADP and 2.9nm/ADP respectively). Filament movements at v_{cross} values above and below this point are plotted in Figure 4.4.14. v_{cross} = 65μm/s exhibits large, distinct steps as new crossbridges can only form much later in the initial crossbridges lever while for the higher v_{cross} value, 225μm/s, steps are shorter and more distributed as new crossbridges formed at a wider range of values.

As an initial crossbridge moves a filament allowing a new crossbridge to form any displacement that initial crossbridge has left may continue to move the filament and the new crossbridge, bending the myosin arm that the new crossbridge is attached to. On levering, the new crossbridge will lose that displacement in straightening the myosin arm (Section 4.2.2). So overlapping crossbridges are inefficient but based on the results it appears to be necessary to generate a stable filament movement: v_{cross} = 65μm/s slips back to its initial position in Figure 4.4.14.

Compromise can be seen in the results between efficiency, speed and sustained movement. In a network of filaments, it may not be necessary to sustain an individual filament's movement as active and pausing filaments may be interspersed to create the overall fibre contraction. v_{cross} demonstrates another means to provide a range of filament performance. Yet, individual filaments in motility studies do maintain movement [59,90,91].

As tension increases, opposing a crossbridge lever event, its release will be slowed effectively increasing v_{cross} and more crossbridges may form. As v_{cross} is dependent on the levering properties, stiffness, k_b, damping, c_b, and distance, b_{max} and tension in the filament the most sensitive range of values is adjustable. With the current model values v_{cross} = 65 to 100μm/s is a significant transition zone. The source of the load on the crossbridge is important. If the load is due to an external opposition to contraction more crossbridges and therefore more potential force is beneficial to the filament/sarcomere's function. However, if the load is due to crossbridges to the left

of the levering crossbridge, towards the M-disc (in the model convention Figure 2.1.1, Figure 3.2.2), more crossbridges may be a hindrance to rapid movement. Strain dependent reaction rates then become important in removing crossbridges that are opposing movement in the direction of contraction.

In muscle fibres it is observed that as contractile speed increases force generation drops [7] and the associated stiffness reduction is attributed to a reduced number of crossbridges. In the model an increased number of crossbridges was associated with increased speed, Figure 4.4.13. The low efficiency indicates a high level of strain energy is lost to the myosin arms (1.4nm/ADP compared to a maximum 7.9nm/ADP) and it is in the early stages of strain release the force expressed is highest. Are the reduced force and stiffness due to the flexed and compliant myosin arms and the loss of energy to the cofilament? This will be considered in Section 4.8 after isometric loading.

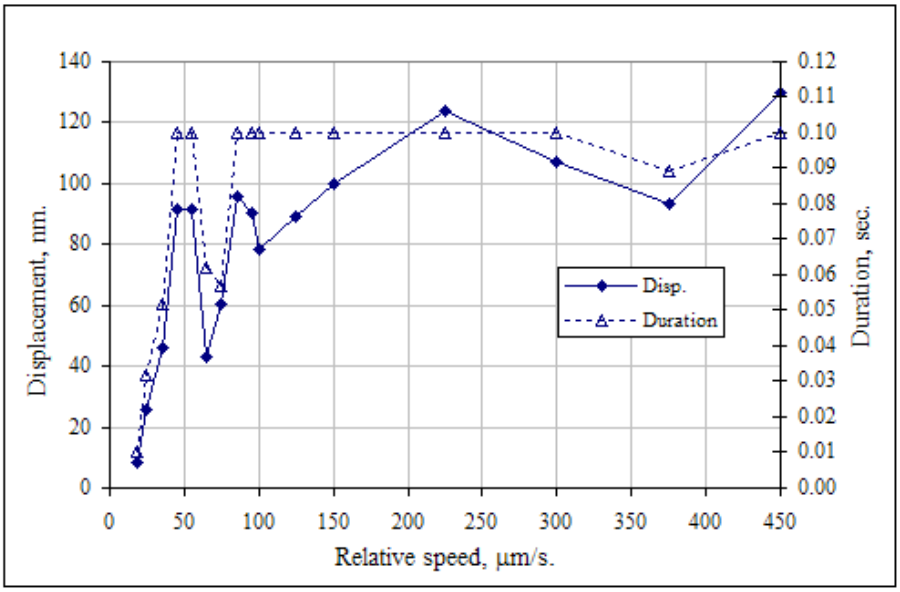

Figure 4.4.12, Displacement of right-hand end of actin and duration of movement up to a maximum of 0.1s.

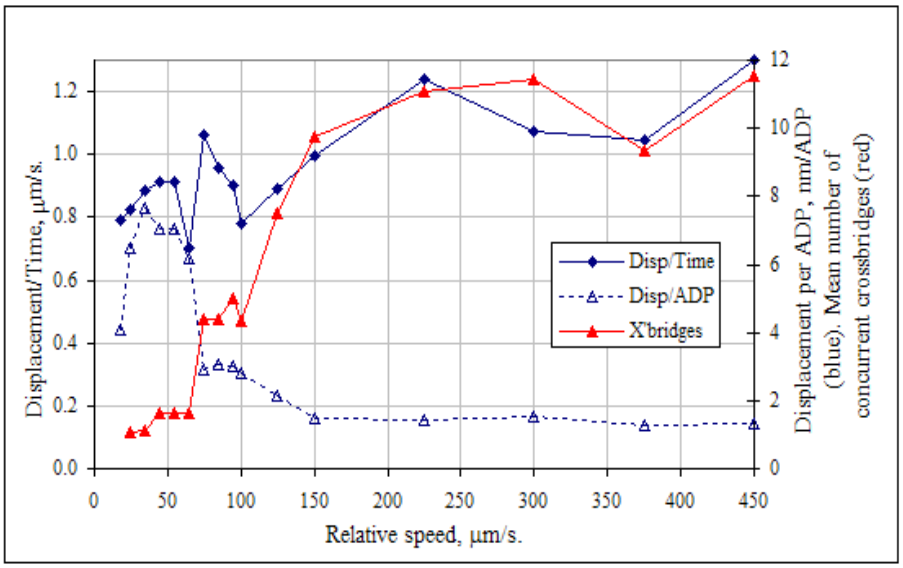

Figure 4.4.13, Displacement of right-hand end of actin filament over time (0.1s), efficiency (displacement per ADP released) and mean number of concurrent crossbridges against the relative speeds of bonds accepted as crossbridges, v_{cross}. k_4^0 =100s^{-1}, x_4 = 80nm and x_{-4} = -60nm.

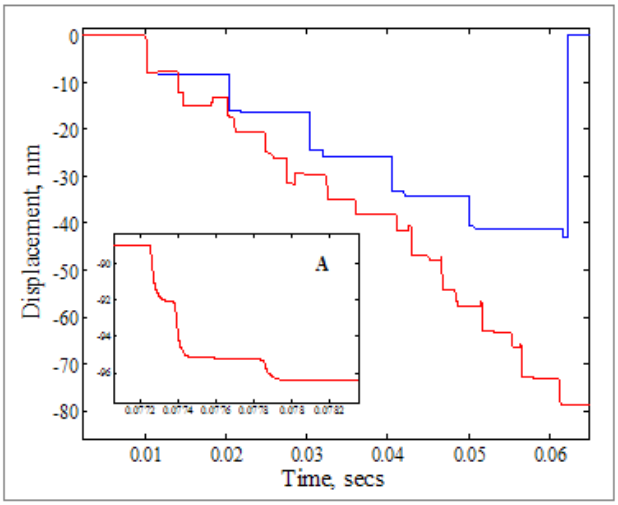

Figure 4.4.14, Displacement of right-hand end of actin filament against time (0.1s), for v_{cross} = 65µm/s (blue) and v_{cross} = 225µm/s (red). k_4^0 =100s^{-1}, x_4 = 80nm and x_{-4} = -60nm. Inset A is an enlargement of a section of filament movement, v_{cross} = 225µm/s.

4.4.9 Crossbridge Attachment Times – the Duty Ratio.

In Section 4.4.4 the interaction of crossbridges along the length of an actin filament was examined. Here the same Baseline Model was used to record the attachment times of crossbridges over 0.1s along a 1µm actin filament (Appendix D). Table 4.4.2 records the duration of crossbridges that completed a reaction cycle being released by ATP. k_4^0 = 100s^{-1} was used as k_4^0= 30s^{-1} failed to generate enough data for a

reasonable experimental time. The attachment time is important in that it limits the type of chemical processes that may occur in the crossbridge to express strain energy.

In vitro motility studies commonly measure the ATPase rate (reaction cycle time) in order to estimate the individual crossbridge attachment times and therefore evaluate their properties. The ATPase rates are taken from a substrate coated with myosin and actin fragments and are therefore not strained. The ATPase rate, filaments speed and the estimated number of concurrent crossbridges are used to determine the percentage of the reaction time a crossbridge is attached (the duty ratio). For skeletal muscle this is recorded as ~5% [89,91] but is dependent on the isoforms of myosin [97].

In analysing the outputs from the model a wide range of attachment times were observed, some much longer than the strain free, dominant k_4^0 =100s^{-1} (10ms duration) pre-lever time, e.g. 20.7ms. From the model the duty ratio varied from 66% to 21% with a mean of 48%. In Section 4.4.6, k_4^0 = 30s^{-1} moves a filament at similar speeds to k_4^0 = 100s^{-1}. If an assumption is made that attachment times have a similar distribution the duty ratio would drop to a minimum of 9% and mean 24%. Increased tension in the filament may further spread the attachment times.

The model demonstrates it is not necessary to have very low duty ratios to move a filament at a reasonable speed, such as 1.0µm/s. The overlapping of crossbridges in time and compliance in the filament enables these time variations. Whether this holds true at faster filament speeds requires further investigation beyond the scope of this project.

Table 4.4.2, Analysis of crossbridge attachment times over 0.1 seconds, k_4^0 =100s^{-1}, x_4 = 80nm and x_{-4} = -60nm.Crossbridges that have completed the reaction cycle and are released by ATP.

	Attachment time, t_{on}, ms.	ATPase, t_{total}, ms.	X'bridge disp. while attached, nm.	Concurrent crossbridges.	Duty Ratio, k_4^0 = 100s^{-1}	Duty Ratio, k_4^0 = 30s^{-1}
max.	20.70	31.20	23.30	17	0.66	
min.	2.85	13.35	7.60	4	0.21	0.090
mean	9.61	20.11	12.90	9.9	0.48	0.240
mode	11.70	22.20	23.30	11	0.53	0.280

Data given for 53 complete cycles.
49 cycles were incomplete: 29 released pre-lever, 15 released during levering, 5 still active at end of time study.

k_4^0 = 100s^{-1}: duration 10ms, without strain ATPase cycle: 21.7ms.
k_4^0 = 30s^{-1}: duration 33ms, without strain ATPase cycle: 45.0ms

Speed of filament = 1µm/s Efficiency = 1.34nm/ADP

4.4.10 Summary

In this section, using the Baseline Model, it has been demonstrated that a longer strain free pre-lever reaction time, as measured in ATPase studies, can accommodate rapid filament movements if the crossbridge reaction duration is made dependent on crossbridge strain. A strain free value for the dominant pre-lever reaction rate k_4^0= $100s^{-1}$ was used, justified by the ordered structure of the actin filament-myosin arrangement in the sarcomere and in motility studies compared to fragments in ATPase studies. Although indications were found that a higher value may also sustain motility in the sarcomere. The peak motility speed measured was 1.24μm/s ($k_4^0 = 100s^{-1}$, x_4 = 100nm, x_{-4} = -50nm) where the forward reaction was shortened in duration and the reverse lengthened in response to strain (positive and negative respectively) compared to the strain independent reaction durations: 0.65μm/s. Efficiency was relatively low (1.55nm/ADP) but was also improved by introducing reaction strain dependency.

The model demonstrated it is not necessary to have very short attachment times to achieve speed but a mixture of long and short attachments allow the filament to move more rapidly and for that motion to be sustained. The wide distribution of attachment times was caused by tension variations along the length of the filament. A large proportion of crossbridges were lost pre-lever (29 compared to 53 complete cycles, Table 4.4.2) potentially conveying stability to the filament's movement without expelling strain energy.

A balance was indicated between preventing the loss of crossbridge strain energy due to the filament slipping and a loss of strain energy due to a crossbridge inhibiting the levering of other crossbridges. Two characteristics were found which influenced this balance. The use of a packing restriction or limit to the displacement of a crossbridge in the direction of contraction in the model, offenders being removed, was found to improve efficiency but not noticeable speed. A second parameter, the relative speed of bond sites, v_{cross}, was found to have potential as a 'tuning' parameter: balancing the number of concurrent crossbridges and distribution in time of levering events, therefore influencing speed and efficiency.

In the next two sections, using the now established strain dependent pre-lever reaction parameters, filament motility is examined in terms of two specific in vitro experiments.

4.5 Motility: the restoring force of titin.

Up to this point in the modelling of motility (Section 4.1 to 4.5), in order to examine the properties of the filament movement against in vitro experiments, where the titin protein was not present, the protein was assigned a relatively low stiffness (0.6μN/m) in order to remove its influence. In this part of the study filament motility under the loading experienced in the sarcomere, that imposed by titin's stiffness is examined using the Baseline Model arrangement from Section 4.3 (with $k_4^0 = 100s^{-1}$, $x_4 = 100nm$ and $x_{-4} = -50nm$).

Titin's stiffness is of interest as not only has it been noted as stabilising the geometry of the sarcomere (Section 3.7), but its resistance to an actin filaments contraction may also be a significant component in the strain distribution within a filament. In Section 4.4.4 the distribution of strain in the actin filament was found to strongly influence the pre-lever reaction rate.

The investigation of titin's stiffness with the Baseline Model will be compared against a related published, in vitro, experiment performed by Kaya and Higuchi [29]. In their experiments, an optical trap, of estimated stiffness 60μN/m, attached to the end of an actin filament monitored the development of force and displacement over time as the filament traversed a substrate bound cofilament. Titin's stiffness, k_{ta}, scaled to the Baseline Model was estimated to also be 60μN/m (Section 3.7). In the Baseline Model all of the myosin heads were available to bond, any reductions in availability due to substrate binding were not made.

4.5.1 Motility in the Baseline Model with a Resistive Load.

In Figure 4.5.1, the actin filament displacement against time generated using the Baseline Model was plotted for the estimated sarcomere stiffness of titin, k_{ta} = 60μN/m. Kaya and Higuchi's [29] force displacement results indicated a resistive stiffness on the actin filament of 33.5μN/m so the model was also run with k_{ta} =

33.5μN/m. Increasing k_{ta} caused the filament to slip, lose all crossbridges and return to its start position, after travelling a short distance. This is shown in red and black in Figure 4.5.1. At k_{ta} = 0.6μN/m slippage occurs at ~40nm (red, Figure 4.5.1) and ~80nm with k_{ta} = 0.335μN/m (black). Filament slippage, in this instance, was found to be due to a modelling issue, described below.

In the model, rapid over-extension of levering crossbridges in the direction of levering generated rapid tension increases in the filament. Two plausible scenarios present themselves when over extension occurs: the crossbridge breaks or is forced into a post-lever stage. The current model is set-up to break, but does not do this quickly enough and the minimum reaction time is currently static. This could not be explored further without modification of the model. Examining the filament behaviour at lower displacements was possible before the development of the error state.

Compared to low load runs (Table 4.4.1, record (4), 0.99μm/s and 1.36nm/ADP) a load on the filament caused it to move more rapidly and with greater efficiency. For k_{ta} = 60μN/m, the mean speed of four events was 1.7μm/s with a range of +16.04% and –13.88% (excluding the rapid end transitions). The displacement per ADP released was 3.05nm (+18.4%, -16.08%). These results were over ~0.024s and are a lower estimate compared to the previous results over 0.1s as the initial, 0.01s, pre-lever pause was a greater proportion of the over all time. Each filament, in all of the experiments in Chapter 4 begins in the same start condition: two crossbridges form, one at the end of the cofilament and the other at ~36μm. At low loads these crossbridges levered together to give a ~7.6nm displacement. The increased resistance to movement from titin offset the levering behaviour (not the pre-load time) creating an initial step of 11.24nm indicating a source of the increased crossbridge efficiency.
A much higher release of crossbridges in pre-lever at higher loads was also noted (6 over 0.014secs compared to 2).

4.5.2 Comparison of the Baseline Model to an In Vitro Experiment.

Setting titin's stiffness to k_{ta} = 33.5 μN/m the displacement and force development (50nm, 1.68pN) approximated to that observed for filaments of comparable length (880 ± 18nm, 3 samples) studied by Kaya and Higuchi [29].

Kaya and Higuchi applied an algorithm to interpret the individual steps of the filament, as there was a thermal noise component in the data. Based on this study they discerned that as resistance increased the individual step size declined and so too, the filament's speed. In the model results shown in Figure 4.5.1 this step pattern can be observed. Increased displacement increases the load consequently, in Kaya and Higuchi*'s* data, this appears to slow the filament down. This characteristic is not clearly visible in the model results but the maximum displacements and loads are lower in the model. For cofilaments of this length Kaya and Higuchi observed movements of ~300nm where as in the model filament movements at this stiffness were ~80nm (black, Figure 4.5.1) due to a modelling characteristic (Section 4.5.1).

Filament speeds in Kaya and Higuchi's data (~0.34µm/s at high loads and ~0.43µm/s low loads) were considerably lower than those observed in the model. Pauses in movement observed in Kaya and Higuchi's data ran for up to ~100ms with backward slips of ~10ms. In the model these pauses and slips were seen in the initial negligible load results and particularly long pauses with $k_4^0 = 30s^{-1}$ (33ms duration) (Figure 4.4.9) but the events were of much lower magnitude with increased titin stiffness. The duration of individual steps in the model were, relatively, much shorter; the model filament took seven or eight steps over the first 40ms compared to Kaya and Higuchi's data where ~5 to ~7 distinct steps per 100ms were observed. Thermal noise may have obscured some of the smaller steps but the dominant steps were distinct.

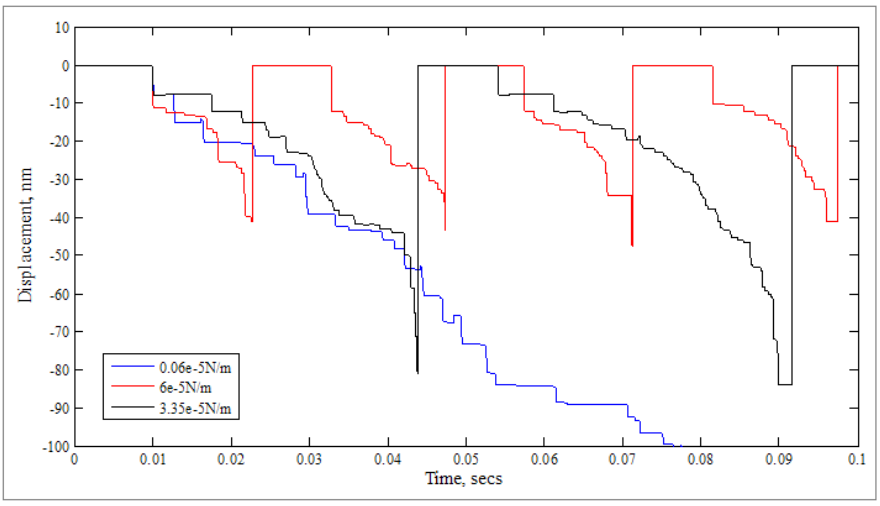

Figure 4.5.1, Displacement of right-hand end of actin filament, $k_4^0 = 100s^{-1}$, x_4 = 80nm and x_{-4} = -60nm, with titin stiffness: k_{ta} =60 µN/m, 33.5µN/m and 0. 6µN/m. At increased k_{ta} values the backward slips are less pronounced. The higher external tension may reduce the compression within the filament which causes the backward movement (Section 4.4.4).

In the following sections the number of concurrent crossbridges, substrate stiffness and post-lever reaction times are considered as possible means to explain these model-in vitro experiment differences.

4.5.3 In Vitro Comparison: concurrent crossbridges.

Kaya and Higuchi [29] measured the number of concurrent crossbridges between actin filaments and a fragment of myosin cofilament bound to a surface. A ratio of 5.2 crossbridges per 370nm of cofilament was determined. The cofilament length excluded an 80nm smooth section at the end where the myosin II tails combined (Section 3.2). As the cofilament was bound to a surface not all of the myosin heads would have been available to bond. Taking into account the overlap between filaments in the Baseline Model study, the maximum number of actin bond sites available was 18 to 19 corresponding to 654.5 to 693nm of overlap. Using Kaya and Higuchi's result, this gives a mean of 9.2 to 9.8 expected crossbridges. The number of concurrent crossbridges in the model are shown in Table 4.5.1.

Table 4.5.1, Number of concurrent crossbridges in the Baseline Model with variation in titin stiffness. 1μm actin filament, k_4^0=100s^{-1}, x_4 = 80nm, and x_{-4} = -60nm. The time period evaluated was the duration of continuous filament movement after a stable pattern of crossbridge formation and release had developed (i.e. after the initial 0.01s).

Titin stiffness, k_{ta}, μN/m.	Period evaluated, s.	X'bridges Min.	X'bridges Max.	X'bridges Mean
33.5	0.01 to 0.04	8	16	11.9
60	0.01 to 0.023	11	16	14.2

As the cofilament in Kaya and Higuchi's experiment was bound to a surface not all of the myosin heads would be available to bond with a loss of 33%, a third of the heads, therefore the mean may rise to 13.8 to 14.7 for an unobstructed cofilament. The number of concurrent crossbridges in the model was dependent on k_{ta}. The force-stiffness relationship of Kaya and Higuchi's experiment indicated k_{ta} = 33.5μN/m so the number of concurrent crossbridges in the model is a little low (11.9 mean at k_{ta} = 33.5μN/m). Although in Table 4.4.1 record (1) and (4) it was shown that a third drop in the number of available myosin bond sites reduced the speed of filament movement by 9.5% and increased efficiency by 36% this does not appear to be the cause of the model filament moving faster than the in vitro data filament (~1.7μm/s compared to ~0.43μm/s).

4.5.4 In Vitro Comparison: post-lever reaction time and a compliant substrate.

In order to investigate the discrepancy in timing between Kaya and Higuchi's [29] motility studies and those of the Baseline Model the significance of ATP availability was considered.

The filament motility study performed by Uyeda *et al* [91], considered in Section 4.6, used an ATP concentration of 2mM at 30°C, Kaya and Higuchi used 20μM, a much lower concentration. Physiological concentrations of ATP in skeletal muscle are dependent on a number of factors: muscle, type, duration and nature of loading. Kushmerick *et al* [98] found concentrations of 5 to 8 mM. The supply of ATP in the Baseline Model was unconstrained but the reaction rate data had a post-lever reaction time (Section 3.3.3) for an assumed ATP concentration of 4mM (temperature not specified [10]). In this study the influence of concentration is not evaluated but in order to obtain an indication as to why the model differed from the test data of Kaya and Higuchi [29] a comparatively slow post-lever, strain independent reaction duration of $k_1^0 = 100s^{-1}$ (10ms duration) was used to generate a set of results for comparison to the Baseline Model where $k_1^0 = 20{,}000s^{-1}$ (0.05ms duration) with k_{ta} = 33.55μN/m. The reduction in reaction rate, k_1^0, by a factor of 200 approximates the low concentration of ATP in Kaya and Higuchi's experiment (20μM.) compared to the data used in the Baseline Model (4mM).

With k_1^0=100s^{-1} the number of small steps (for example between 0.03 to 0.033s, red in Figure 4.5.2) were significantly reduced and replaced with more clearly defined filament movements. Up to ~0.035s in Figure 4.5.2 filament speeds are similar 1.16μm/s ($k_1^0 = 20{,}000s^{-1}$) and 1.25μm/s ($k_1^0 = 100s^{-1}$) but the longer post-lever reaction time doubled the efficiency: 4.08nm/ADP compared to 2.33Nm/ADP. Examination of the number and state of concurrent crossbridges in the results showed an increase in crossbridges from ~1 to ~3 in a post-lever state. Although the attachment time increased, the overall filament movement was not greatly hindered as the protracted post-lever time ran in parallel to the pre-lever duration of other crossbridges. By demonstrating the post-lever reaction time changes the distribution of reaction states of the concurrent crossbridges and the timing of new crossbridges forming indicates post-lever strain dependent reactions are an important part of the filament's movement but its investigation is beyond the scope of this project.

Examination of the post-lever reaction time did not explain why the model filaments still moved more quickly than those in Kaya and Higuchi*'s* data.

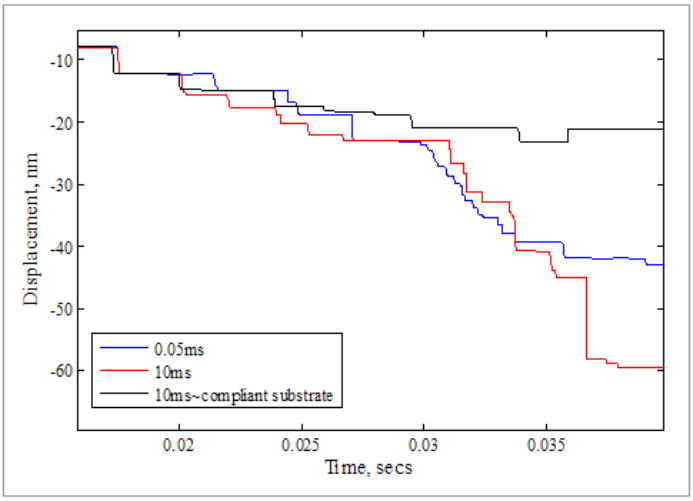

Figure 4.5.2, Increased strain independent post-lever reaction rate, $k_{tm} = k_{ta}$ =33.5 μN/m. k_1^0 = 20,000s^{-1} (0.05ms duration) and k_1^0 = 100s^{-1} (10ms duration).

Kaya and Higuchi [29] estimated the combined substrate and cofilament compliance, this was examined in Section 3.2.6, Figure 3.2.5 and was found to greatly influence the apparent stiffness of an individual crossbridge. Kaya and Higuchi were not able to separate the cofilament and substrate stiffness so the low stiffness may refer to the cofilament or the cofilament-substrate interface. In the model the cofilament is anchored at one end not along its length, in order to examine this stiffness property, the cofilament stiffness between myosin arms was reduced. In Figure 4.5.2 (black line) with a long post-lever time a filament's movement in the Baseline Model was plotted with reduced cofilament stiffness. In alignment with Kaya and Higuchi's cofilament-substrate estimate 9.2 x 10^{-3}N/m per 14.3nm was used the standard model value being 4.61N/m per 14.3nm (Appendix B, Table 2).

The model filament was slowed considerably by reducing the cofilament stiffness while maintaining the force-displacement relationship and the number of concurrent crossbridges (mean 13.4 of two runs), Figure 4.5.2 (black line) indicating the substrate-cofilament stiffness is a potential cause of the difference between the model's performance and the in vitro test data. A loss of displacement from each crossbridge would be expected as more movement was put into extending the more compliant cofilament resulting in less actin filament movement and therefore a lower apparent lever distance with less opportunity to form new crossbridges. This

highlights the importance of the cofilaments stiffness relative to the other components in regulating movement, a point for future investigation.

4.6 Displacement: actin length and myosin concentration.

Comparison of the Baseline Model's performance to an in vitro motility study performed by Uyeda *et al* [91] where actin length and myosin concentrations were varied provided a means to further examine the interaction of crossbridges in the propulsion of actin filaments in low load scenarios. In addition to actin length and myosin concentrations the comparison was used to examine the sensitivity of the filament movement to the compliance of actin filaments, and the myosin II S1 and S2 components which were examined as individual crossbridges in Chapter 3.

4.6.1 Results of Actin Length Study.

Uyeda *et al*'s in vitro experiment used HMM fragments randomly distributed across a nitrocellulose surface. Fluorescent-tagged actin filament movements across the surface were then studied via video recorder. Two clear trends in actin-myosin behaviour were observed: increasing the concentration of myosin fragments increased the actin filament's speed and increasing the actin filament's length increased speed until a maximum speed was reached for the given concentration. For comparison with this data the Baseline Model as described in Section 4.2 was used with pre-strain reaction durations used, which provided greater speeds (k_4^0 =100s^{-1} (10ms duration), x_4 = 80nm and x_{-4} = -60nm, Section 4.4.3). Titin's stiffness was returned to its initial, negligible level (0.6 μN/m). The myosin cofilament was increased in proportion to the actin filament in order to provide enough myosin bond sites for the actin filament to traverse.

The speed and efficiency against actin filament length generated by the model are plotted in Figure 4.6.1. The model speed increased with length and began to plateau towards 9μm/s at a length of 7 to 8 μm. Efficiency decreased with length levelling off at 8μm length of myosin cofilament in the model.

Uyeda at al found peak values of ~8µm/s, these speeds, at high HMM concentrations, were achieved with 1 to 2µm lengths of actin. At lower concentrations, the plateaux speed dropped and longer filament lengths were required to achieve that plateau. The model's peak speed corresponded to the high concentration result of Uyeda *et al*, but the length required to achieve it did not. By considering the differences between the set-up of the two experiments and the results, a number of filament and sarcomere characteristics were considered.

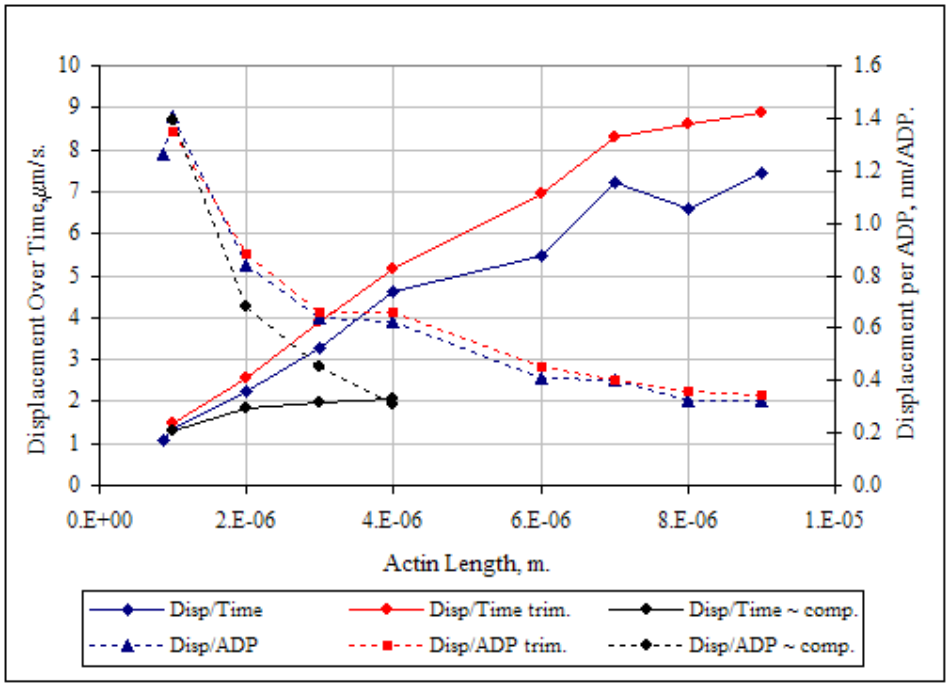

Figure 4.6.1, Displacement over time of right hand end of actin filament and displacement per ADP plotted against actin filament length. Trimmed values consider events between 0.03 and 0.1 s as there was a pause in filament motion for several of the filaments. $k_4^0 = 100s^{-1}$, x_4 = *80nm and* x_{-4} = *-60nm.*

4.6.2 Motility: concentration of myosin heads.

The impact on motility of the number of myosin bond sites available and how this number compared to the number available in Uyeda *et al's* experiment were considered as a potential explanation of the speed-length differences between in vitro and model results. The Baseline Model spacing for myosin bond sites along a cofilament was 14.3nm corresponding to those available to actin filament in a sarcomere. At this concentration, 68 pairs of myosin heads per 1µm, the actin filament speed was 2.52µm/s for a 2µm length where actin has 26 bond sites per 1µm. In Table 4.6.1, the result in the model of reducing the myosin bond site spacing,

effectively increasing the concentration, shows that although more crossbridges are formed the overall speed of movement does not increase but the efficiency of each crossbridge use is slightly reduced.

Blocking every third myosin bond site, effectively reducing the bond site concentration, produced a drop in speed of 33% for a 1µm filament with increased efficiency of 40% was recorded in the model (see Table 4.4.1, Section 4.4.5). *Uyeda et al* measured a drop in motility of ~ 25% for a 1µm actin filament between 870/µm^2 (a saturation level) of HMM to 540 HMM/µm^2 (approximately a drop of a third). The specific number of crossbridges per actin length in the in vitro experiment could not be measured.

Increasing the myosin concentration will not raise the speed of a 2µm actin filament in the model from 2.52µm/s to the ~8µm at this length, measured by Uyeda *et al* at high HMM concentrations.

Table 4.6.1, Model output for a 2µm length of actin (52 actin sites available). Note actin initially overhangs the myosin cofilament so 8 actin bond sites are not initially accessible to myosin bond sites.

					Concurrent crossbridges.	
Myosin spacing, nm.	Heads per 1µm of myosin.	Filament speed, µm/s.	Efficiency, nm/ADP	ADP molecules expelled.	max	mean
14.3	68	2.43	0.85	286	44	27
7.2	136	2.47	0.75	328	45	34.8
3.6	273	2.35	0.65	363	49	38.8

4.6.3 Cofilament Stiffness and Myosin Arm Stiffness (S2).

In the model the myosin bond sites were part of a relatively stiff cofilament anchored at one end. In the in vitro motility study, HMM fragments were randomly bound to a nitrocellulose surface. How those attachments perform under loading is not clear. The Baseline Model stiffness, 4.61N/m per 14.3nm (Appendix B, Table 2) was reduced to 9.2 x 10^{-3}N/m per 14.3nm (a cofilament –substrate stiffness derived in another in vitro experiment [29] see Section 3.2.4). In Figure 4.6.1 the result of reducing the myosin cofilament stiffness between S2 attachment points, i.e., HMM components (see Figure 3.2.1) in the model are plotted. A lower plateau stiffness developed at much shorter lengths. This aligns with Section 3.2.7 where strain energy was lost distorting the

substrate/cofilament rather than propelling the filament forward. At the Baseline Model stiffness the distortion of the cofilament relative to myosin S2 was negligible. Changing the cofilament stiffness in the model would have altered the spacing of myosin bond sites. In the in vitro experiment the relative positions of HMM fragments bound to a substrate may change without influencing one another's position. In the model the HMM components of myosin are interconnected by the myosin cofilament, as in the sarcomere, so bond-site spacing was not investigated further.

A second consequence of embedding HMM fragments into a substrate is that the performance of the myosin arms (S2) may be restricted. The effect of increasing the S2 stiffness, k_m, was evaluated. The longitudinal stiffness was not considered as the measured extension of the arm with the Baseline Model stiffness was low, the in vitro attachment would not be expected to be stiffer and greater compliance would slow the filament in a similar way to the cofilament stiffness.

In Figure 4.6.2 the speed of the right hand end of a 2μm actin filament dropped rapidly as k_m increased above 25μN/m. In Figure 4.6.3 filaments with a high k_m stiffness paused and slip back to the start position under the returning force of the protein titin. As k_m increased the strain on pre-lever crossbridges increased so fewer were maintained, and so, movement could not be maintained. In the extreme, beyond k_m = 40μN/m, after the initial lever event occurred no further crossbridges were formed. However, increasing stiffness a small amount from the model's Baseline value of 10μN/m to 20 - 22μN/m generated a small speed increase. Neighbouring points indicated an improving trend rather than an anomaly or random variation. The optimum value of k_m was interdependent on the strain dependent reaction rates. So ideally, the parameters would be examined together.

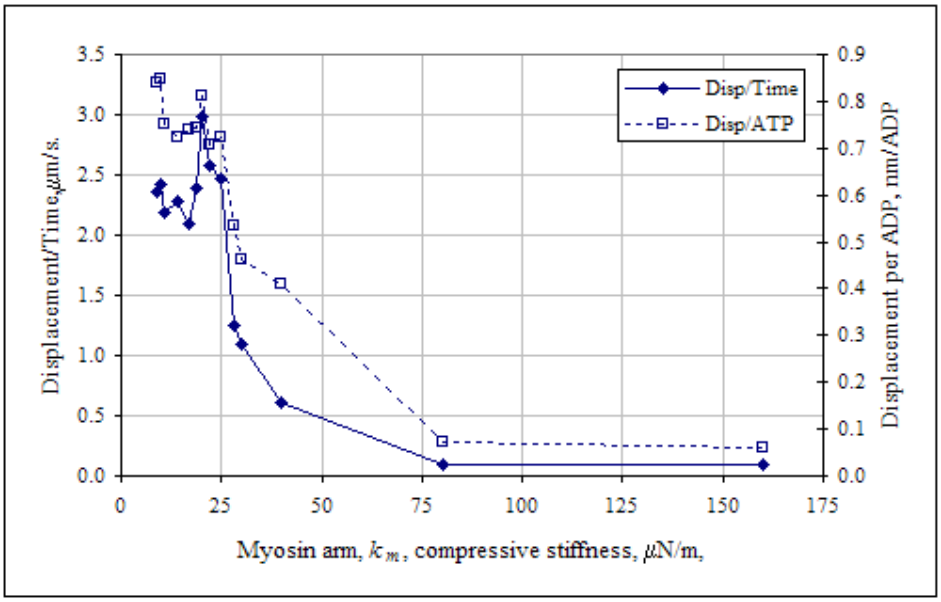

Figure 4.6.2, Model sensitivity to the compressive stiffness of the myosin arm, k_m. Speed of right hand end of actin filament and displacement per ADP. $k_4^0 = 100s^{-1}$, x_4 = 80nm and x_{-4} = -60nm.

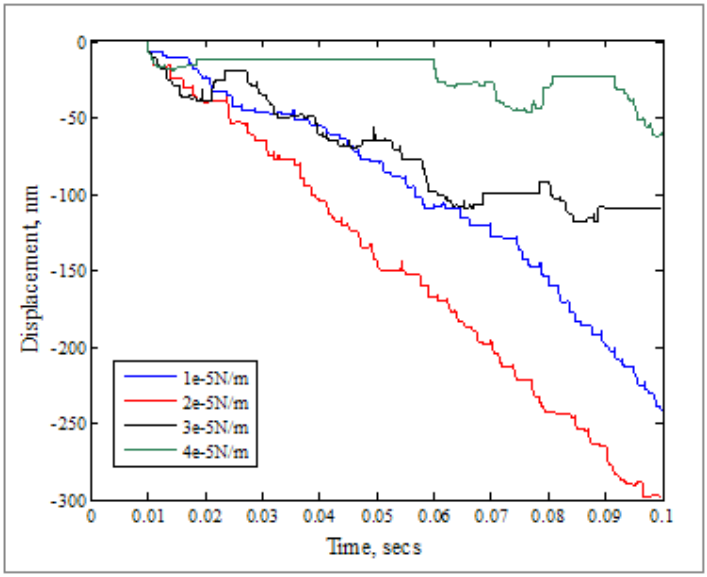

Figure 4.6.3, Sensitivity of actin filament displacement (right-hand end) over time to variation in myosin arm compressive stiffness, S2. Values used for S2 stiffness: k_m = 10, 20, 30 and 40μN/m. $k_4^0 = 100s^{-1}$, x_4 = 80nm and x_{-4} = -60nm.

4.6.4 Comparison of Characteristics of Actin Lengths: 2, 4, 6 and 8μm.

An analysis of the results shown in Figure 4.6.1 is presented in Table 4.6.2. As actin filament length increases, (Table 4.6.2) the mean and maximum number of crossbridges does not change greatly from the variation in a single run although there

does appear to be a decline in the mean at longer actin lengths. As length increases the ADP expelled per unit length increases combined with only a small change in the mean number of crossbridges the time crossbridges are attached and levering must be shorter but this also has the consequence of being less efficient. From the model data used to generate Figure 4.6.1 the changing length of the actin filaments over time was extracted and the mean bond-site-to-bond-site (38.5nm) tension and movement in the actin filaments was determined. Within the filaments, compression predominated with peaks in tension of 1.3pN (per 38.5nm) at 2µm and 7.29pN (per 38.5nm) for a 8µm filament. The mean level of movement was small, 5.2pm/38.5nm (8µm filament). The strain dependent reaction durations will potentially have been affected by these load changes.

To increase the tension in an actin filament of 2µm the actin stiffness was modified in the model. A range of 0.53 x 10^{-3} to 530 x 10^{-3} N/m per unit length where the Base line Model value was 53 x 10^{-3} N/m was examined. This had little influence on filament speed or efficiency that could not be attributed to variations in results with common parameters (Table 4.4.1), e.g. 15.6% change for a factor of 10 increase in stiffness. Bond-site-to-bond-site tension increased to 1.8pN peak from 1.3pN peak. In the model, a distinction could not be made between the stiffness of the filament in compression and extension. In vitro an actin filament may have space to bend giving an apparent lower stiffness in compression. The model assumes this type of distortion would not be possible in the close packing of the sarcomere but this could have influence on the crossbridge strain response.

Table 4.6.2, Changing actin length, details of runs plotted in Figure 4.6.1. Note actin initially overhangs the myosin cofilament so 8 actin bond sites are not initially accessible to myosin bond sites.

				Concurrent crossbridges.	
Actin Filament length, µm.	Speed (0.03 - 0.1s), µm/s.	Efficiency, nm/ADP	ADP expelled per 1µm.	max per µm of actin.	mean per µm of actin.
2	2.52	0.83	135	21	14.2
4	5.14	0.62	185	21	14.2
6	6.93	0.41	222	20	12.5
8	8.61	0.33	254	23.4	11.9

From these length-tension observations further examination of the strain dependency of crossbridge reaction rates may make the crossbridge interactions more productive

in terms of increased filament speed and efficiency. Such potential improvements will be interdependent on stiffness parameters and parameters such as v_{cross}.

4.6.5 Myosin II, S1 Component.

In Section 3.2 the different isoforms of the myosin II S1 component were introduced and in Section 3.2.6 an experiment was performed to identify values for the lever arm in S1, k_{mh}, and the flexure length, l_{head}, how far the lever arm can bend before it becomes rigid. The stiffness of S1 has been demonstrated in in vitro studies to have a strong influence on motility [52,58,59]. Here, these two parameters were examined using the Baseline Model and a 1μm length of actin (a shorter length enables a greater number of variations to be examined more quickly using the model). Baseline Model pre-, post- and levering stiffnesses, k_{mh} (2.7, 3.03, 3.53pN/nm respectively, Table 2, Appendix B) were increased by the same factor.

In the model results for k_{mh} (Figure 4.6.4) and l_{head} (Figure 4.6.5) there was a clear cyclic sensitivity to the parameters. In Figure 4.6.4 below 0.8 times the Baseline Model value (Section 3.3.6) the speed rose as k_{mh} decreased. Compared to lower values a mean increase of ~18% occurred between 0.8 and 1.2. Above this level, higher speeds were also indicated but were unclear due to the cyclic characteristics. No clear trends appeared when changing l_{head} (Baseline Model value 6nm).

The performance of the lever arm stiffness in S1 is bound to the stiffness of the myosin arm (S2). Under compression S2 (0.01pN/nm, Appendix B) is considerably more compliant than S1 (k_{mh}) and so dominates the combined stiffness. Under extension S2 stiffness increases (70pN/nm) and so S1 (k_{mh}) becomes significant and dominates the combined stiffness (Section 3.2.2). When a crossbridge releases strain energy, it reacts against the myosin head and arm (S1 and S2). A reduced stiffness of S1 (k_{mh}) would allow more movement to occur in the myosin II rather than propelling the actin filament aligning with the in vitro observation that reducing S1 stiffness reduces speed. Correspondingly, efficiency would be reduced. In the model, l_{head} limited this myosin displacement as it dictated the transition point to the longitudinal, S2 stiffness of the arm (Section 3.3.2). Therefore, in the model results, the reduction in stiffness may have less effect than anticipated. The interdependency of l_{head} and k_{mh} is an area which requires further work. Individually, displacement with the Baseline Model value for k_{mh} may mean the movement of in S1 is not enough to make l_{head}

significant. Figure 4.6.4 demonstrates the Baseline parameters for k_{mh} are at a transition point for higher speeds and slightly more efficient crossbridge use.

The cyclic behaviour in the results requires further examination but a cyclic characteristic was also noted in the number of concurrent crossbridges. The mean number of crossbridges closely follows the filament speed for changing k_{mh}. In Figure 4.6.6, the number of concurrent crossbridges is constantly changing but when the filament is short a periodicity in the number of crossbridges is visible, at 2µm this is about 0.035-0.04s, at 3µm about 0.015s as length increases beyond 4µm this periodic characteristic is no longer clear. As the model uses distinct transitions for arm stiffness such as those for S2 and time steps there may be an interaction with this overall cycle. The frequencies contained within these responses were not analysed further but examination of this characteristic may provide insight into whether it is a model characteristic or a true characteristic of a filament's behaviour.

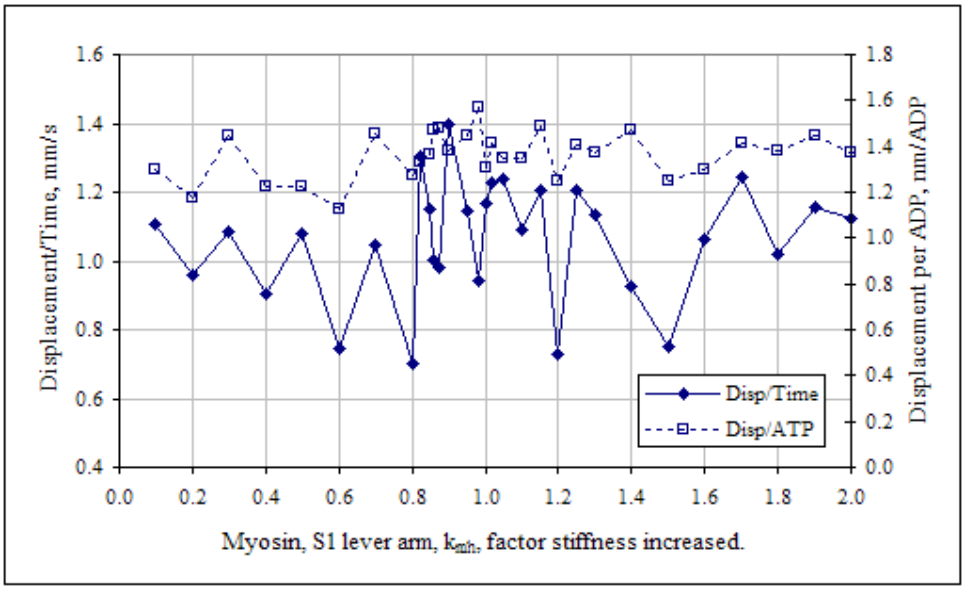

Figure 4.6.4, Model actin filament (1µm): speed of right-hand end of actin filament and efficiency over 0.1s with variation in S1 lever arm stiffness. 1.0 in the plot is the Baseline Model result. $k_4^0 = 100s^{-1}$, $x_4 = 80nm$ *and* $x_{-4} = -60nm$.

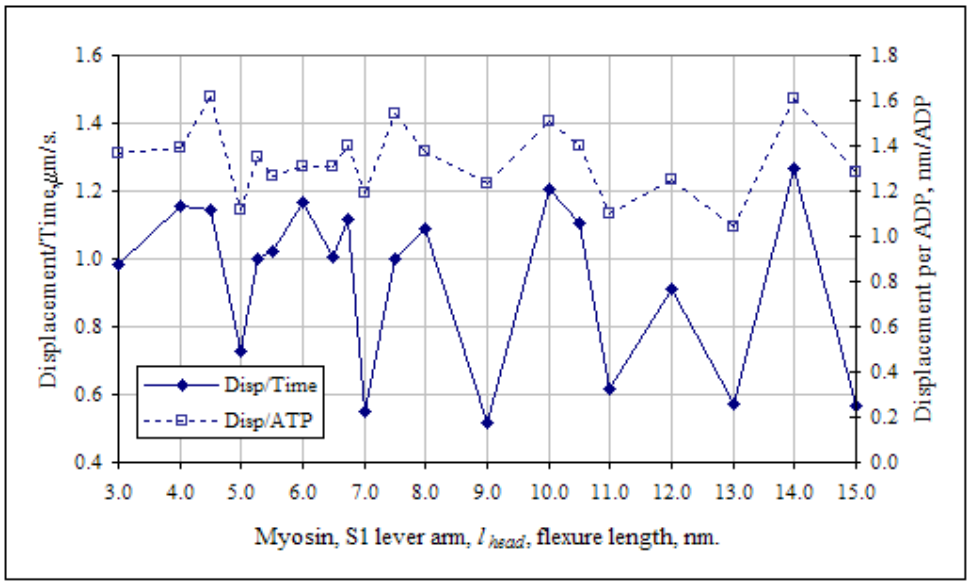

Figure 4.6.5, Model actin filament (1μm): speed of right-hand end of actin filament and efficiency over 0.1s with variation in S1 lever arm flexure length.
k_4^0 =100s^{-1}, x_4 = 80nm and x_{-4} = -60nm.

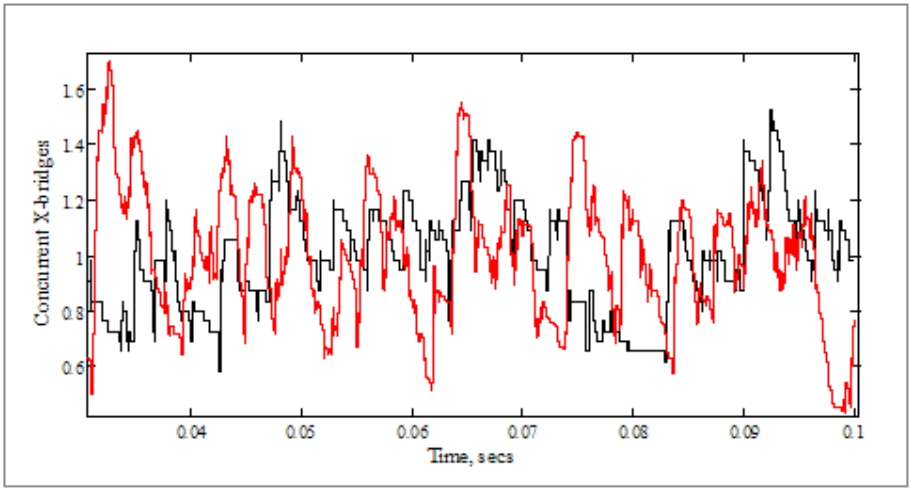

Figure 4.6.6, Normalised (to mean for each filament) concurrent number of crossbridges against time in the Baseline Model during a motility study that generated the speed and efficiencies plotted in Figure 4.6.2, actin length 2μm (black) and 8μm (red).
Data normalised to mean number of crossbridges for the individual filament. k_4^0 =100s^{-1}, x_4 = 80nm and x_{-4} = -60nm.

4.6.6 Summary

Using the model, peak filament speeds identified in vitro could be reached but longer filaments were required to achieve them and the efficiency of energy usage was very low. While the model was sensitive to decreasing the number of myosin bond sites increasing the concentration of myosin sites caused more crossbridges to form and lever less efficiently but without increasing filament speed. These differences

indicated the proportion of the crossbridge's strain energy driving filament movement in the model could be improved. A number of parameters were examined; the connection between them is that they changed the strain distribution within the system and consequently the importance of examining the strain dependency of the reaction durations was further highlighted. This will be discussed in a summary of Chapter 4 where the results of the chapter will be considered in terms of different isoforms, fibre characteristics and in vitro observations.

The importance of the compliance of myosin II S2 under compression was demonstrated. A point for further investigation was how S1 crossbridges maintain in vitro filament movement, although at reduced speeds [52,59], without pushing each other off the actin filament. The difference in tension between 2μm and 8μm actin filaments in the model was identified and consequently the actin filament stiffness was investigated and found to not influence the filament speed in the model. Examination of the S1 stiffness parameters indicated the k_{hm} stiffness identified in Section 3.2.6 provided improved speed and efficiency compared to more compliant values. l_{head}, a limiter on the flexure of S1 was found ineffectual which may have been a consequence of low loads in the filament due to an interaction with k_{hm}. It was reasoned that in future the two parameters should be examined as a pair. A cyclic component in the number of concurrent crossbridges occurring over time in the model was recorded. A cyclic characteristic was found when varying parameters k_{hm} and l_{head}. This may be partially due to the properties of the model, e.g. transitions between stiffness and time steps and is sensitive to tension in the filament but requires further investigation.

4.7 Force Development Under Isometric Loading.

The influence of the strain dependent pre-lever reaction parameters x_4 and x_{-4} on filament motility was examined in a set of experiments in Chapter 4 (summarised in Appendix C). For each of these experiments, after the displacement data had been recorded, at 0.11s the right-hand end of the actin filament was immobilised. Force was allowed to develop in the filament and the response at the right hand end of the actin filament was recorded providing a representation of isometric loading.

4.7.1 Characterisation of the Isometric Load.

In order to characterise the force response over time (see Figure 4.7.1 for examples) and compare one set of pre-lever parameters, x_4 and x_{-4}, against another the response was assessed in terms of the following:

1. Peak isometric force.
2. Time to peak isometric force.
3. ADP released up to peak force.
4. Impulse form onset to peak isometric force.
5. Impulse: percentage of total impulse released up to peak force, (0.11 to 0.124s).
6. Efficiency: Impulse to peak force/ADP released.

Characteristics 1-3 describe the speed and magnitude of the filament's response to loading and the efficiency of that process. Characteristics 4-6 evaluated the overall force generated in terms of an impulse, I_F extracted from the data using Simpson's approximation method:

$$I_F = \int_{t_1}^{t_2} F \cdot dt \approx \sum_{i}^{n} \frac{f_i + f_{i+1}}{2} \cdot dt \,, \qquad (4.7.1),$$

where i, in this instance, is t_1/t_{step}, the initial time divided by the time step used in the model and n is (t_2/ t_{step})-1, the penultimate time step. The average force is denoted by F and the initial and final force levels during the time step are f_i and f_{i+1}.Visually evaluating the data, after the onset of loading in the majority of cases the events had completed before 0.013s so this was used as a cut off point.

The results were considered in three stages, firstly the trends in the parameter-output relationship, sources of variability in this data and finally a more detailed examination of the processes at work in some of the key results.

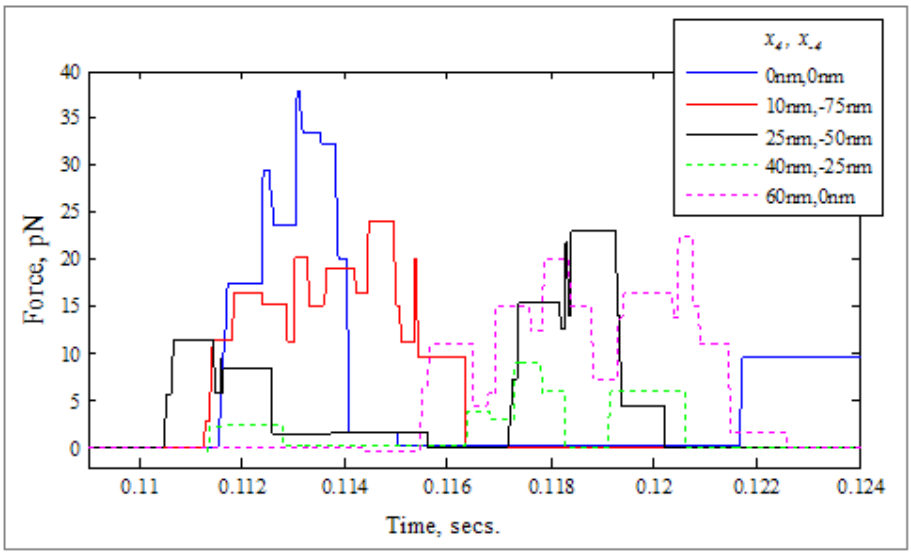

Figure 4.7.1, The isometric force response for a selection of values from the study range.

4.7.2 Isometric Force: pre-lever strain dependent reaction.

The results of the experiment are recorded in Appendix C, matrices 3-8. A high level of variation in individual runs obscured the response of the system to changes in the parameter values x_4 and x_{-4} but some trends were still indicated. Figure 4.7.2, B plots the peak isometric forces against the changing pre-lever reaction parameters. Peak values of 37.8pN (x_4 = 0nm, x_{-4} = 0nm) and 34.8pN (x_4 = 5nm, x_{-4} = -100nm) were observed. Plot A is a simplification of plot B: where x_4's value was held and x_{-4} was adjusted, the mean value observed and range has been plotted for x_4 and vice-a-versa providing generalised trends. Plot A indicates higher peak forces occur when x_4 < 25nm and x_{-4} = -50nm. The detailed results of plot B show these higher forces occur below x_4 = 25nm but also occur at higher values if x_{-4} = -50nm to –75nm. Lowering the value of x_4 makes the forward pre-lever reaction duration less sensitive to strain. Reducing the strain sensitivity reduced the distribution of crossbridges across time (Figure 4.4.8). Examination of the number of crossbridges below x_4 = 25nm a higher minimum and lower maximum number of crossbridges was recorded compared to the other parameter settings resulting in a lower spread of crossbridge values but a greater probability of having a high number of crossbridges active when loading was applied (Appendix C matrices 9-12). The x_{-4} = -50nm to –75nm results indicate benefits to making the pre-lever reaction more sensitive to strain. There may be a balance between number of crossbridges, removal of crossbridges that have travelled since forming and so release no useful strain energy or oppose strain production characteristics examined in Section 4.7.4.

How rapidly the peak force was reached varied without a clear pattern, from 1.2ms (x_4 = 60nm, x_{-4} = -50nm) to ~10ms (Appendix C, matrix 5). Two potential regions of higher values (min. 6.3ms) occurred above x_4 = 35nm where x_{-4} –50 to -75nm and below x_4 = 35nm where –125nm < x_{-4} < -50nm. The strain independent values (Figure 4.7.1 blue) provided the highest and most rapid force.

In vitro experiments measuring the deflection of glass micro needles holding an actin filament on a surface of HMM fragments measured forces per unit actin length of 11.8 ± 1.0 pN/μm [57], 12.2 ± 1.5pN/nm [99], S1 fragments 5.4pN/μm, monomeric myosin 9.6pN/μm Kishino and Yanagida [100] (*n.b*. Kishino and Yanagida's actin tensile strengths were double those currently measured using optical traps). Kawai *et al* [30] used optical traps to measure actin filaments across a surface of HMM fragments and determined ~6pN/μm. In Kaya and Higuchi*'s* [29] (Section 4.6) experiment filaments moved against the resistance of an optical trap. Near the peak force displacement ceased and ~13pN per 1μm of actin filament was measured. Therefore, the peak isometric forces generated in the model appear to be high. The difference could be explained by a greater compliance of the myosin-substrate in the in vitro experiments spilling more of the reacted load. In the model, the cofilament was set to represent the arrangement in a sarcomere so the results may be more representative.

Impulse to peak force and the number of ADP released showed similar trends, as would be expected, as the ADP release precedes the release of strain energy (Figure 4.7.3). Below x_4 = 60nm as x_{-4} increased in magnitude the number of ADP and impulse level was highest. These parameter changes had the effect of making the forward and reverse reactions more sensitive to strain changing the distribution of crossbridges in the pre-lever state.

Points x_4 = 0 to 30nm with x_{-4} at –125nm have previously been identified as anomalous points (Section 4.3.2) where there is a sudden drop in the number of concurrent crossbridges and a drop in the impulse. Few crossbridges, mostly zero or one, were released after the peak force was expressed. Above x_4 =40nm a scatter of events occurred where 3-5 crossbridges remained. No trends were found in efficiency: the ratio of impulse to peak force and ADP released.

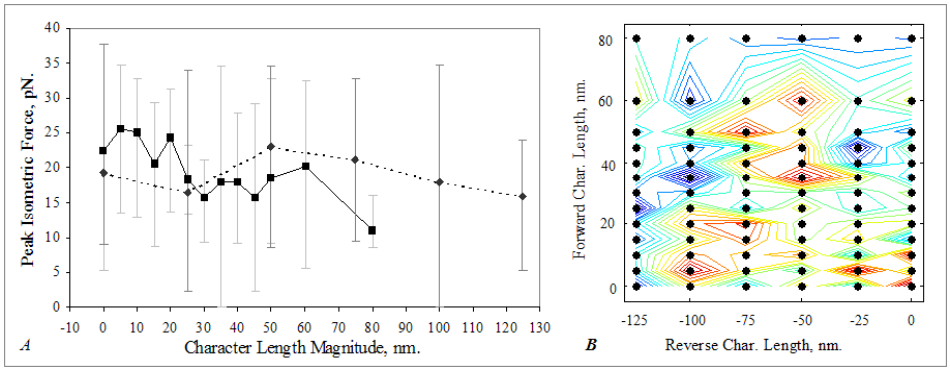

Figure 4.7.2, Peak isometric force at right-hand end of actin filament: Plot A: mean and range of values plotted for the responses at that parameter value dashed line $-x_{-4}$ and solid line x_4. Plot B: black dots indicate a result; colour indicates the peak force, red max. 37.8pN, blue min. 0pN.

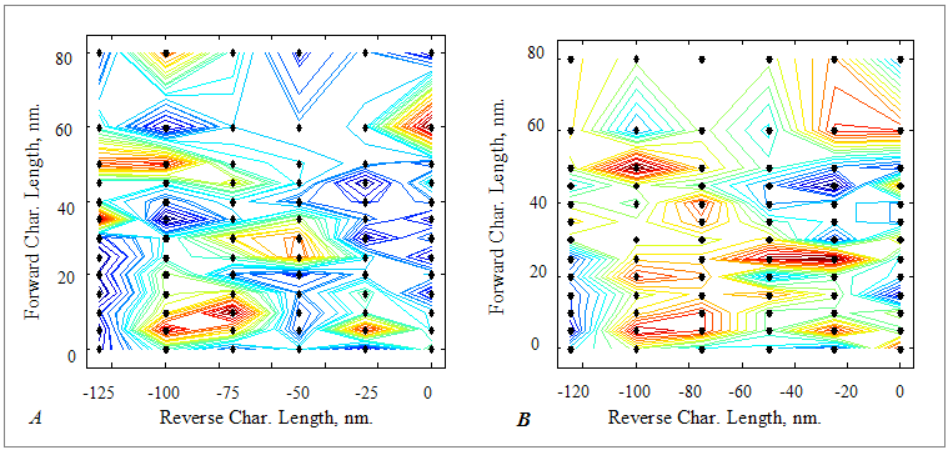

Figure 4.7.3, Plot A: impulse up to peak force, max. 7.1 x 10^{-14}Ns (red), min. 0.1 x 10^{-14}Ns (blue). Plot B: ADP released up to peak force, max 12 (red), min. 1 (blue).

4.7.3 Isometric Force: variation in an individual result.

In reviewing the modelss sensitivity to the pre-lever parameter values, a high level of variability in the model,s output was recorded. To gauge that variability five repeat runs were made with the same pre-lever parameter set of x_4 =10nm and x_{-4} =-75nm which is associated with a high peak isometric force and impulse. A summary of these five results is recorded in record (3) of Table 4.4.1. The mean peak force was 26.5pN (range +16%, -9.4%). The other performance characteristics were more sensitive to the changing initial conditions: time to reach the peak force varied by +45% and –29.6% and the ADP released by ± 25% and impulse from load onset to peak force varied by +90%. The force against time for these five filaments is plotted in Figure 4.7.4.

The only random component in the Baseline Model was the time of release of levering crossbridges that are unable to complete or reverse through the reaction cycle (Section 3.5.7). This has been shown to change the pattern of filament movement (Figure 4.4.7 and Table 4.4.1). In was noted in Section 4.6.5 that the number of concurrent crossbridges changes over time for a 1μm actin filament (see Appendix D, Figure D2).

At the time the load was applied, the number of and reaction stages of the filament's crossbridges would have been different. This is demonstrated in Figure 4.7.4 where the number of concurrent crossbridges when the load is applied varies, as does the time of release of the crossbridges and ADP.

In addition to the variation in a single filament, the myosin concentration was evaluated. Table 4.4.1 records (1) and (3) x_4 = 10nm, x_{-4} =-75nm, every third myosin bond site was blocked to mimic a reduction in the concentration of myosin. There was a drop in peak force from 26.05pN (+16% to –9.4%) to 14.3pN (+31% to -53%). The time to peak force increased from 4.6 to 8.5ms and the number of ADP released dropped from 8 (10 to 6) to 5.2 (7 to 3) indicating the presence of fewer crossbridges in line with the lower peak force.

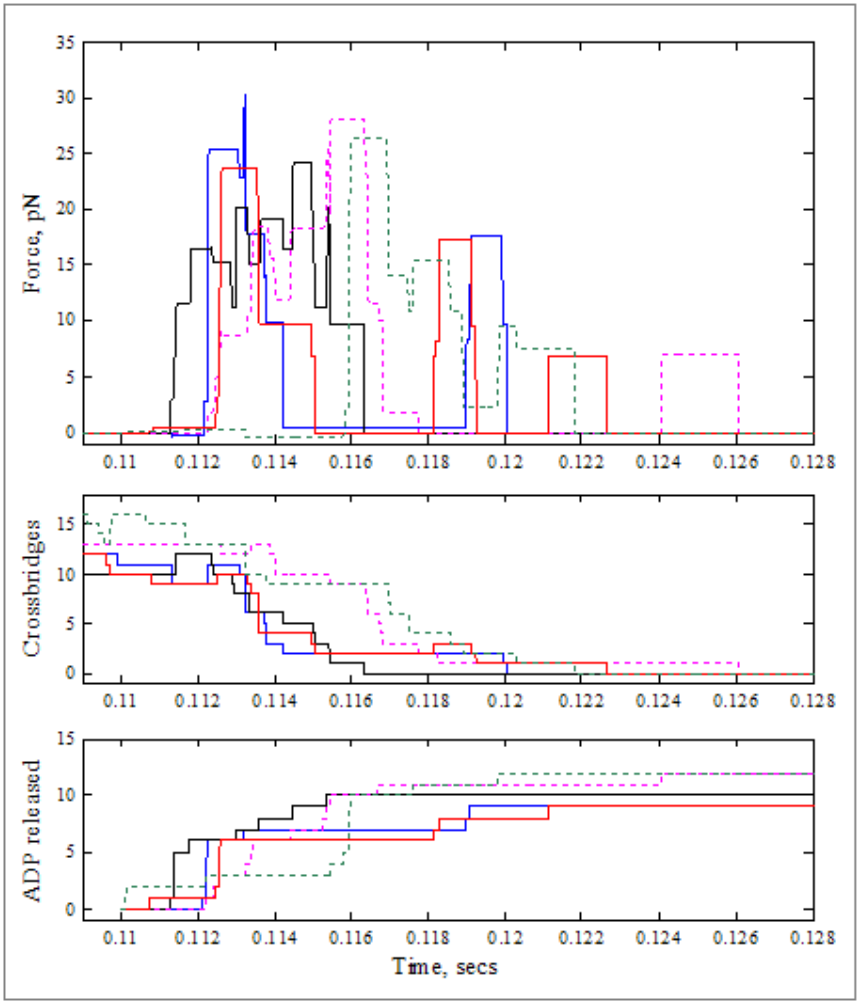

Figure 4.7.4, Isometric force response at right-hand end of actin filament for five results, parameter values: k_4^0=100s^{-1}, x_4 =10nm and x_{-4} =-75nm. Force is shown in the upper plot, the middle plot records the number of concurrent crossbridges and the lower plot the number of ADP molecules released: a release indicates the onset of a levering event.

4.7.4 Crossbridge Interaction During Isometric Loading.

To better understand the processes at work under isometric loading the interaction of crossbridges for two parameter settings was examined in more detail: x_4 = 10nm, x_{-4} =-75nm and x_4 = 40nm, x_{-4} =-25nm. The right end of the filament position was held and the left was free to move.

The two results started with similar numbers of crossbridges in similar states but generated different peak forces. In Figure 4.7.5, A, loading on the filament began with nine crossbridges in a pre-lever state (black) and 3 levering (red) resulting in a peak force of 24pN (Figure 4.7.5, A) while the second example (Figure 4.7.6, A) also had

nine pre-lever crossbridges (black) and 3 levering (red), but generates 5.6pN at most (Figure 4.7.6, C).

In both examples, there was very little movement of the filament, which limits the forming of new crossbridges and the generation of more force. The crossbridges present release and are not replenished. A single new crossbridge formed at actin bond site 8, Figure 4.7.5, A.

In plot A Figure 4.7.5, the individual reaction cycles show most of the crossbridges are released during or linger in the levering stage (red) strongly influencing the expression of the stored crossbridge energy. More crossbridges with the lower peak force result, Figure 4.7.6, complete the reaction cycle, being released by ATP (blue) demonstrating a much lower tension within the filament.

Some crossbridges, in both examples, contribute little or nothing to the overall force production e.g. actin site 4 in Figure 4.7.6, A, C and actin sites 13,16,17,19 Figure 4.7.5, A, C. At the onset of loading they have already expressed their strain energy or the crossbridge has moved so much since forming that its strain energy straightens the myosin arm it is attached to diverting the energy to the cofilament. The lower value of x_{-4} =-75nm would have made the filament in Figure 4.7.5 more sensitive to negative loading than that in Figure 4.7.6 (x_{-4} =-25nm) removing crossbridges that had travelled excessively more rapidly.

Crossbridges occurred which acted as blocks in the tension distribution along the filament's length. The most notable of these was at actin site 15, Figure 4.7.5, A, which remained in the levering state throughout the study period. In plot B it can be seen to have caused a disruption in the filament tension; the tension to the right changed but was consistently lower than the tension to the left. Such behaviour could prevent the filament from slipping if a sudden loss in tension occurred.

Examination of the initial length of the filaments showed the first, fast filament was under extension and the second under compression. This is highlighted by the negative force detected in Figure 4.7.6, C after the right hand crossbridges are released. Examining other examples showed no clear pre-load – peak force relationship.

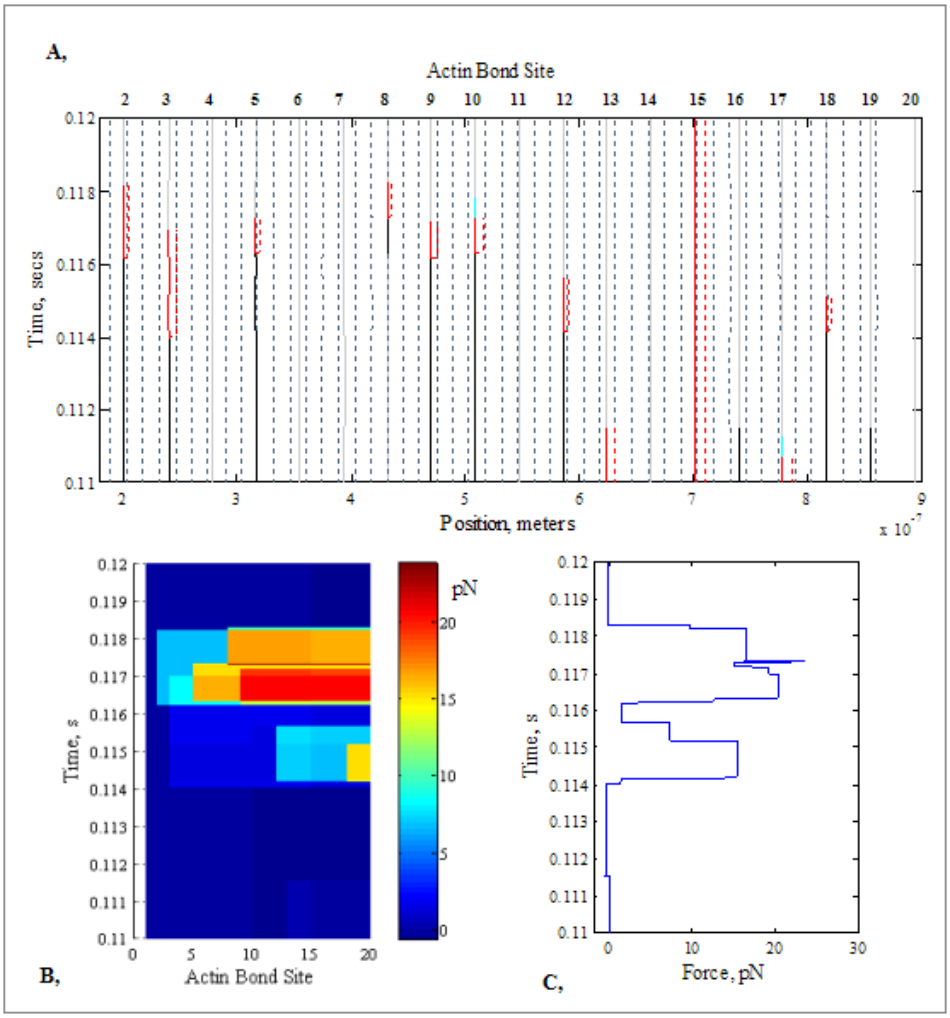

Figure 4.7.5, The isometric loading of an actin filament with parameter settings x_4 = 10nm, x_{-4} =-75nm A: the reaction state, position and timing of crossbridge interactions (see Figure 4.3.2 for a detailed description), B: the change over time of tension between bond sites along the length of the actin filament and C: the force level at the right-hand end of the actin filament against time.

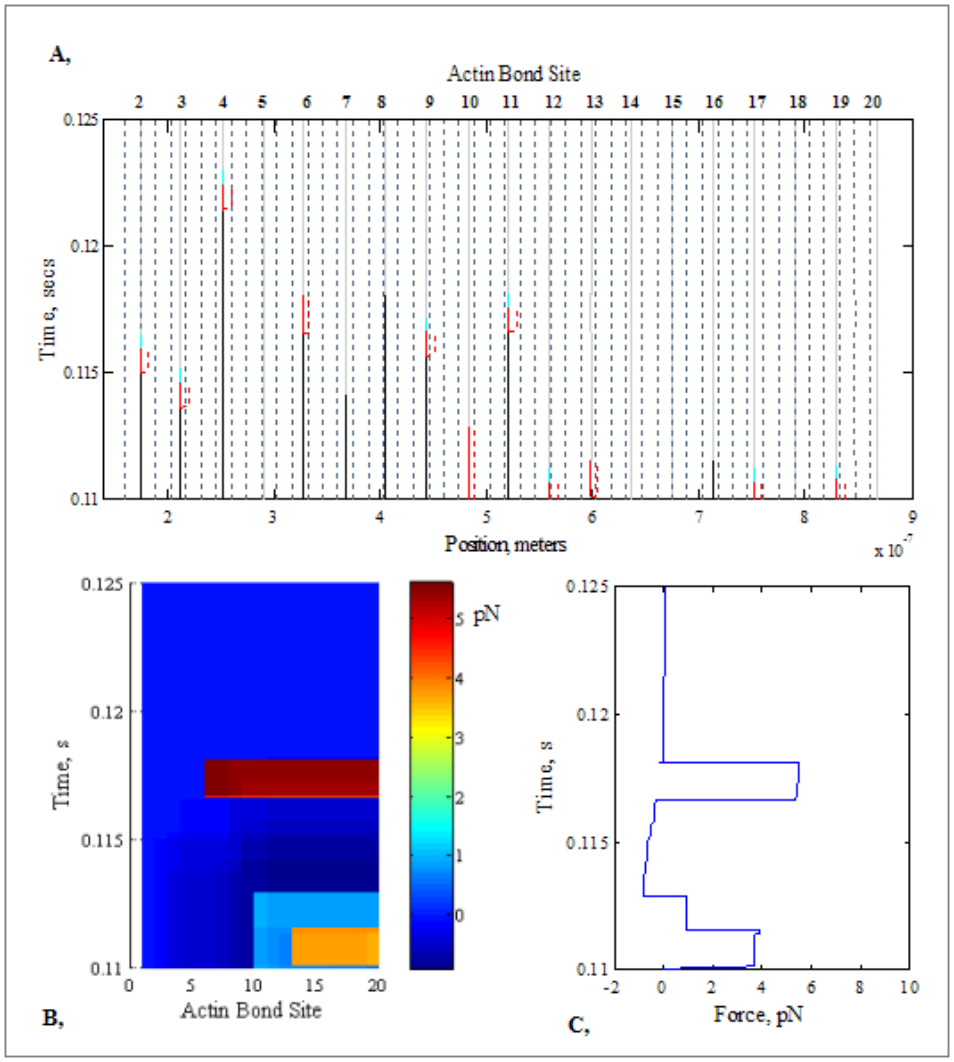

Figure 4.7.6, The isometric loading of an actin filament with parameter settings x_4 = 40nm, x_{-4} =-25nm A: the reaction state, position and timing of crossbridge interactions (see Figure 4.3.2 for a detailed description), B: the change over time of tension between bond sites along the length of the actin filament and C: the force level at the right-hand end of the actin filament against time.

4.7.5 Summary.

Examination of the results of Section 4.7 show there were two key stages to the development of isometric force. The first was the number and state of the filament crossbridges at the onset of loading and the second was the expression of those crossbridges as force began to develop.

Making the pre-lever strain dependent reaction less sensitive to load opposing the direction of compression maintained crossbridges in the forward pre-lever state for longer. With the onset of loading this increased the chance of more crossbridges being

present with stored strain energy with an increased potential for higher peak forces and impulses. However, once formed, a crossbridge that travelled too far released strain energy into the cofilament rather than the actin filament and could inhibit the release of strain energy from other crossbridges. The benefits were observed in impulse results of removing these crossbridges by reducing the value of the reverse reaction, increasing the rate of removal of crossbridges loaded in the direction of contraction. There was a balance demonstrated between the forward and reverse reaction strain sensitivity in order to maintain a higher number of crossbridges in readiness for the load onset.

After the onset of loading, force developed but was not sustained. Due to a lack of movement in the filament, few new crossbridges were formed; the recycling of the initial crossbridges seems necessary to maintain force for longer periods of time as observed in vitro [30,57]. However it is notable, that the filaments in vitro tend to be much longer, have more crossbridges and may experience more internal tension and shifting bond site positions due to the higher number of crossbridges. In the experiment, a perfect equilibrium in force and displacement was imposed. In a sarcomere and fibres, more movement may be expected as filaments potentially jostle one another generating more bonding opportunities. After the onset of force, a fast turn-over in response to filament tension may generate more force. This may be in contradiction to the pre-lever parameter settings for the initial onset of force, but without the formation of new crossbridges, cannot be gauged here.

A large proportion of crossbridges was held in the levering stage highlighting the importance of this reaction stage in force development and indicating, that further investigation of it is required. Again, greater movement in the sarcomere through the interaction of filaments may reduce this occurrence. There is some experimental evidence for the increased duration and detachment during the levering stage: In in vitro experiments at higher loads, the rate of ATP utilisation in fibres declines [101,102] and the lever stroke is shorter and slower in in vitro filament studies [103].

In comparison to in vitro data, the peak, forces for a single filament under isometric loading generated by the model (~37pN) were higher by a factor of 3. In vitro the substrate against which the filament force was reacted has been demonstrated to be more compliant than the cofilament in the model (Section 3.2.6), which may account for the difference. The model's stiffer cofilament was more representative of the stiffness in the sarcomere. The distribution of peak forces in time, demonstrated here,

may be beneficial in a fibre, avoiding a sharp, potentially damaging stab of force under initial loading.

4.8 Summary of Chapter 4.

Motility has been examined in terms of 1μm lengths of actin filament traversing substrate bound myosin proteins; this can approximate a contracting filament under low load in a sarcomere. Primarily the parameters defining the strain dependent pre-lever reaction duration were examined. By comparison with specific in vitro experiments, it was also possible to consider the influence on motility of a number of other model parameters.

The issue was raised as to how to accommodate the long pre-lever reaction duration measured in solutions of fragments while obtaining a feasible crossbridge attachment duration that would correlate with observed in vitro filament speeds. By reducing the pre-lever attachment duration model filaments moved more quickly but movement was not sustained: the actin filament disconnected from the myosin surface. In a sarcomere with filaments working together, this may not be a problem as movement in one filament may offset a pause in another. However, the in vitro evidence shows single filaments of 1μm, the length used in the model, can move at high speeds so persistence of movement and speed of movement were considered to be of equal importance. In vitro, such filaments may have maintained their position (the model filament has a low load returning it to its initial position when no crossbridges are present) and be 'nudged' on by thermal noise. In order to improve speeds without resorting to introducing a stochastic element to the model the reaction stage with the longest duration, pre-lever, was examined in more detail.

A strain independent duration of 10ms, k_4^0 =100s^{-1} was used. The structured arrangement of bond sites in the sarcomere and filament in vitro studies was argued to decrease the pre-lever reaction duration in comparison to fragments measured in solution (k_4^0=30s^{-1}, 33ms duration). In order to increase speed, it was found, when a load opposing contraction was applied, the forward reaction is favoured with a reduced duration. In response to increasing loads in the direction of contraction, the reverse reaction is favoured and the duration increased. Filament speeds rose from strain free 0.65μm/s to 1.24μm/s with k_4^0 =100s^{-1}. Increasing k_4^0 to 30s^{-1} generated

surges of similar speed to k_4^0 =100s^{-1} but were interspersed with long pauses in motion.

The strain on the crossbridges comes from the external load and the internal filament tension created by the crossbridges. The effect of the strain dependent pre-lever duration was a broad distribution of crossbridge attachment times. Some cycled rapidly, as would be expected for increased speed, while other crossbridges were of longer duration, some drifting between forward and reverse reactions and remaining attached longer than the strain free reaction time. Crossbridges of longer duration provided stability to the filament's movement by holding the filament's position if no other crossbridges were levering and by maintaining crossbridges that could quickly transfer to releasing strain energy if needed or be quickly removed if excessively loaded in the direction of contraction. A pattern emerges where the long strain free reaction times from fragments in solution and the in vitro filament speeds measured can be represented in the model dynamics. Strain dependency could also explain the observation that single crossbridges studied in vitro release strain energy almost immediately after forming.

Increasing resistance to the filament's movement by applying the stiffness of titin in the sarcomere increases the effect of the strain dependent reactions causing increased filament speed and efficiency. The results of in vitro fibre studies analysing force-velocity-displacement data show that as the force increases the speed of contraction decreases. This raises the question as to whether there is a non-zero optimum loading of the sarcomere, that is, is it dictated by the titin in the sarcomere? Model refinements, discussed later, are required to examine this in more detail.

By increasing the actin filament's length, the filament speed was also increased up to a peak of ~9μm/s which approximates the peak filament speeds observed in vitro. However, the length of filament required to achieve this speed was longer than that observed in vitro (7μm vs. 2μm). Cross-referencing this result with other, in vitro, results suggests the number of concurrent crossbridges per unit length of actin is reasonable and increasing the number of myosin sites incurred no increase in speed or in the number of crossbridges. The longer actin filaments did have increased internal tension, which appeared to cause a wider distribution over time in levering events and sustain a slightly high number of concurrent crossbridges.

Examining the influence of structural components of the sarcomere it was found that reducing the cofilament stiffness, which approximates to the in vitro substrate stiffness, reduced filament speeds as crossbridge strain energy is converted to deforming the cofilament rather than propelling the actin filament forward. The actin filament's stiffness had no influence on its speed in the model: importantly the model did not distinguish between the filament under compression and extension. Actin stiffness may be sensitive to the load direction due to its helical structure in addition to lateral bending. A slight increase (~20μN/m) in the myosin II arm stiffness, S2, in compression improved speed but greater stiffness increases inhibited the formation of new crossbridges and movement. A high compressive stiffness of S2 is equivalent to removing the S2 component leaving the stiffness of the myosin head, S1, to operate in isolation. In vitro, S1 fragments of myosin where the S2 component is chemically removed, can sustain actin filament movement but the concentration of myosin must be greatly increased and the filament speed is greatly reduced. In an example in vitro motility experiment [59], myosin fragments with the S2 component intact (HMM fragments) sustained actin filament movement at 7.5μm/s but with the S2 component chemically removed the speed fell to 1-2μm/s with similar rates of ATP consumption. In the model, movement was not sustained but a higher concentration was not examined in relation to this. It is a point for future work.

In the model, the efficiency with which energy in the form of ATP was used was considered in terms of the actin filament movement achieved per ADP released, the maximum efficiency being a complete lever distance, b_{max}, divided by one ADP. This maximum was reduced by how far a crossbridge travelled from its point of formation before releasing its strain energy, the relative stiffness and loading of the actin filament and cofilament components and the overlap of levering events.

In response to applying the strain dependent pre-lever reaction duration, efficiency improved approximately in line with increased filament speed. Effectively, crossbridges that opposed levering experienced increased strain in the direction of contraction so were reversed and removed. If the reverse reaction was made too sensitive to loading, the efficiency increased, but not enough crossbridges were maintained for filament motion to persist. However, peak efficiency still appeared to be quite low (1.55nm/ADP).

By removing crossbridges that had travelled in the pre-lever state, efficiency was improved (~2.5nm for 25% for a maximum travel of ~7.6nm). The interpretation of

this in the sarcomere is that there is limited space between the actin and myosin filaments such that the myosin head would incur increased loading due to spatial restrictions. Increasing the tension gradient across the filament by applying a higher external load increased the number of concurrent crossbridges but offset them in such a way as to increase efficiency.

Two other parameters were examined which also influenced the offset in crossbridge formation and levering events. Efficiency was strongly influenced by the relative speed of bond sites forming crossbridges, v_{cross}. v_{cross} could be used to shift the output between high efficiency and slow, less stable speeds and higher speeds with lower efficiency. One interpretation of v_{cross} would be the affinity between actin and myosin. Extending the post-lever reaction duration increased efficiency to 75% (4.08nm/ADP from 2.33nm/ADP k_{ta}=0.335μN/m). The uptake of new crossbridges was slowed down. Further investigation of the strain dependency of the post-lever reaction duration would therefore seem important in improving efficiency without compromising motility speed.

In vitro, at low temperatures (12^{o}C) [104], different reaction stages were found to be important to different fibre types. Contraction speeds in fibres with the slow isoforms of myosin II were dominated by the rate of ADP release. In fibres with fast myosin II isoforms the release of ATP, corresponding to the release of the crossbridges, had greatest influence on speed. Indications are that this may not carry through to human body temperatures, 37^{o}C, where ADP release may dominate both fibre types. By focusing the study on the pre-lever period the model's behaviour may have been limited to that of slow filaments. Therefore, completing an evaluation of all of the reaction stages will be important future work. In shorter actin lengths, in motility studies, the number of concurrent crossbridges observed in the model was cyclic and this characteristic decayed as the filament length increased and more crossbridges became active. Initial indications are that this behaviour is dependent on the strain response of the reaction durations and the selection criteria for new crossbridge formation. The mean number of crossbridges in the model approximates the number measured in vitro but it is not clear whether this cyclic characteristic is representative. The multiple filaments in a sarcomere may even out this cyclic characteristic.

The cyclic number of concurrent crossbridges was significant in the results of the isometric loading as at the on-set of loading it changed the number of crossbridges the filament had to generate force with. The lack of filament movement and generation of

new crossbridges amplified this effect after initial loading. Contrary to the properties for motility, the isometric loading favoured strain dependent pre-lever forward reactions of longer duration, that is, less sensitive to strain. As the forward reaction became more sensitive to strain, the reverse reaction had to increase sensitivity to maintain a higher level of force over time (impulse). A faster turn-over of forward reactions increased filament movement so the reverse reaction must remove over-travelled crossbridges more efficiently, but over zealous removal left too few crossbridges available to generate displacement and force ($x_{-4} > 100$nm). As force development was so dependent on the initial state when loading began the output was heavily influenced by the low load contraction behaviour. The peak levels of force generated in the model were higher than comparable data measured in vitro, the difference may be attributable to greater, in vitro, substrate compliance.

Two aspects of the crossbridge model in the levering stage were influential in the isometric loading and motility studies: how an individual crossbridge in the levering stage should respond to being in an isometric state; and the model's response to rapid over-loading of the levering crossbridge. The first of these states strongly influences the isometric force development and the second the stability of the model as filament loading increases. Both require consideration before loading can be examined in more detail.

Having many concurrent crossbridges appears to be useful; the crossbridges are then available to be used for force production and as part of the contraction movement but it is important that the system is 'tuned' to efficiently use them. Efficiency in this instance means quickly removing crossbridges which are opposing movement or have moved and lost their potential contribution to force production before they release their strain energy, but that efficient use may vary between isometric force generation and speed of contraction. In vitro the number of crossbridges that have occurred is gauged by the concentration of γ-phosphate or rate of ATP hydrolysis. The model suggests many crossbridges are present which do not reach one of these chemical stages and so are not detected in vitro but still contribute to the filament's function.

Chapter 5

5 Conclusion.

5.1 Single and Multiple Crossbridge Modelling Compared.

Force and displacement in a muscle contraction are powered by interactions between bond sites on actin and myosin filaments. At these crossbridges chemical energy is converted to mechanical energy. In vitro data are beginning to identify the components of the sarcomere and crossbridge, particularly the isoforms of myosin II (Section 3.2.1), that define the overall character of a motor unit's output within the muscle bulk. The number of filaments, sarcomere, fibre dimensions and distribution contribute to the bulk muscle characterisation (Figure 1.1.1, Section 2.1).

Models, which currently exist, tend to focus on either extreme of the muscle's function. There are models based on the bulk output of the muscle with no regard for the composite components, e.g. Hill models. At the other extreme thermodynamic models represent the individual chemical events of the crossbridge with some reference to the filament structures before extrapolating to bulk fibre behaviour. In this project, a mathematical model has been developed which represents a subsection of a half-sarcomere (Appendix A, Diagram A, D, Figure 3.8.1 model overview). The subsection is the basic functional unit of a muscle which repeats across the sarcomere and along the length of the myofibril. The model relates the chemo-mechanical cycle of individual crossbridges to the transfer of mechanical energy through an actin filament, myosin cofilament and, by incorporating the protein titin, the mechanical properties of the interconnecting proteins in a section of sarcomere. This allowed the complexities of the individual crossbridge events to be studied while moderating their potential number; in a fibre there can be in excess of 10^{15} bond sites (Figure 1.1.1).

The mathematical model is composed of various modelling approaches to accommodate the interdependency of the chemical cycle of the bond sites, crossbridges and the mechanical output. A reaction equation (Section 3.3, Equation

3.3.7) determines a minimum duration for each reaction stage of a myosin bond site as it develops strain energy, binds to an actin bond site, releases the strain energy and then separates from the actin bond site in readiness to recharge with energy (Figure 3.3.1). However, this chemical cycle is constrained by geometric and mechanical properties. A crossbridge's formation is limited by the relative speed and position of bond sites (Section 3.4). Over time, with changing patterns of crossbridges, the length and, therefore, compliance of actin filament and myosin cofilament between crossbridges can change, consequently, the spring-damper representation of the filament system is reformulated at each model time step (Section 3.6) and the duration of the reaction stages which may be strain dependent (Equation 3.3.7). The release of a crossbridge's stored strain energy is expressed as a displacement (a conformation change) between actin and myosin bond sites. The model approximation of this is a compressed spring-damper (Section 3.5, Equation 3.5.1). The release of this spring-damper allows the reaction cycle to proceed or it may inhibit the cycle or change its direction. Functions fitted to in vitro obtained empirical data were used to define the separation of actin and myosin bond sites of a levering crossbridge that could not recover or release its strain energy (Section 3.5.7) and to define the rupturing of crossbridges due to excessive load rates (Section 3.3.3, Figure 3.3.2). Appendix A and Figure 3.8.1 show overviews of the model.

The model required a high number of parameters, (summarised in Appendix B). While there is a consensus in the literature as to some of the experimentally determined values, other parameters of a smaller magnitude or which relate to transient events are more difficult to measure and are therefore inaccurate, imprecise or unknown. With improvements in in vitro experimental techniques, for example optical trap manipulation of individual crossbridges and filaments, the consensus as to some experimentally derived values is improving, for example the lever distance b_{max} (Table 3, Appendix B). Using the model developed in this project the underlying behaviour of individual and multiple interacting crossbridges, which currently cannot be observed in vitro, could be evaluated by comparing the resultant outputs with those that have been measured in vitro.

Initially, the model of a single crossbridge was developed in stages testing the representation and selected parameters against published data of single crossbridges manipulated in vitro with optical traps. By this means, the expression of the chemical energy of the crossbridge in-to mechanical energy was examined using an isometric loading scenario (Section 3.5.3). This experiment enabled the examination of the

model levering parameters (b_{max}, k_b, k_{mh} and c_b see Appendix B, Table 3). The force-displacement generated by the model corresponded with the in vitro data and the individual parameter values, which generated this correlation, aligned with in vitro data from several other literature sources.

All of the model's components, actin filament, myosin cofilament and titin protein, were brought together in a scenario that approximated to a low-load high-speed concentric muscle fibre contraction (Section 4.1). In vitro motility studies where single actin filaments traverse substrate bound myosin cofilaments and myosin fragments provided filament speed, resultant force and an overall estimate of ATP consumption against which the model could be compared.

The model simulation of motility studies demonstrated how strain dependent reaction durations could accommodate the apparently contradictory in vitro results of the long duration of the chemical cycle of the crossbridge (the ATPase rate) and the speed with which an actin filament can traverse a surface coated with myosin and consequently how rapidly a muscle can contract (Section 4.4.6). Measurement of actin and myosin fragments in solution has shown a long reaction cycle dominated by the duration of the pre-lever reaction stage where actin and myosin link to form a crossbridge (Section 3.3, Figure 3.3.1, Table 3.3.1). To achieve the filament speeds seen in vitro, speculation in the literature suggests that the attachment time of the crossbridge must be short. In the model, filament movement was not maintained if the pre-lever attachment was simply shortened (Section 4.3). However, with a strain dependent pre-lever duration in the model at low strain, the duration could be made comparable to the low strain scenario of filaments in solution while in motility studies actin filament speeds, obtained in the model, were comparable to those observed in vitro. The durations of the crossbridge attachments were not necessarily short in the motility studies. Tension within the actin filament caused a distribution of attachment times, some quite short and others longer than the strain-free attachment cycle (Section 4.4.9). These longer attachment times increased the persistence of the actin filament's movement by reducing pauses in motion and maintaining an interaction between the actin filament and myosin cofilament.

Application of the stiffness, estimated from in vitro data (Section 3.7), of the titin protein in the sarcomere to the model caused a passive resistance to the actin filament's movement causing an increase in filament speeds (Section 4.5). The light load improved the performance of the strain dependent reactions demonstrated by an

increase in the filament movement imposed on the actin filament by each crossbridge despite an increased number of concurrent crossbridges. This result contradicts the in vitro observation that as load increases the speed of fibre contraction decreases, but this may indicate there is a non-zero load for maximum contraction speeds. These results suggest that the passive structure of the fibre may 'tune' the optimum output of the crossbridges. This observation highlights the limitations of prematurely extrapolating the output of a few individual crossbridges to the bulk muscle behaviour and vice-a-versa.

Actin filament speeds, filament force generated under isometric loading (Section 4.7) and the number of concurrent crossbridges (Section 4.5.3) observed in the model are comparable to in vitro data indicating the model's crossbridge levering stage generates an appropriate amount of force and displacement conferring confidence in the single crossbridge study of Section 3.5.3. In this project a number of parameters have been identified that influence crossbridges and how they may be adjusted in order to modify the output characteristics of the sarcomere system i.e. speed of contraction, the actin filament displacement achieved per ATP (efficiency) and isometric force development. The parameter settings for these characteristics may be in opposition; for example, the pre-lever reaction strain parameters for speed of contraction do not correspond to those for isometric force development. There is a balance between the number of crossbridges and their state and spatial distribution in order to support filament movement and the onset of loading while removing crossbridges that may inhibit the output force and displacement.

The number of and offset in timing of crossbridge formation can be adjusted by modifying the affinity of actin for myosin (parameter v_{cross}, Section 4.4.8) and the strain dependency of the duration of reactions. The pre-lever reaction stage's influence (Section 4.4.3) has been examined in detail and based on an initial investigation; the strain dependency of the post-lever reaction (Section 4.5.4) also appears significant in the crossbridge distribution. Once the crossbridges have formed, the tension in the sarcomere system feeds back into the character and distribution of the strain dependent crossbridges. The structural components identified as being of key significance to that tension level and distribution were the myosin II arm (S2), head (S1) stiffness and the cofilament (substrate) stiffness. An over-compliant cofilament (substrate) deforms under the crossbridge strain rather than providing resistance against which the crossbridge can load the actin filament (Sections 3.2.6, 4.6.3). Similarly, the tensile stiffness of the myosin II S2 arm forces the crossbridge energy into the actin filament.

However, its low compressive stiffness reduces inter-crossbridge strain allowing multiple crossbridges to be sustained. In the model, efficiency of energy usage could be improved if the movement under compression of S2 is limited and at that limit, crossbridges are broken. This approximates to saying there is no more space to move in the sarcomere, ramping up the strain on the crossbridge causing it to rupture (Section 4.4.7). The expression of S2's stiffness is modified by its connection to S1. The stiffness values of S1 were set in a single crossbridge experiment using the model (Section 3.2.4) by comparison with in vitro data. The values obtained corresponded to the values for S1 that provided a stable rapid filament movement (Section 4.6.5).

In developing and experimenting with the model three particular points of interest for future study were identified. (1) By concentrating on the pre-lever reaction stage the study may have limited the filament behaviour. In vitro evidence indicates different types of fibre (fast or slow) are influenced more strongly by different reaction stages. Sensitivity to the reaction stage can also be temperature dependent. Therefore, further study of the reaction cycle is indicated. (2) In vitro, the movement of actin filaments on a substrate coated with S1 myosin heads has been observed. In the model, without the flexibility of the myosin II arms, S2, the actin filament movement is not sustained (Section 4.6.4, Figure 4.6.2). Investigation of this difference may expand the understanding of the S1 structural components that are strongly associated with different isoforms of myosin and therefore different fibre types. (3) In the model a linear approximation has been used for many of the parameters, e.g. k_{ta}, k_{tm} and k_m. In some instances, e.g. the combined S1 and S2 stiffness, the stiffness transitions through different linear states. This approximates to test data for the level of force and displacement examined here (lower force and shorter contractions) but for larger sarcomere distortions other non-linear behaviour should be considered, e.g. titin's stiffness becomes non-linear and appears to have a yield-point at ~3.8μm (Section 3.7.3).

The model described in this project has been compared to in vitro data from a number of laboratories using samples from a variety of muscles and types of animal. To advance the model it would be beneficial to have a coherent set of data for a single crossbridge, a filament and a myofibril (a number of sarcomere) such that force, displacement and ATP consumption can be gauged across the levels and where possible isoforms and fibre types identified.

Further parameter investigation and refinement of the model as it stands has been indicated and the need to extend the model in two directions. Firstly, the development of the mechanical structure to a larger cross-section of sarcomere, multiple sarcomere in series to form a fibre incorporating connective structures in order to study the transfer of strain energy. This may not necessarily entail creating many copies of the model as it stands but may be achievable by defining the external input to the model or the interplay between several models. There are a great deal of in vitro data available both animal [104-109] and human [15,21,22,110-113] at the fibre level such as fibre type specific stretch activation data (step changes to fibre with the recovery of tension monitored) which can be used to test a model and takes the model closer to the function of a motor unit. Secondly, the stimulation of the muscle to contract involving the import and export of chemicals and heat into and out of the bulk muscle should be considered. In the current model temperature and chemical concentrations are modelled as components of the reaction rates (see Equation 3.3.7, Figure 3.8.1 and Appendix E, Function: ReactionRate) and variation in stimulation (in terms of modifying how receptive actin is to myosin) can be simulated, however, bulk muscle makes these properties more complex; for example, temperature may influence the elastic properties of components. Across a muscle, activated fibres are interspersed with inactive and different fibre types. A fibre cell's structure is modified to accommodate different time profiles of energy supply; the movement of the muscle influences the blood supply and there may be temperature gradients across the filament.

5.2 Conclusion.

To adequately simulate muscular diseases and their treatments a model is required that incorporates the internal processes and structures of muscle. Previous models have focused on either the chemical processes or the bulk muscle output. The aim of this project was to build a model that would bridge the gap between individual crossbridge chemistry and bulk muscle output providing a means to investigate those internal processes and structures and their influence on the force-displacement output of muscle.

A prominent difficulty in generating this chemical-bulk muscle output link is the high number of individual, complex crossbridge interactions that combine to generate a

muscle's force-displacement output. To address this difficulty a model of a repeat unit within the sarcomere was constructed consisting of an actin filament, composite myosin filament and a composite titin protein. The selection of this unit enabled the examination of individual crossbridges, the interaction of multiple crossbridges and part of the passive mechanical structure of the sarcomere. The identification of this repeat unit provides future potential for scaling the input and output functions of the unit to the myofibril and motor unit level.

At the scale of the model, in vitro data were available for comparison in the form of chemical, chemo-mechanical data for a single crossbridge and actin filament force and displacement. The availability of in vitro data at different length scales proved useful in addressing the issue of the high number of model parameters. Some parameter values have been identified with high confidence in the literature; others are ambiguous or unknown. Whilst ongoing advancements in experimental techniques improve that understanding, the model described in this project provides a means to examine the parameter values and associated mechanisms across several length scales.

The model generated force and displacement results comparable to in vitro data for a single crossbridge and multiple crossbridges acting along a filament in isometric loading and low load contraction scenarios. The importance was observed of the mechanical structure of the sarcomere in defining the timing and state across the actin filament of the individual crossbridges resulting in variations in filament speed and efficiency. Some elements of refinement and further parameter study have been identified in the current model, e.g. post-lever reaction duration strain dependency. In this project, in vitro data have been used from a variety of experimental sources where muscle samples have been taken from a diverse selection of muscles and animals. To refine and further exploit the model it would be useful to have coherent in vitro data, that is, samples which relate chemical, crossbridges, filament and myofilament characteristics to chemical and force-displacement data from common sources and where possible with identified isoforms.

The work described in this thesis has demonstrated the principles for implementing a chemo-mechanical model of the most fundamental reactions and structures that determine the function of a muscle. It provides a foundation from which to develop models of myofibril, fibre, motor unit and finally, bulk muscle. As the length scale of the model increases to that of the myofibril and fibre, in vitro data become more readily available. With these increases in scale, additional properties become

significant and will require consideration: the chemical activation of the muscle, delays in the diffusion of that stimulation through a motor unit, the input and export of chemicals and heat. The structure of the model provides a means to cross-reference and test the in vitro data at different length scales as these refinements are made providing a means to improve the understanding of muscle function.

Bibliography

[1] R. L. Lieber, Skeletal Muscle Structure, Function and Plasticity: The physiological basis of rehabilitation. Second Edition, Lippincott, Williams and Wilkins, Baltimore, (2002).

[2] E. N. Marieb, Human Anatomy & Physiology, Fifth Edition, Addison Wesley Longman Inc., Baltimore, (2001).

[3] G. E. Loeb, C. A. Pratt, C. M. Chanaud, F. J. R. Richmond, Distribution and innervation of short, interdigitated muscle fibres in parallel-fibred muscles of the cat hind limb. J. of Morphology, (1987), 191, 1-15.

[4] M. Ounjian, R. R. Roy, E. Eldred, A. Garfinkel, J. R. Payne, A. Armstrong, A. W. Toga, V. R. Edgerton, Physiological and developmental implications of motor unit anatomy. J. of Neurobiology, (1991), 22, 547-559, 1991.

[5] S. F. Street, Lateral transmission of tension in frog myofibers: a myofibrillar network and transverse cytoskeletal connections are possible transmitters. J. of Cellular Physiology, (1983), 114, 346-364.

[6] S. C. Bodine, R. R. Roy, E. Eldred, V. R. Edgerton, Maximal force as a function of anatomical features of motor units in the cat tibialis anterior. J. of Neurophysiology, (1987), 6, 1730-1745.

[7] Y. V. Pereverzev, O. V. Prezhdo, M. Forero, E. V. Sokurenko, W. E. Thomas, The two-pathway model for the catch-slip transition in biological adhesion. Biophysical Journal, (2005), vol:89, 1446-1454.

[8] A. F. Huxley, Muscle structure and theories of contraction, Prog. Biophys. Biophys. Chem., (1957), 7: 255-318.

[9] T. J. Burkholder, R. L. Lieber, Sacromere length operating range of vertebrate muscles during movement. The Journal of Experimental Biology, (2001), 204, 1529-1536.

[10] J. Howard, Mechanics of Motor Proteins and the Cytoskeleton. Sineauer Associates, Sunderland, Massachusetts, (2001).

[11] J. A. Spudich, How molecular motors work. Nature, (1994), 372, 515-18.

[12] R. C. Woledge, N. A. Curtin, E. Homsher, Energetic aspects of muscle contraction, Monogr. Physiol. Society, (1985) 41:1-357.

[13] J. B. Peter, R. J. Barnard, V. R. Edgerton, C. A. Gillespie, K. E. Stempel, Metabolic profiles on three fibre types of skeletal muscle in guinea pigs and rabbits. Biochemistry, (1972), 11, 2627-2733.

[14] M. Barany, ATPase activity of myosin correlated with speed of muscle shortening. Journal of General Physiology, (1967), 50, 197-216.

[15] C. Reggiani, R. Bottinelli, G. J. M. Stienen, Sarcomere myosin isoforms: fine tuning of a molecular motor. News. Physiol. Sci, (2000), 15: 26-33.

[16] D. I. Resnicow, J. C. Deacon, H. M. Warrick, J. A. Spudich, L. A. Leinwand, Functional diversity among a family of human skeletal muscle myosin motors. Proc. National Academy of Science, Biochemistry, (2009), 107,3, 1053-1058.

[17] S. Schiaffino, C. Reggiani , Molecular diversity of myofibrillar proteins: gene regulation and functional significance. Physiological Reviews, (1996), 76, 2, 371 – 423.

[18] T. P. Martin, S. Bodine-Fowler, R. R. Roy, E. Eldred, V. R. Edgerton, Metabolic and fibre size properties of cat tibialis anterior motor units. American J. of Physiology, (1988), 255, C43-C50.

[19] R. E. Burke, Motor unit types of cat triceps surae muscle. J. of Physiology (London), (1967), 193, 141-160.

[20] R. E. Burke, D. N. Levine, F. E. Zajac, P. Tsairis, W. K. Engel, Mammalian motor units: physiological-histochemical correlation in three types in cat gastrocnemius. Science, (1971), 174, 709-712.

[21] K. Hilber, S. Galler, B. Gohlsch, D. Pette, Kinetic properties of myosin heavy chain isoforms in single fibres from human skeletal muscle. FEBS Letters , (1999), 455, 267-270.

[22] G. J. M. Stienen, J. L. Kiers, R. Bottinelli, C. Reggiani, Myofibrillar ATPase activity in skinned human skeletal muscle fibres: fibre type and temperature dependency. Journal of Physiology, (1996), 493:2 299-307.

[23] D. Pette, R. S. Staron, Myosin isoforms, muscle fibre types, and transitions. Microscopy Research and Technique. (2000), 50:500-509.

[24] J. F. Finer, R. M. Simmons, J. A. Spudich, Single myosin molecule mechanics: piconewton forces and nanometre steps. Nature, (1994), 368.

[25] M. P. Sheetz, J. A. Spudich, Movement of myosin-coated fluorescent beads on actin cables in vitro. Nature, (1983), 303, 31-35.

[26] M. P. Sheetz, S. M. Block, J. A. Spudich, Myosin movement in vitro: a quantitative assay using oriented actin cables from Nitella. Methods in Enzymology, (1986), 134, 531-544.

[27] T. R. Hynes, S. M. Block, B.T. White, J. A. Spudich, Movement of myosin fragments in vitro: domains involved in force production. Cell, (1987), 48, 953-963.

[28] S.J. Kron, J. A. Spudich, Fluorescent actin filaments move on myosin fixed to a glass surface. Proc. Natl. Acad. Sci, USA, (1986), 83, 6272-6276.

[29] M. Kaya, H. Higuchi, Nonlinear elasticity and an 8nm working stroke of single myosin molecules in myofilaments. Science, (2010), vol. 329, 686-689.

[30] M. Kawai, K. Kawaguchi, M. Saito and S. Ishiwata, Temperature change does not affect force between single actin filaments and HMM from rabbit muscles. Biophysical Journal, (2000), 78, 3112-3119.

[31] M. Kawai, T. Kido, M. Vogel, R. H. A. Fink and S. Ishiwata, Temperature change does not affect force between regulated actin filaments and heavy meromyosin in single-molecule experiment. J. Physiology, (2006), 574.3, 877-887.

[32] J. A. Spudich, Optical trapping: motor molecules in motion. Nature, (1990), 348, 284-285.

[33] S. J. Kron, Y. Y. Toyoshima, T. Q. P. Uyeda and J. A. Spudich, Assays for actin sliding movement over myosin-coated surfaces. Methods in Enzymology. (1991), 196, 399-416.

[34] G. T. Yamaguchi, Dynamic modelling of musculoskeletal motion: a vectorised approach for biomechanical analysis in three dimensions. Kluwer Academic Publishers, Dordrecht, (2003), pp5.

[35] A. V. Hill, The Effect of Load on the Heat of Shortening of Muscle. Proceedings of the Royal Society of London, Biological Sciences, (1964), vol. 159, 975, 297-318.

[36] E. J. Perrault, C. J. Heckman, T. G. Sandercock, Hill muscle model errors during movement are greatest within the physiologically relevant range of motor unit firing rates. Journal of Biomechanics, (2003), 36: 211-218.

[37] D. G. Thelen, F. C. Anderson, Using computed muscle control to generate forward dynamic simulations of human walking from experimental data. J. Biomechanics, (2006), 39: 1107-1115.

[38] G. H. Shue, P. E. Crago, Muscle-tendon model with length history-dependent activation-velocity coupling. Annals of Biomedical Engineering, (1998), 26: 369-380.

[39] L.A. Gilchrist, D.A. Winter, A multi-segment computer simulation of normal human gait. IEEE Transactions on Rehabilitation Engineering, (1997) 5:4, 290-299.

[40] K. S. Campbell, Interactions between connected half-sarcomeres produce emergent mechanical behaviour in a mathematical model of muscle. PloS Computational Biology, (2009), 5 (11): e1000560.

[41] D.A. Martyn, P.B. Chase, M. Regnier, a. M. Gordon, A simple model with myofilament compliance predicts activation-dependent crossbridge kinetics in skinned skeletal fibers. Biophysical Journal, (2002), vol. 83, 3425-3434.

[42] I. A. Telley, J. Denoth, E. Strussi, G. Pfitzer, R. Stehle, Half-sarcomere dynamics in myofibrils during activation and relaxation studied by tracking fluorescent markers. Biophysical Journal, (2006), vol. 90, 514-530.

[43] D. A. Smith, The theory of sliding filament models for muscle contraction. II. Biochemically-based models of the contraction cycle. (1990) 146, 157-175.

[44] D. A. Smith, S. Sicilia, The theory of sliding filament models for muscle contraction. I. The two state model. J. Theoret. Biology, (1987) , 127, 1-30.

[45] D. A. Smith, The theory of sliding filament models for muscle contraction. III. Dynamics of the five state model. (1990), J. Theoret. Biology (1990), 146, 433-466.

[46] T. Hill, E. Eisenberg, Y. Chen, R. J. Podolsky, Some self-consistent two state sliding filament models of muscle contraction. Biophysical Journal, (1975) vol. 15, 335-372.

[47] T. A. J. Duke, Molecular model of muscle contraction. Proc. Natl. Academy of Science , U.S.A., (1999), 96 (6): 2770-2775.

[48] M. P. Slawnych, C. Y. Seow, A. F. Huxley, L. E. Ford, A program for developing a comprehensive mathematical description of the crossbridge cycle of muscle. Biophysical Journal, (1994), vol. 67, 1669-1677.

[49] C. R. Bagshaw, Muscle Contraction. Chapman & Hall, Cambridge, UK, (1993).

[50] R. D. Keynes, D. J. Aidley, Nerve and Muscle. Third Edition, Cambridge University Press, New York, (2001).

[51] I. Rayment, H. M. Holden, The three-dimensional structure of a molecular motor. Trends in Biochemical Sciences, (1994), 19, 129.

[52] S. Lowey, G. S. Waller, K. M. Trybus, Function of skeletal muscle myosin heavy and light chain isoforms by an in vitro motility assay. The Journal of Biological Chemistry, (1993), vol. 268:27, 20414-20418.

[53] K. Wakabayashi, Y. Sugimoto, H. Tanaka, Y. Ueno, Y. Takezawa, Y. Amemiya, X-ray diffraction evidence for the extensibility of actin and myosin filaments during muscle contraction. Biophysical Journal, (1994), 67, 2422-2435.

[54] Y. E. Goldman, A. F. Huxley, Actin compliance: are you pulling my chain? Journal of Biophysics, (1994), 67 (6): 2131-2133.

[55] H. Kojima, A. Ishuima, T. Yanagida, Direct measurement of stiffness of single actin filaments with and without tropomyosin by in vitro nanomanipulation. Proc. Natl. Acad. Sci. USA, (1994), vol. 91 12962-12966.

[56] Y. Tsuda, H. Yasutake, A. Ishijima, T. Yanagida, Torsional rigidity of single actin filaments and actin-bond breaking force under torsion measured directly by in vitro micromanipulation. Proc. Natl. Acad. Sci. USA, (1996), vol. 93 12937-12942.

[57] P. VanBuren, G. S. Waller, D. E. Harris, K. M. Trybus, D. M. Warshaw and S. Lowy, The essential light chain is required for full force production by skeletal muscle myosin. Proc., National Acad. Science, (1994), 91, 12403-12407.

[58] J. J. Sherwood, G. S. Waller, D. M. Warshaw and S. Lowy, A point mutation in the regulatory light chain reduces the step size of skeletal muscle myosin. PNAS, (2004), vol. 101, 30, 10973-10978.

[59] Y. Y. Toyoshima, S. J. Kron, E. M. McNally, K. R. Niebling, C. Toyoshima, J. A. Spudich, Myosin subfragment-1 is sufficient to move actin filaments in vitro. Nature, (1987), vol. 328.

[60] H. E. Huxley, Sliding filaments and molecular motile systems. The Journal of Biological Chemistry, (1990), vol.265-15, 8347-8350.

[61] I. Adamovic, S. M. Mijailovich, M. Karplus, The elastic properties of the structurally characterized myosin II S2 subdomain: a molecular dynamics and normal mode analysis. Biophysical Journal, (2008), 94, 3779-3789.

[62] A. Lewalle, W. Steffen, O. Stevenson, Z. Ouyang, J. Sleep, Single-molecule measurement of the stiffness of the rigor myosin head. Biophysical Journal, (2008), 94, 2160-2169.

[63] Y. Takagi, E. E. Homsher, Y. E. Goldman, H. Shuman, Force generation in single conventional actomyosin complexes under high dynamic load. Biophysical Journal, (2006), vol. 90, 1295-1307.

[64] J. E. Molloy, J. E. Burns, J. C. Sparrow, R. T. Tregear, J. Kendrick-Jones and D. C. S. White, Single-molecule mechanics of heavy meromyosin and S1 interacting with rabbit or drosophila actins using optical tweezers. Biophysical Journal, (1995), vol.68, 298s-305s.

[65] J. E. Molloy, J. E. Burns, J. Kendrick-Jones, R. T. Tregear, D. C. S. White, Movement and force produced by a single myosin head. Nature, (1995), vol. 378, 9, November.

[66] H. Higuchi, T. Yanagida, Y. E. Goldman, Compliance of thin filaments in skinned fibres of rabbit skeletal muscle. Biophys J., (1995), 69(3), 1000-1010.

[67] M. J. Tyska, D. E. Dupuis, W. H. Guilford, J. B. Patlak, G. S. Waller, K. M. Trybus, D. M. Warshaw, S. Lowey, Two heads are better than one for generating force and motion. Proc. Natl. Acad. Sci. U.S.A., (1999), 13:96(8):4402-7.

[68] M. R. Webb, D. R. Trentham, Chemical mechanism of myosin-catalyzed ATP hydrolysis. Handbook of Physiology (1983), American Physiological Society (237-255).

[69] R. W. Lymn, E. W. Taylor, Mechanism of adenosine triphosphate hydrolysis by actomyosin. Biochemistry, (1971), 10, 4617- 4624.

[70] J. A. Spudich, J. Finer, B. Simmons, K. Ruppel, B. Patterson, T. Uyeda, Myosin structure and function. Cold Spring Harbour, Symposium Quant. Biol. (1995), 60, 783-91.

[71] A. Ishijima, H. Kolima, T. Funatsu, M. Tokunaga, H. Higuchi, H. Tanaka and T. Yanagida, Simultaneous observations of individual ATPase and mechanical events by a single myosin molecule during interaction with actin. Cell, (1998), vol. 92, 2, 161-171.

[72] R. Ait-Haddou, W. Herzog, Force and motion generation of myosin motors: muscle contraction. Journal of Electromyography and Kinesiology, (2002), 12, 435-445.

[73] B. Guo, W.H. Guilford, Mechanics of actomyosin bonds in different nucleotide states are tuned to muscle contraction. PNAS, (2006), 103:26, 9844-9849.

[74] G. I. Bell, Model for the specific adhesion of cells to cells. Science, (1978) vol. 200, 618-627.

[75] E. Evans, K. Ritchie, Dynamic strength of molecular adhesion bonds. Biophysical Journal, (1997), vol:72, 1541-1555.

[76] R. Cooke, Actomyosin interaction in striated muscle. Physiological Review, (1997), 77, 671-697.

[77] J. A. Dantzig, Y. E. Goldman, N. C. Millar, J. Lacktis, E. Homsher, Reversal of the crossbridge force-generation transition by photogeneration of phosphate in rabbit psoas muscle fibres. Journal of Physiology, (1992), 451, 247-278.

[78] M. G. Hibberd, J.A. Dantzig, D.R. Trentham, Y.E. Goldman, Phosphate release and force generation in skeletal muscle fibres. Science, (1985), 228, 1317-1319.

[79] E. Homsher, N.C. Millar, Caged compounds and striated muscle contractions. Annual Review Physiol., (1990), 875-896.

[80] Y. Y. Toyashima, C. Toyoshima, J. A. Spudich, Bidirectional movement of actin filaments along tracks of myosin heads. Nature, (1987), 341 154-156.

[81] L. E. Ford, A. F. Huxley, R. M. Simmons, Tension transients during steady shortening of frog muscle fibres. Journal of Physiology. (1985), 361, 131-150.

[82] E. Eisenberg, T. L. Hill, A crossbridge model of muscle contraction. Prog. Biophysics & Mol. Biology. (1979) 33: 55-82.

[83] R. C. Woledge, N. A. Curtin and E. Homsher, Energetic aspects of muscle contraction. Monogr. Physiology Society, (1985), 41:1-357.

[84] A. F. Huxley, R. M. Simmons, Proposed mechanism of force generation in striated muscle. Nature, (1971), 233, 533-538.

[85] Y. M. Haddad, Viscoelasticity of Engineering Materials. Chapman & Hall, London, (1995), P49.

[86] G.Wang, M. Kawai, Effect of temperature on elementary steps of the cross-bridge cycle in rabbit soleus slow-twitch muscle fibres. Journal of Physiology, (2001), 531.1, 219-234.

[87] T. J. Lorenzen, V. L. Anderson, Design of Experiments: A No-Name Approach. Marcel Dekker Inc. New York, (1993).

[88] G. E. P. Box, J. S. Hunter, W. G. Hunter, Statistics for Experimenters. Second Edition, John Wiley & Sons, Hoboken, (2005).

[89] D. E. Harris and D. M. Warshaw, Smooth and skeletal muscle myosin both exhibit low duty cycles at zero load in vitro. The Journal of Biological Chemistry, (1993), 268: 20, 14764-14768.

[90] Y. Y. Toyoshima, S. J. Kron, E. M. McNally, K. R. Niebling, C. Toyoshima, J. A. Spudich, Myosin subfragment-1 is sufficient to move actin filaments in vitro. Nature, (1987), 328, 536-539.

[91] T. Q. P. Uyeda, S. J. Kron, J. A. Spudich, Myosin step size, estimation from slow sliding movcement of actin over low densities of heavy meromyosin. Journal of Molecular Biology, (1990), 214, 699-710.

[92] C. Veigel, M. L. Bartoo, D. C. S. White, J. C. Sparrow, J. E. Molloy, The stiffness of rabbit skeletal actomyosin cross-bridges determined with an optical tweezers transducer. Biophysical Journal, (1998), 75, 1424-1438.

[93] K. Wang, R. McCarter, J. Wright, J. Beverly, R. Ramirez-Mitchell, Viscoelasticity of the sacromere matrix of skeletal muscles; the titin-myosin composite filament is a dual-stage molecular spring. Biophysical Journal, (1993), 64, 1161-1177.

[94] A. M. Gordon, A. F. Huxley, F. J. Julian, The variation in isometric tension with sarcomere length in vertebrate muscle fibres, Journal of Physiology, (1966), 184, 170-192.

[95] B. R. Eisenberg, Quantitative ultrastructure of mammalian skeletal muscle. Skeletal Muscle, MD: American Physiological Society, (1983), 10, 73-112.

[96] W. H. Guilford, D. E. Dupuis, G. Kennedy, J. Wu, J. B. Patlak, D. W. Warshaw, Smooth muscle and skeletal muscle myosins produce similar unitary forces and displacements in the laser trap. Biophysical Journal, (1997), 72: 1006-1021.

[97] Y. S. Han, P. C. Geiger, M. J. Cody, R. L. Macken, G. C. Sieck, ATP consumption rate per crossbridge depends on myosin heavy chain isoform. J. Appl. Physiology, (2003) 94: 2188-2196.

[98] M. J. Kushmerick, T. S. Moerland, R. W. Wiseman, Mammalian skeletal muscle fibres distinguished by contents of phosphocreatine. ATP and Pi. Proc. Natl. Acad. Sci. USA, (1992), 89, 7521-7525.

[99] P. VanBuren, S. S. Work, D. M. Warshaw, Enhanced force generation by smooth muscle myosin in vitro. Proceeds National Academy of Science, USA, (1994), 91, 202-205.

[100] A. Kishino and T. Yanagida, Force measurements by micromanipulation of a single actin filament by glass needles. Nature, (1988), 334, 74-76.

[101] M. J. Kushmerick, R. E. Davis, The chemical energetics of muscle contraction. Proceed. Royal Society, London, (1969), B 174, 315-353.

[102] Y. B. Sun, K, Hilber, M. Irving, Effect of active shortening on the rate of ATP utilisation by rabbit psoas muscle fibres. Journal of Physiology (London), (2001) 431, 781-791.

[103] A. Ishijima, Y. Harada, H. Kojima, T. Funatsu, Single_molecule analysis of the actomyosin motor using nano-manipulation. Biomedical and Biophysical Research Communications, (1994), vol. 199:2, 1057-1063.

[104] M. Nyitrai, R. Rossi, N. Adamek, M. A. Pellegrino, R. Bottinelli, M. A. Geeves, What limits the velocity of fast-skeletal muscle contraction in mammals? J. Molecular Biology, (2006) 355, 432-442.

[105] R. Bottinelli, M. Canepari, C. Reggiani, G. J. M. Stienen, Myofibrillar ATPase activity during isometric contraction and isomyosin composition in rat single skinned muscle fibres. Journal of Physiology, (1994) 663-675.

[106] R. Bottinelli, R. Betto, S. Schiaffino, C. Reggiani, Unloaded shortening velocity and myosin heavy chain and alkali light chain isoform composition in rat skeletal muscle fibres. Journal of Physiology, (1994) 341-349.

[107] C. Reggiani, E.J. Potma, R. Bottinelli, M. Canepari, M. A. Pellegrino, G. J. M. Stienen, Chemo-mechanical energy transduction in relation to myosin isoform composition in skeletal muscle fibres of the rat. Journal of Physiology, (1997) 502.2, 449-460.

[108] E. Thedinga, N. Karim, T. Kraft, B. Brenner, A single-fibre in vitro motility assay. In vitro sliding velocity of F-actin vs. unloaded shortening velocity in skinned muscle fibres. (1999) Journal of Muscle Research and Cell Motility, 20, 785-796.

[109] P. Hook, L. Larsson, Actomyosin interactions in a novel single muscle fibre in vitro motility assay. Journal of Muscle Research and Cell Motility, (2000) 21, 357-365.

[110] S. D. R. Harridge, R. Bottinelli, M. Canepari, M. A. Pellegrino, C. Reggiani, M. Esbjörnsson, B. Saltin, Whole-muscle and single-fibre contractile properties and myosin heavy chain isoforms in humans. European Journal of Physiology, (1996) 432: 913-920.

[111] L. Larsson, R. L. Moss, Maximum velocity of shortening in relation to myosin isoform composition in single fibres from human skeletal muscles. Journal of Physiology, (1993) 472, 595-614.

[112] R. Bottinelli, M. Canepari, M. A. Pellegrino, C. Reggiani, Force-velocity properties of human skeletal muscle fibres: myosin heavy chain isoform and temperature dependence. Journal of Physiology, (1996) 495.2, 573-586.

[113] Z. H. He, R. Bottinelli, M. A. Pellegrino, M. A. Ferenczi, C. Reggiani, ATP consumption and efficiency of human single muscle fibres with different myosin isoform composition. Journal of Biophys. (2000) 79, 945-961.

[114] M. J. Tyska, D.M. Warshaw, The myosin power stroke. Cell Motility and the Cytoskeleton, (2002), 51:1-15.

Appendix A:

Summary of Half-Sarcomere Sub-Unit Model.

The model represents the section of the sarcomere highlighted in red in Diagram A. This incorporates an actin filament, a composite myosin filament and a composite titin protein see Figure 2.1.1, Section 1.1.2 and Diagram D. Fig. 3.8.1 and App. E give schematics of the Matlab script.

A.

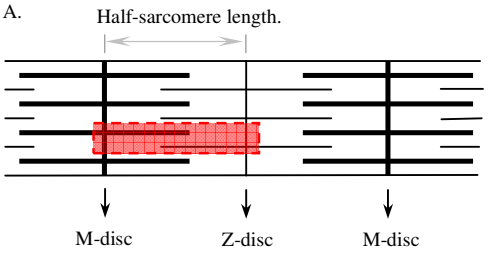

B.

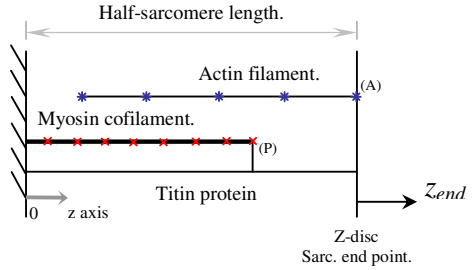

Crossbridge formation (Section 3.4).

The receptive myosin bond site position relative to the actin bond sites is considered. The actin site must be to the right of the myosin site and within the distance identified by z_{range} (see Diagram C) or have transition through this position in the previous time step. The relative speed of the bond sites must be below a maximum defined by v_{cross}.

If these criteria are met, an actin-myosin crossbridge is recorded and the myosin bond site assigned the state A.M.ADP.Pi. If a crossbridge does not form the myosin bond site remains unbound but in a receptive state.

All actin bond sites which are not in a crossbridge are considered receptive to bonding. Each myosin S2 arm has two bond sites; only one can form a crossbridge at a time.

C.

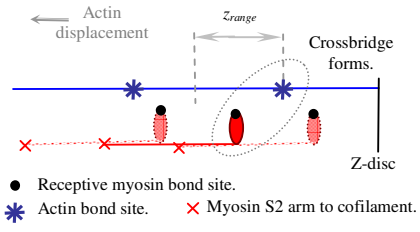

1, Define the model parameters and external loading.
Parameters are summarised in Appendix B.

2, Calculation of initial geometry.

The M-disc acts as the fixed origin from which the the following geometry points are measured (see Diagram B):

~ actin bond sites.
~ S2, myosin arm, to myosin cofilament junctions (see Section 3.2).
~ point (A) marks the Z-disc/end of the titin protein.
~ point (P) is a rigid connection between the myosin cofilament and titin protein (see Section 3.7).

It is not necessary to define the orthogonal offset between the filaments and titin protein for this model.

Each myosin position is assigned two bond sites (Section 3.2.9), the position of which are offset laterally from the S2-cofilament position by the length of S2 the myosin arm (see Section 3.1 and Figure 3.2.1).

Next time step.

A

3, Reaction stages (Section 3.3):

The reaction state of individual bond sites are evaluated. Each myosin bond site maintains a record of its reaction state. At the initial model time step (t_0) a random unattached state, M.ATP or M.ADP.Pi, is assigned to each myosin bond site, see Figure 3.3.1 for the complete reaction cycle.

In subsequent time steps/cycles each myosin bond site is evaluated against the following criteria:

~ Each reaction stage has a minimum duration governed by:

$$k_i\,(T, F) = k_i^0 \exp(F x_{ai} / kT) \qquad \text{(Eq. 3.3.7, Sec. 3.3)}$$

For the purposes of this model k, T are fixed, x_{ai} is empirically defined and examined in Section 4.4. Where the strain, F, is zero for example in unattached crossbridges, Equation 3.3.7 simplifies to k_i^0. Strain free reaction values, k_i^0 , are taken from Table 3.3.1. The reaction stage of shortest duration is taken, forward or reverse, where the potential paths are shown in Figure 3.3.1.

~ Unattached myosin bond sites receptive to actin (M.ADP.Pi) are evaluated for crossbridge formation.

~ If the strain on the crossbridge, F, changes the reaction duration is re-evaluated. Strain is determined by comparing the actin filament tension either side of the crossbridge.

~ For the transition between levering to post-levering states the crossbridge must have released all of its strain energy (A.M. to A.M.ATP).

~ If all of the lever strain energy remain a reversal to the pre-lever state is considered (A.M. to A.M.ADP).

~ If the lever stage exceeds a minimum duration, k_6^0, without releasing all of its energy a separation of the crossbridge is considered, see Section 3.5.7: Isometric loading on a crossbridge.

Continue...

Continue...

4, Evaluation of crossbridges/ filaments as a system

Having identified the reaction state of each bond site the interactions between the model's crossbridges and filaments are determined. Explanation of the modelling process is made via an example. Consider the model to have progressed through a number of time cycles and to be in the equivalent state of Diagram D. Three crossbridges are present: one pre-lever, one levering and a third is in a post-lever state. To evaluate how these crossbridges interact with one another and the actin filament, the system was represented as a spring and damper system, Diagram E.

Stiffness is assigned to the lengths of filaments between the crossbridges: $k_a p_i$ and $k_{ms} n_i$ where i= 1 to 4 (see see Section 3.2.2).

The different types of crossbridge are represented:

~ In a pre-lever crossbridge, the actin bond site c is coincident with the myosin bond site b, forming an effectively rigid connection.

~ The levering crossbridge has strain energy to release into the system (Section 3.5.2) represented by k_{b1} and c_{b1} from Equation 3.5.1:

$$F_{bridge} = (b_{\max} - z)k_b = c_b \frac{dz}{dt} + k_b \cdot z \,,$$

If the crossbridge has released no strain energy the points f and e are coincident, if in previous time steps energy has been released f and e are off-set in proportion to the energy already released into the system.

~ In the post-lever crossbridge, myosin and actin bond sites are off-set by the lever distance b_{max} (Section 3.5, 3.5.2), the displacement imparted to the actin and myosin bond sites by the completion of the levering stage.

The combined stiffness of the myosin head S1 and myosin arm S2 are determined for each crossbridge (k_{mi} , where i =1,2,3 in Diagram E) by applying the lengths of a-b, d-e and g-h to the criteria in Section 3.2.2, Equations 3.2.1, 3.2.2 and 3.2.3.

As each node, a-j in the example, is in equilibrium The system can be written in the form of an equation set (Section 3.6). External loads are applied at node j. The equation set is then solved (Equation 3.6.6) to determine the displacements of the nodes.

The equations are reformulated and re-evaluated if a crossbridge is excessively loaded and therefore removed based on the criterion of rupturing crossbridges Section 3.3.3 and Figure 3.3.2. If the length of a myosin arm changes enough to change the stiffness representation of the arm the equations are revaluated over shorter time steps in order to capture the change (Section 3.2.2).

The positions of the actin bond sites and myosin S2-to-cofilament junctions are updated, as is the strain energy remaining in each crossbridge and the state of crossbridges which have ruptured.

A

Next time step.

5, Output.

At the end of each time step the following data are recorded:

~ Displacement of the nodes.

~ Position of actin bond sites and myosin S2-cofilament junction.

~ Reaction state of bond sites and the remaining crossbridge strain energy.

After a number of cycles the displacement and force generated can be plotted against time: e.g. Diagram F. By colour coding the reaction stages and positions of the bond sites the interaction and contribution of individual crossbridges to the overall filament movement can be explored. Diagram G represents a potential out come of solving the system in Diagram E, see also Figure 4.3.2.

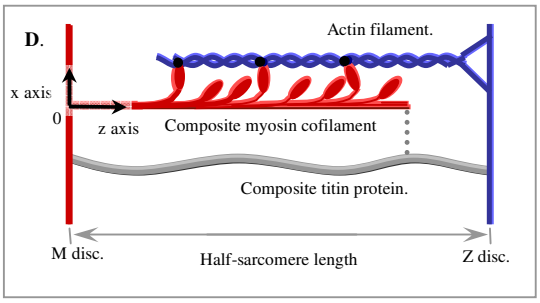

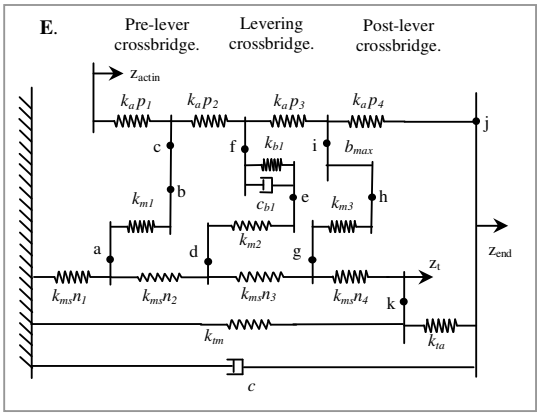

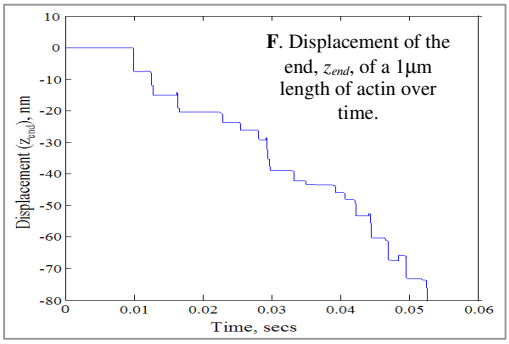

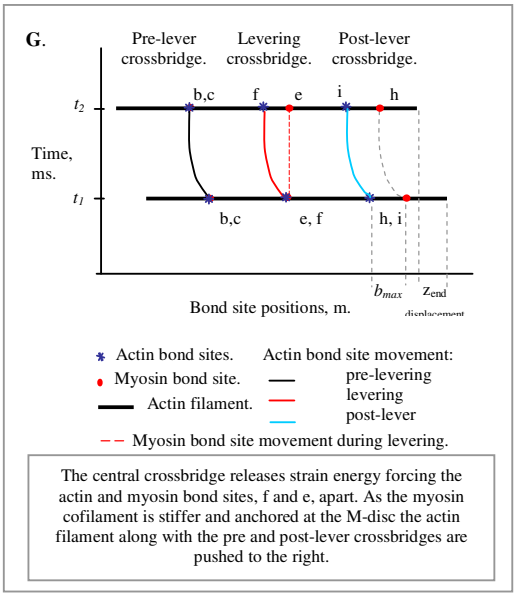

The central crossbridge releases strain energy forcing the actin and myosin bond sites, f and e, apart. As the myosin cofilament is stiffer and anchored at the M-disc the actin filament along with the pre and post-lever crossbridges are pushed to the right.

Appendix B:

Tabulation of model parameters.

Table 1, Cofilament and filament Geometry Parameters.

	Parameter Description	Value	Sect. Intro.	Source/Notes
1	Single myosin cofilament: spacing between S1-S2 junctions.	42.9nm *(a)*	3.1	[49] [50] Determined from X-ray diffraction, micrographs, chemical analysis.
2	Cofilament length S2 to S2, M_{head}.	14.3nm*(a)*	3.1	[49] [50] (as above)
3	Myosin S2 length.	60nm to 65nm	3.2	[11,49,61] 60nm, [51] 65nm, Determined from X-ray diffraction, micrographs, chemical analysis. 60nm most commonly measured.
5	Sarcomere length	1.01 – 4.41μm.	3.7	Example range given, great variability, see Section 3.7, [9].
6	Myosin cofilament length.	1.6μm*(b)*	3.7	[9,50]
7	Myosin cofilament smooth mid-section.	0.2μm	4.1	[50]
8	Actin length.	2.0μm*(b,c)*	3.7	[9]
9	Actin bond site-to-bond site length.	38.5nm	4.1	[49] [50] Determined from X-ray diffraction, micrographs, chemical analysis.

(a) Model, as combination of three myosin, uses a repeat sequence of 14.3nm (42.9nm/3).
(b) Full length given, full-length/two is used in the model.
(c) Some variability dependent on muscle type, 2.0μm is the most common see ref [9].

Table 2, Cofilament, Myosin II and filament Stiffness Parameters.

	Parameter Description	Value	Sect. Intro.	
1	S2 longitudinal stiffness, k_m	70± 10pN/nm per 60nm length.	3.2	Taken form [46], modal analysis of Myosin II, S2.
2	S2 bending stiffness, k_m	~0.01pN/nm per 60nm length.	3.2	Taken form [46], modal analysis of Myosin II, S2.
3	Actin with tropomyosin, k_a. stiff. between bond sites. [(b)]	65.3 ± 6.3pN/nm per 1µm length	3.2	Taken from [55], a direct measurement of filament stiffness. Second source: 53pN/nm per 1µm length [10(p138)] tropomyosin unspecified.
4	Actin without tropomyosin, stiff. between bond sites, k_a.	43.7± 4.6pN/nm per 1µm length	3.2	Taken from [55], a direct measurement of filament stiffness.
5	S1 pre-lever stiffness, k_{mh}.	2.70pN/nm (k_{cross} 2.6pN/nm) [(c,b)]	32	Model experiment derived from reference [61].
6	S1 post-lever stiffness, k_{mh}.	3.03pN/nm (k_{cross} 2.9pN/nm) [(b)]	3.2	"
7	S1 stiffness during levering, k_{mh}.	3.53pN/nm	3.5	Lower estimate based on isometric study using the model.
8	Pre-lever max. head flexure, l_{head}.	3.62 ± 0.09nm to 16.5nm	3.2	Length deduced via model experiment.
9	Post-lever max. head flexure, l_{head}.	3.23 ± 0.08nm to 16.5nm	3.2	"
x	Myosin cofilament, S2 to S2 stiffness, k_{ms}.	4.61N/m per 14.3nm + 62% [(d)]	3.2	Based on extrapolation for compliance devision in fibres, [53],[66].
y	Titin parallel to actin, k_{ta}.	58.9µN/m [(e)]	3.7	Estimated from myofibril x'section [93].
z	Titin parallel to myosin, k_{tm}.	58.9µN/m	3.7	Estimated from myofibril x'section [93].

(a) Due to helical structure, scaling for length may be approximate.
(b) Apparent crossbridge stiffness in model matched to ref [61] where error is not explicitly given but estimated as ± 0.1pN/nm.
(c) k_{cross} crossbridge stiffness.
(d) Lower estimate used as a magnitude of ten greater than the stiffness of actin for the same length.
(e) Error is not given although assumed high as extrapolated from fibre data. Significance of parameter examined in Section 4.3.

Table 3, Crossbridge Parameters.

	Parameter Description	Value	Sect. Intro.	
1	Max. lever displacement, b_{max}. [(a)]	7.9nm	3.5	Value established in model corresponds to [29,63,65,114][(b)]
2	Elastic component of lever, k_b.	1.923pN/nm	3.5	Value established in isometric study using model.
3	Viscous damping of lever, c_b.	0.04pN/μm/s	3.5	Value established in isometric study using model.
4	Range of electrostatic attraction between bond sites, z_{range}.	2.2×10^{-22}m	3.4	Kept small to avoid energy input into model, see Section 4.1.3.
5	Max relative speed of bond sites forming a X'bridges, v_{cross}.	10μm/s[(c)]	3.4	Arbitrary value based on peak filament speeds, see Section 4.3.3

(a) Displacement put into model at crossbridge, min. percentage required for crossbridge to progress to post-lever state is 7.6nm.
(b) Reference [114] summarises length measurements from a number of sources for pre- 2002 with results ranging from 4.7 to 13.5nm, also ~4nm [65,1995]. More recent results determined values of ~7.6nm [29, 2010] and ~7.5nm [110, 2006]. Kaya and Higuchi [29] highlights the apparent displacement (actin movement) may appear shorter than the distance levered, which includes myosin cofilament/substrate movement (see Section 4.3, Figure 4.3.2).
(c) Constraint placed on maximum value: (v_{cross}/t_{step}) ≤ max filament velocity see Section 3.4.

Table 4, Reaction Parameters.

	Parameter Description	Value	Sect. Intro.	
1	Unstrained reaction values.			See Table 3.3.1.
2	Strain dependency of pre-lever reaction, Character length x_4			See Section 4.4 and 4.7.
3	Rupture Stage 1: inner, Pre-lever character length, x_1	0.10 ± 0.01nm	3.3	Guo and Guilford's [73] model of optical trap test data.
4	Rupture Stage 1: inner, Post-lever character length, x_1	0.51 ± 0.04nm	3.3	"
5	Rupture Stage 1: inner, Pre-lever reaction rate, k_1^0	4.4 ± 0.2s^{-1}	3.3	"
6	Rupture Stage 1: inner, Post-lever reaction rate, k_1^0	0.9 ± 0.2s^{-1}	3.3	"
7	Rupture Stage 2: outer, Pre-lever character length, x_2	2.6 ± 1.0nm	3.3	"
8	Rupture Stage 2: outer, Post-lever character length, x_2	2.1 ± 0.7nm	3.3	"
9	Rupture Stage 2: outer, Pre-lever reaction rate, k_2^0	0.02 ± 0.04s^{-1}	3.3	"
x	Rupture Stage 2: outer, Post-lever reaction rate, k_2^0	0.2 ± 0.1s^{-1}	3.3	"
y	Rupture during levering assigned post-lever values.		3.3	"

Appendix C:

Summary of Pre-Lever Strain Dependency Results.

Summary of the results of Section 4.4 and 4.7: the influence of pre-lever strain dependent reactions on the motility and isometric force generation of an actin filament. Colour coding indicates high and low values. Each matrix shows the response for changing x_4 (the forward reaction) and x_{-4} (the reverse reaction).

1, Displacement/Time Time = 0.1 sec

Foreward Δx, nm \ Reverse Δx, nm.	0	-25	-50	-75	-100	-125
0	0.648	0.637	0.605	0.606	0.572	0.458
5	0.682	0.724	0.694	0.8	0.649	0.495
10	0.725	0.713	0.713	0.66	0.704	0.582
15	0.65	0.902	0.701	0.715	0.692	0.743
20	0.639	0.902	0.968	0.846	0.769	0.637
25	0.779	0.769	0.921	0.921	0.821	0.69
30	0.782	0.864	0.844	0.867	1.051	0.781
35	0.674	0.888	0.935	0.812	0.992	0.9
40	0.885	0.757	1.098	0.907	1.009	0.801
45	0.815	0.853	0.96	0.978	0.963	0.888
50	0.779	1.021	0.935	0.901	1.15	1.01
60	0.901	1.011	1.096	0.934	1.184	0.803
80	0.929	1.108	1.096	1.04	0.913	1.045

Key	μm/s
0.45	0.598
0.598	0.746
0.746	0.894
0.894	1.042
1.042	1.19

min/max 0.378

15/-125 slips ~ duration 0.0529 secs

Slips: 0/35 -50/30 -50/45 and -100/35 -50/100 slips

2, Efficiency ~ Displacement/ADP

Foreward Δx, nm \ Reverse Δx, nm.	0	-25	-50	-75	-100	-125
0	0.90	0.95	1.08	1.10	1.00	2.08
5	1.18	1.08	1.02	1.08	1.10	2.60
10	1.29	1.00	1.15	1.03	1.13	2.16
15	1.41	1.17	1.23	1.13	1.19	2.18
20	1.56	1.17	1.36	1.32	1.26	1.99
25	1.39	1.28	1.20	1.20	1.24	2.30
30	1.35	1.27	1.34	1.28	1.28	1.24
35	1.53	1.31	1.48	1.23	1.26	1.30
40	1.55	1.54	1.29	1.37	1.44	1.38
45	1.25	1.52	1.35	1.38	1.34	1.25
50	1.53	1.38	1.44	1.31	1.17	1.37
60	1.45	1.44	1.52	1.37	1.36	1.30
80	1.39	1.37	1.31	1.35	1.32	1.24

Key	nm/ADP
0.9	1.26
1.26	1.62
1.62	1.98
1.98	2.34
2.34	2.7

min/max 0.333

3, Peak Isometric force

Foreward Δx, nm \ Reverse Δx, nm.	0	-25	-50	-75	-100	-125
0	37.77	13.49	24.81	12.14	23.76	5.166
5	20.08	34.04	15.4	23.42	34.75	13.49
10	32.74	12.85	27.45	24.03	27.96	15.05
15	9.701	25.2	18.62	29.3	20.33	8.694
20	22.57	21.95	17.88	31.16	28.03	13.59
25	18.03	14	23.18	13.31	23.23	(a)
30	21.03	15.53	17.44	17.42	13.07	9.294
35	11.51	24.34	34.52	21.21	0.053	16.11
40	15.42	9.155	27.85	26.98	11.05	17.18
45	21.17	2.294	29.15	14.52	9.684	17.66
50	9.192	14.53	21.68	32.78	21.33	11.23
60	22.45	16.55	32.49	19.59	5.661	23.91
80	8.949	9.227	8.648	9.594	13.99	15.99

Key	pN
0	7.56
7.56	15.12
15.12	22.68
22.68	30.24
30.24	37.8

min/max 0

(a) 0.445

4, Impulse to Peak Isometric Force

Foreward Δx, nm \ Reverse Δx, nm.	0	-25	-50	-75	-100	-125
0	3.500	0.776	2.624	1.685	3.190	0.882
5	2.523	5.856	1.391	4.691	6.228	0.395
10	2.518	2.976	1.423	6.871	4.286	1.234
15	0.792	3.380	1.928	4.227	3.722	0.136
20	2.367	2.210	1.189	1.857	3.861	0.727
25	0.527	2.631	5.408	3.278	2.853	0.224
30	2.019	0.478	5.177	4.508	2.709	1.165
35	0.857	1.841	3.804	2.123	(b)	6.406
40	1.826	1.233	1.746	2.556	1.684	2.733
45	2.862	0.322	2.559	4.226	2.854	2.915
50	1.423	2.235	2.587	2.799	5.862	5.376
60	7.046	2.451	2.089	2.346	0.526	2.931
80	0.800	2.135	1.179	2.849	5.353	1.329

Key	10^{-14}Ns
0.1	1.5
1.5	2.9
2.9	4.3
4.3	5.7
5.7	7.1

min/max 0.014

(b) Negligible force.

5, Time to Peak Isometric Force

Foreward Δx, nm \ Reverse Δx, nm.	0	-25	-50	-75	-100	-125
0	3.18	1.93	5.71	4.47	4.88	11.9
5	5.75	5.56	1.8	7.45	6.48	4.12
10	5.02	5.76	2.1	7.6	4.48	4.48
15	2.11	2.73	6.29	6.99	3.84	4.35
20	4.69	2.83	8.48	5.32	4.96	10.4
25	9.51	5.73	8.93	8.05	3.34	10.1
30	3.28	1.53	7.38	7.69	3.64	2.07
35	2.42	3.98	1.73	3.65	(c)	(d)
40	10.4	7.76	1.34	6.5	2.91	8.61
45	4.79	3.62	6.18	6.67	7.22	8.11
50	2.43	2.64	3.68	2.88	10.4	7.31
60	10.7	5.45	1.2	2.11	3.69	3.05
80	3.17	10.5	3.85	6.48	9.62	4

Key	msec
11.9	9.74
9.74	7.58
7.58	5.42
5.42	3.26
3.26	1.1

min/max 0.09

(c) 13.49

(d) 17.36

6, Efficiency ~ Impulse to peak/ADP

Foreward Δx, nm \ Reverse Δx, nm.	0	-25	-50	-75	-100	-125
0	0.35	0.26	0.52	0.34	0.46	0.18
5	0.42	0.59	0.23	0.47	0.57	0.2
10	0.36	0.5	0.24	0.69	0.54	0.41
15	0.4	0.48	0.21	0.53	0.53	0.05
20	0.47	0.37	0.3	0.21	0.39	0.18
25	0.11	0.22	0.49	0.41	0.36	0.07
30	0.25	0.16	0.65	0.64	0.39	0.17
35	0.11	0.37	0.76	0.24		0.8
40	0.46	0.25	0.44	0.26	0.28	0.39
45	0.32	0.32	0.64	0.7	0.41	0.58
50	0.47	0.56	0.43	0.35	0.49	0.77
60	0.7	0.25	0.42	0.34	0.13	0.37
80	0.2	0.24	0.17	0.41	0.76	0.17

Key	10^{-14}Ns/ADP
0	0.18
0.18	0.36
0.36	0.54
0.54	0.72
0.72	0.9

7, Impulse ~ Percentage of total released upto peak force, 0.11s to 0.124 secs.

Foreward Δx, nm \ Reverse Δx, nm.	0	-25	-50	-75	-100	-125
0	45.5	26.6	48.2	36.7	63.2	80.4
5	42.1	89.4	33.3	51.6	70.8	29.0
10	34.8	76.7	18.3	69.7	75.8	39.2
15	57.1	61.3	46.9	39.7	52.9	6.6
20	30.6	43.6	52.1	36.7	34.8	33.8
25	16.7	66.1	80.3	67.9	48.0	63.4
30	30.9	9.4	83.3	79.9	51.0	67.3
35	20.1	32.6	45.8	44.9		128.9
40	39.1	49.4	50.8	51.1	55.5	76.3
45	69.0	83.6	66.6	75.5	83.6	60.0
50	61.0	47.9	47.3	69.3	83.3	74.4
60	86.1	58.7	60.0	56.6	27.8	65.6
80	48.1	78.3	49.4	68.8	84.3	54.1

Key	10^{-14}Ns
6.5	31
31	55.5
55.5	80
80	104.5
105	129

min/max 0.05

8, ADP expelled upto Peak Isometric Force.

Foreward Δx, nm \ Reverse Δx, nm.	0	-25	-50	-75	-100	-125
0	10	3	5	5	7	5
5	6	10	6	10	11	2
10	7	6	6	10	8	3
15	2	7	9	8	7	3
20	5	6	4	9	10	4
25	5	12	11	8	8	3
30	8	3	8	7	7	7
35	4	5	6	9		8
40	4	5	4	10	6	7
45	9	1	4	6	7	5
50	3	4	6	8	12	7
60	10	10	5	7	4	8
80	4	9	7	7	7	8

Key	10^{-14}Ns/ADP
1	3.2
3.2	5.4
5.4	7.6
7.6	9.8
9.8	12

min/max 0.08

9, Motility, concurrent crossbridges - mean.

Foreward Δx, nm \ Reverse Δx, nm.	0	-25	-50	-75	-100	-125
0	10.3	10.4	10.3	10.0	10.0	
5	10.1	10.8	10.7	11.1	10.5	
10	10.6	10.8	10.9	10.9	10.7	
15	10.0	11.4	10.0	10.6	10.2	
20	9.2	11.6	11.6	10.2	10.8	
25	11.2	10.7	11.7	11.3	10.7	
30	11.1	11.3		10.4	11.7	11.1
35		11.4	10.6	11.0		11.0
40		10.4	11.3	10.9	11.2	10.2
45	11.5	10.6		11.1	11.7	10.1
50	11.0	11.6	10.2	10.9	12.2	11.2
60	11.4	11.5	11.2	10.0	11.4	10.0
80		11.7	11.8	11.7		11.3

Key	pN
9.2	9.82
9.82	10.44
10.44	11.06
11.06	11.68
11.68	12.3

min/max
0.748

10, Motility, concurrent crossbridges - spread of values.

Foreward Δx, nm \ Reverse Δx, nm.	0	-25	-50	-75	-100	-125
0	10	10	10	9	11	
5	8	9	8	8	10	
10	10	8	11	8	10	
15	13	12	17	15	11	
20	16	13	11	13	12	
25	10	12	11	14	11	
30	11	12		13	13	12
35		12	12	10		12
40		16	13	11	11	13
45	11	13		13	14	12
50	12	10	12	11	11	11
60	10	12	15	13	12	16
80		11	13	14		13

Key	10^{-14}Ns
8	9.8
9.8	11.6
11.6	13.4
13.4	15.2
15.2	17

11, Motility, concurrent crossbridges - minimum.

Foreward Δx, nm \ Reverse Δx, nm.	0	-25	-50	-75	-100	-125
0	8	6	6	7	5	
5	7	7	7	7	6	
10	6	7	5	7	6	
15	3	5	1	3	6	
20	1	5	7	4	5	
25	7	5	7	4	6	
30	6	7		4	4	5
35		6	5	6		6
40		1	5	6	6	4
45	6	4		6	4	6
50	5	7	6	7	6	6
60	7	5	2	4	5	2
80		6	4	5		4

Key	msec
1.0	2.4
2.4	3.8
3.8	5.2
5.2	6.6
6.6	8.0

min/max
8

12, Motility, concurrent crossbridges - maximum.

Foreward Δx, nm \ Reverse Δx, nm.	0	-25	-50	-75	-100	-125
0	18	16	16	16	16	
5	15	16	15	15	16	
10	16	15	16	15	16	
15	16	17	18	18	17	
20	17	18	18	17	17	
25	17	17	18	18	17	
30	17	18		17	17	17
35		18	17	16		18
40		17	18	17	17	17
45	17	17		19	18	18
50	17	17	18	18	17	17
60	17	17	17	17	17	18
80		17	17	19		17

Key	10^{-14}Ns/ADP
15	15.8
15.8	16.6
16.6	17.4
17.4	18.2
18.2	19

(1) Matrix 7, some percentages are higher than 100: titin provides a returning force, which may cause a negative load on the held end of the actin filament. For x_{-4} = 35, -125nm, this was expressed after the peak force disrupting the calculation required to summarise the results, the results in some instances are therefore not shown.

(2) Displacements are shown as positive but in the convention of the model they are negative, being movements to the left.

(3) Below the x_4=30nm the model script was modified to include a packing restriction (see Section 4.3.2).

Appendix D:

Example Set of Data for a Baseline Model Motility Run.

Data for a Baseline Model run monitored in more detail. $k_4^0 = 100s^{-1}$, x_4 = 80nm and x_{-4} = -60nm. Table D1 summarises the filaments movement and the performance of individual crossbridges. Figure D1 plots the reaction state and position of those crossbridges relative to one another over time. Figure D2 summarise the number of crossbridges and their states over time and Figure D3 maps the position of the right hand end of the actin filament as it moves over time.

Table D1, Analysis of crossbridge attachment times over 0.1 seconds, $k_4^0 = 100s^{-1}$, x_4 = 80nm and x_{-4} = -60nm.Crossbridges that have completed the reaction cycle and are released by ATP.

	Attachment time, t_{on}, ms.	ATPase, t_{total}, ms.	X'bridge disp. while attached, nm.	Concurrent crossbridges.	Duty Ratio, $k_4^0 = 100s^{-1}$	Duty Ratio, $k_4^0 = 30s^{-1}$
max.	20.70	31.20	23.30	17	0.66	
min.	2.85	13.35	7.60	4	0.21	0.090
mean	9.61	20.11	12.90	9.9	0.48	0.240
mode	11.70	22.20	23.30	11	0.53	0.280

Data given for 53 complete cycles.
49 cycles were incomplete: 29 released pre-lever, 15 released during levering, 5 still active at end of time study.

$k_4^0 = 100s^{-1}$: duration 10ms, without strain ATPase cycle: 21.7ms.
$k_4^0 = 30s^{-1}$: duration 33ms, without strain ATPase cycle: 45.0ms

Speed of filament = 1μm/s Efficiency = 1.34nm/ADP

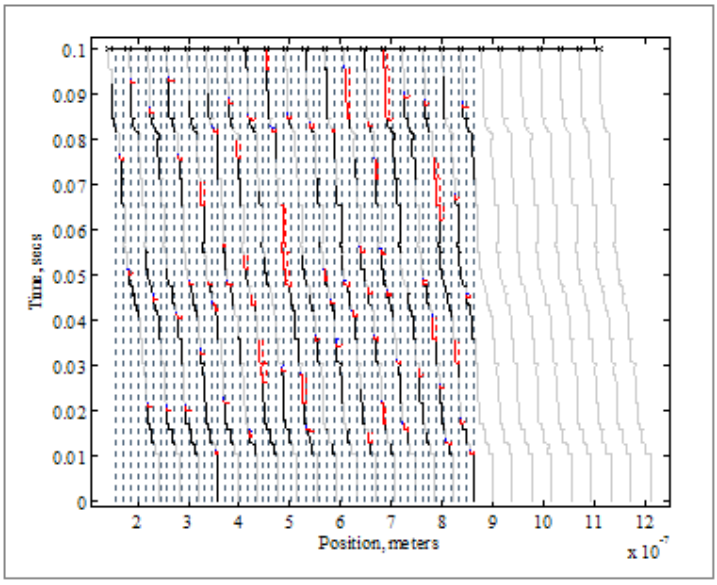

Figure D1, Crossbridge behaviour over 0.1 seconds, $k_4^0 = 100s^{-1}$, x_4 = 80nm and x_{-4} = -60nm.

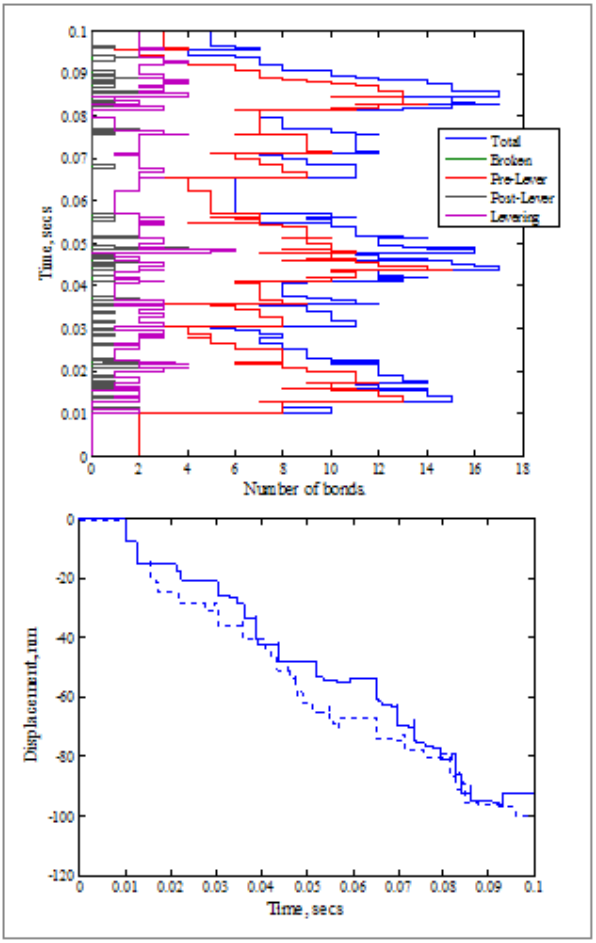

Figure D2, Number of concurrent crossbridges and there reaction states against time. k_4^0 *=100s*$^{-1}$*,* x_4 *= 80nm and* x_{-4} *= -60nm.*

Figure D3, Displacement against time of two filaments. 0.1 seconds, k_4^0 *=100s*$^{-1}$*,* x_4 *= 80nm and* x_{-4} *= -60nm. Data for the dark blue result is recored in figures D1, D2 and Table D1.*

Appendix E:

Schematics of key functions used in the Matlab model.

Figure 3.8.1 outlines the interaction of these functions: ResolveLoad, HeadBonding, HeadProcessing and ReactionRate.

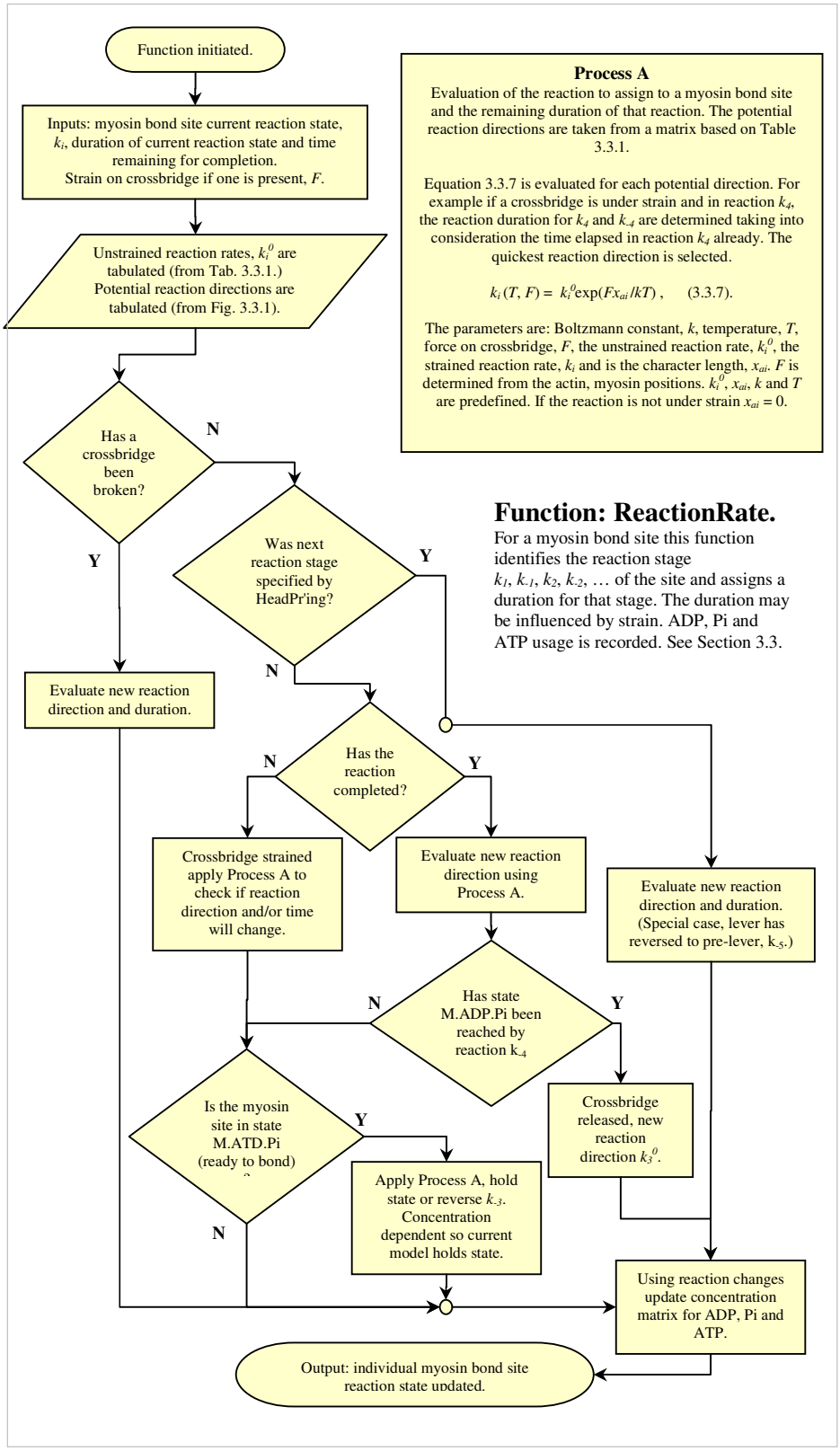
Function initiated.
Inputs: myosin bond site current reaction state, k_i, duration of current reaction state and time remaining for completion.
Strain on crossbridge if one is present, F.
Unstrained reaction rates, k_i^0 are tabulated (from Tab. 3.3.1.)
Potential reaction directions are tabulated (from Fig. 3.3.1).
Has a crossbridge been broken?
N
Y
Was next reaction stage specified by HeadPr'ing?
Y
N
Evaluate new reaction direction and duration.
Has the reaction completed?
N
Y
Crossbridge strained apply Process A to check if reaction direction and/or time will change.
Evaluate new reaction direction using Process A.
Evaluate new reaction direction and duration. (Special case, lever has reversed to pre-lever, k_{-5}.)
Has state M.ADP.Pi been reached by reaction k_{-4}
N
Y
Is the myosin site in state M.ATD.Pi (ready to bond)
Y
N
Crossbridge released, new reaction direction k_3^0.
Apply Process A, hold state or reverse k_{-3}. Concentration dependent so current model holds state.
Using reaction changes update concentration matrix for ADP, Pi and ATP.
Output: individual myosin bond site reaction state updated.
Process A
Evaluation of the reaction to assign to a myosin bond site and the remaining duration of that reaction. The potential reaction directions are taken from a matrix based on Table 3.3.1.
Equation 3.3.7 is evaluated for each potential direction. For example if a crossbridge is under strain and in reaction k_4, the reaction duration for k_4 and k_{-4} are determined taking into consideration the time elapsed in reaction k_4 already. The quickest reaction direction is selected.
$k_i(T, F) = k_i^0 \exp(F x_{ai}/kT)$, (3.3.7).
The parameters are: Boltzmann constant, k, temperature, T, force on crossbridge, F, the unstrained reaction rate, k_i^0, the strained reaction rate, k_i and is the character length, x_{ai}. F is determined from the actin, myosin positions. k_i^0, x_{ai}, k and T are predefined. If the reaction is not under strain $x_{ai} = 0$.
Function: ReactionRate.
For a myosin bond site this function identifies the reaction stage k_1, k_{-1}, k_2, k_{-2}, … of the site and assigns a duration for that stage. The duration may be influenced by strain. ADP, Pi and ATP usage is recorded. See Section 3.3.

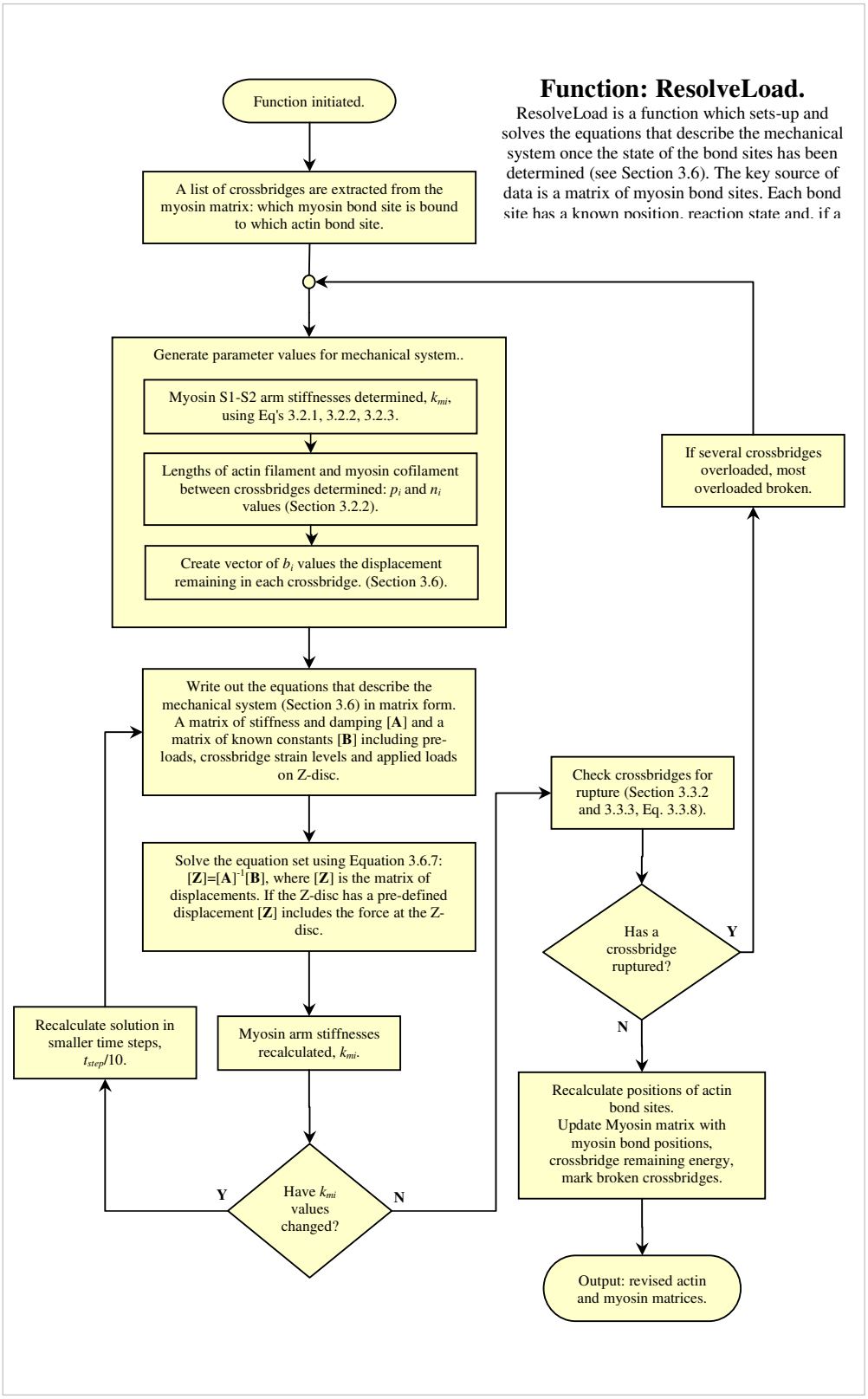
Function: ResolveLoad.
ResolveLoad is a function which sets-up and solves the equations that describe the mechanical system once the state of the bond sites has been determined (see Section 3.6). The key source of data is a matrix of myosin bond sites. Each bond site has a known position, reaction state and, if a
Function initiated.
A list of crossbridges are extracted from the myosin matrix: which myosin bond site is bound to which actin bond site.
Generate parameter values for mechanical system..
Myosin S1-S2 arm stiffnesses determined, k_{mi}, using Eq's 3.2.1, 3.2.2, 3.2.3.
Lengths of actin filament and myosin cofilament between crossbridges determined: p_i and n_i values (Section 3.2.2).
Create vector of b_i values the displacement remaining in each crossbridge. (Section 3.6).
Write out the equations that describe the mechanical system (Section 3.6) in matrix form. A matrix of stiffness and damping [**A**] and a matrix of known constants [**B**] including pre-loads, crossbridge strain levels and applied loads on Z-disc.
Solve the equation set using Equation 3.6.7: $[\mathbf{Z}]=[\mathbf{A}]^{-1}[\mathbf{B}]$, where [**Z**] is the matrix of displacements. If the Z-disc has a pre-defined displacement [**Z**] includes the force at the Z-disc.
Myosin arm stiffnesses recalculated, k_{mi}.
Have k_{mi} values changed?
Y
N
Recalculate solution in smaller time steps, t_{step}/10.
Check crossbridges for rupture (Section 3.3.2 and 3.3.3, Eq. 3.3.8).
Has a crossbridge ruptured?
Y
N
If several crossbridges overloaded, most overloaded broken.
Recalculate positions of actin bond sites.
Update Myosin matrix with myosin bond positions, crossbridge remaining energy, mark broken crossbridges.
Output: revised actin and myosin matrices.

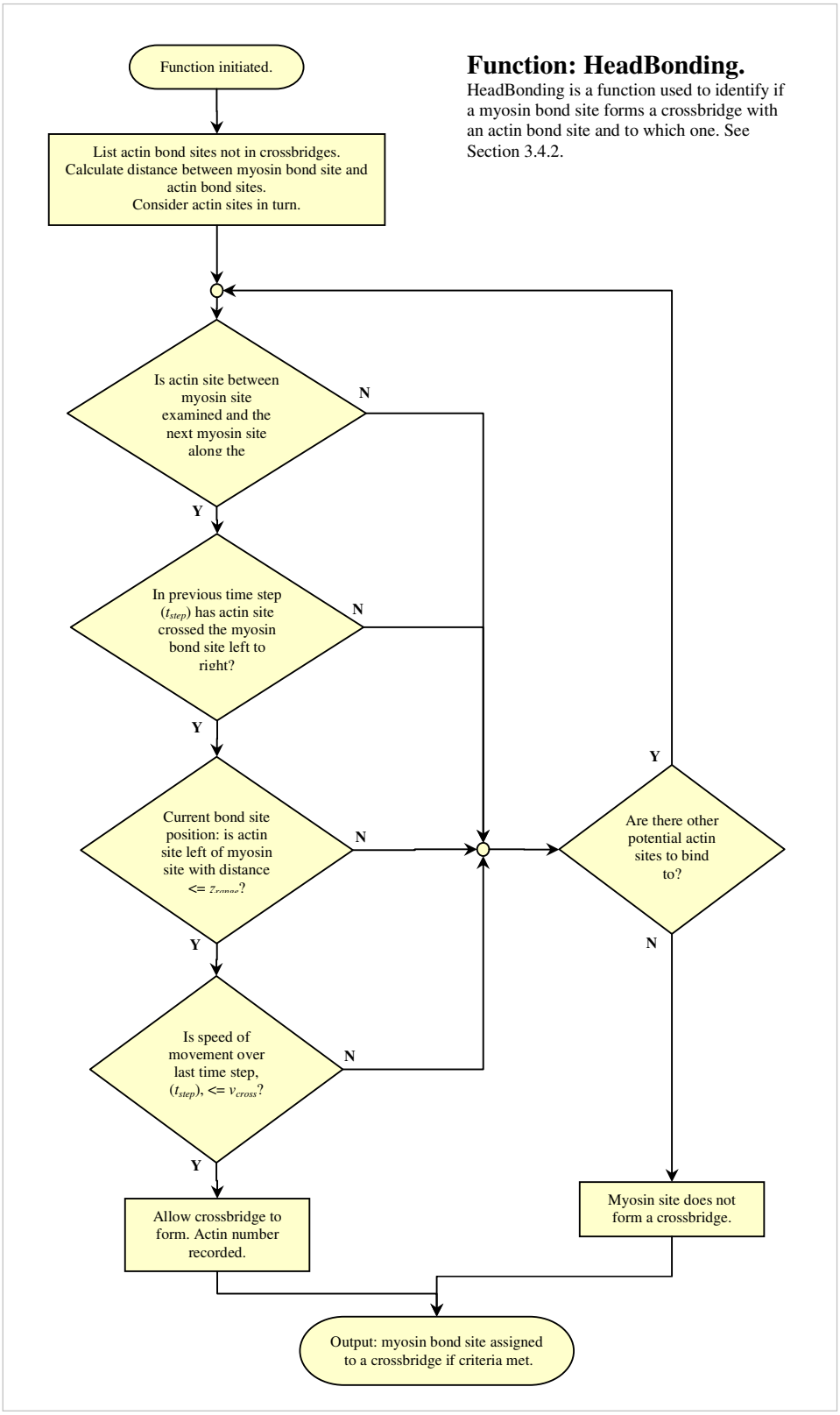

Function: HeadBonding.

HeadBonding is a function used to identify if a myosin bond site forms a crossbridge with an actin bond site and to which one. See Section 3.4.2.

Function: HeadProcessing.

The HeadProcessing function evaluates the status of each myosin bond site: its reaction state, if it is ready to bind whether it finds an actin to bind to and to which one. Strain energy is assigned to new crossbridges.